JOURNAL OF TELECOMMUNICATIONS AND INFORMATION TECHNOLOGY

1/2003

Special issue edited by Józef Modelski

New approach to computer aided design of coupled resonator filters

P. Kozakowski and M. Mrozowski — Paper — 3

Modulator structures for radio-on-fiber applications

S. V. Hum, M. Okoniewski, and R. J. Davies — Paper — 8

A 24 GHz PHEMT-based oscillator

A. Lewandowski et al. — Paper — 15

Synthesis method for distributed amplifiers

A. Zólomy — Paper — 20

Reliability and low-frequency noise measurements of InGaAsP MQW buried-heterostructure lasers

S. Pralgauskaite et al. — Paper — 24

Optical control of semiconductor synchronized microwave oscillators in the power suppression mode

D. A. Usanov, A. V. Skripal, and A. V. Abramov — Paper — 30

Vertical cavity surface emitting lasers in radio over fiber applications

T. Marozsák and E. Udvary — Paper — 36

Evaluation of near field of the GSM base station antennas in urban environment

D. Wójcik — Paper — 41

ISSN 1509-4553

Circulation: 300 copies

Sowa - Druk na życzenie, tel. 022 431-81-40, www.sowadruk.pl

JOURNAL OF TELECOMMUNICATIONS AND INFORMATION TECHNOLOGY

Preface

This special issue is devoted to the *14th International Conference on Microwaves, Radar and Wireless Communications* MIKON-2002, which was held on May 20–22, 2002, in Gdańsk, the charming old capital of Pomerania, well known around the world for its major historical landmarks. This volume contains 13 papers presented by the finalists of the Young Scientists Contest, which is traditionally organized during the conference.

In the course of MIKON's over 30-year long history, the last conference was already the fifth truly international meeting. MIKON assembles the whole Polish microwave and radiolocation community as well as numerous representatives of our immediate neighbours (especially from the East and South of Europe). MIKON is also privileged to host the leaders of other foreign research centres collaborating with Poland and the Polish origin, now working and living abroad. In 1994, thanks to the IEEE Microwave Theory and Techniques Society support MIKON received the status of an international conference (permanently marked in the world conferences calendar). Since then it has been organized every two years in May and it has been hosted by various Polish cities – biggest research and culture centres.

Last year MIKON moved to Gdańsk, with the record number of 177 papers accepted for presentation: 90 from Poland and 87 from 25 countries all around the world. A majority of foreign papers was submitted by the neighbouring countries, particularly the former Soviet Union – Ukraine, Russia, Belarus, and Lithuania. From Western Europe, the biggest contribution of papers came from the Netherlands. Hungary and the Czech Republic were also well represented. Out of the accepted papers, 98 were oral and 79 poster presentations. We also heard 17 invited speakers, some of the world's leading experts, who agreed to present their works. The MIKON-2002 program comprised 29 sessions in total – 24 oral and 5 poster ones, held in 3 parallel streams. The number of contributions from the area of radar technology has been constantly increasing, and that year 7 sessions were organized on the subject. Traditional MIKON topics such as antennas, CAD methods, measurement techniques and passive components were also very well covered. Although active devices, integrated circuits and optoelectronics attracted less interest in regular papers, they were well represented by invited speakers. The total number of attendees was 263: 172 from Poland and 91 from abroad and among them were many prominent members of the world microwave community, regularly participating in this event.

MIKON-2002 continued the **Young Scientists Contest** addressed to the young engineers and Ph.D. students. That year 41 foreign and Polish young authors presented their papers. Due to the high prestige of MIKON, the European Microwave Association was a co-sponsor of the event for the first time. The winners received diplomas of recognition and financial prizes: the first prizes *Piotr Kozakowski* from Technical University of Gdańsk and *Sean Hum* from University of Calgary, the second prizes Arkadiusz Lewandowski from Warsaw University of Technology and *Attila Zólomy* from Technical University of Budapest, the third prizes *Sandra Pralgauskaitė* from Semiconductor Physics Institute (Vilnius) and *Anton Abramov* from Saratov State University. I hope this volume will find the Reader's interest and will prove to be for practical usage.

Józef Modelski
Guest Editor

Paper

New approach to computer aided design of coupled resonator filters

Piotr Kozakowski and Michał Mrozowski

Abstract — A gradient based optimization technique along with a new definition of cost function is applied to synthesis of coupled resonators filters. The cost function is defined using location of zeros and poles of the filter's transfer function. The topology of the structure is enforced on each step of optimization and its physical dimensions are used as independent variables.

Keywords — CAD, microwave filters, optimization.

1. Introduction

Coupled resonator filters have found many applications in communication systems. Synthesis techniques of this class of filters have been known for long time [1, 2]. Unfortunately, some of those synthesis techniques do not always converge with [6] others, such as those based on equivalent circuits, and provide only approximation of filter parameters. This results, in many cases, in the necessity to apply certain optimization methods to meet electrical specifications.

Recently, a gradient based optimization method along with relatively simple definition of the cost function was used for synthesizing coupled resonators filters and excellent results have been reported in [6]. Unfortunately, this technique requires at least rough synthesis serving as a starting point for the optimization method to ensure good quality of the final solution.

This paper presents new approach to the coupled resonator filters synthesis which allows to find physical parameters of filter with a given topology without any prior synthesis. The method is partly similar to one described in [6]. It uses gradient based optimization technique along with modified cost function. The cost function is based on direct analysis of zeros and poles location of filter's transfer function. Physical dimensions of the structure are then used as variables in the optimization procedure. The superiority of the proposed approach is evident as a starting guess for a gradient optimization method can be chosen almost at random.

To illustrate application of the method three kind of filters were synthesized:

- an E-plane metal insert filter of the fourth order (Fig. 1),
- a filter based on inductive irises of the third order (Fig. 2),
- same filter as above, but with rounded corners (Fig. 3).

The first two filters were analyzed using the mode-matching technique (MM) and the third one by means of the Finite Difference-Time Domain (FD-TD) method. We have chosen a gradient technique based on the Sequential Quadratic Programming (SQP) method as optimization tool. This method is implemented in the Matlab Optimization Toolbox.

2. Cost function

The centerpiece of the new CAD procedure is a new definition of cost function which involves quantities uniquely describing the filtering character of electrical prototype. To derive this cost function let us recall that for the generalized Chebyshev approximation of the filter composed of series of N coupled resonators the transfer function $S_{21}(\omega)$ of the electrical prototype is given by

$$\left|S_{21}\right|^2 = \frac{1}{1+\varepsilon^2 F_N^2(\omega)}, \tag{1}$$

where ε is a constant related to the passband return loss and $F_N(\omega)$ is the filtering function given by

$$F_N(\omega) = \cosh\left(\sum_{n=1}^{N} \cosh^{-1}(x_n)\right), \tag{2}$$

where

$$x_n = \frac{\omega - 1/\omega_n}{1 - \omega/\omega_n}, \tag{3}$$

ω_n is the position of the nth transmission zero.

If all n transmission zeros are at infinity, the filtering function becomes a pure Chebyshev polynomial defined as

$$T_N(\omega) = \cosh\left(N \cosh^{-1}(x_n)\right). \tag{4}$$

$F_N(\omega)$ and $T_N(\omega)$ are rational functions. For instance $F_N(\omega)$ can be expressed as [7]

$$F_N(\omega) = 0.5\left[\frac{\prod_{n=1}^{N}(a_n + b_n) + \prod_{n=1}^{N}(a_n - b_n)}{\prod_{n=1}^{N}\left(1 - \frac{\omega}{\omega_n}\right)}\right], \tag{5}$$

where

$$a_n = \omega - 1/\omega_n, \quad b_n = \left[(\omega^2 - 1)\left(1 - 1/\omega_n^2\right)\right]^{1/2}. \tag{6}$$

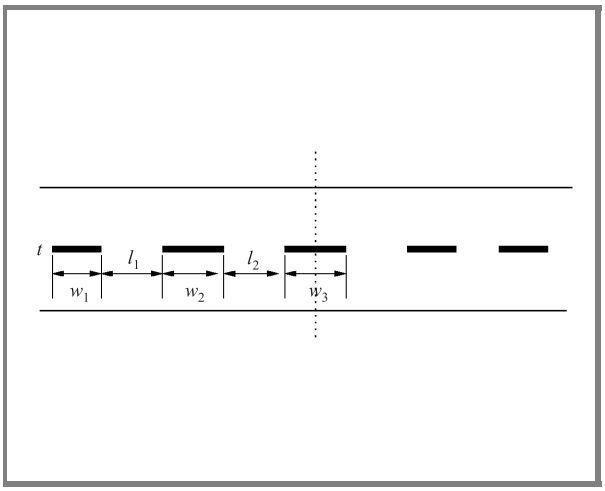

Fig. 1. E-plane metal insert filter (WR-75 waveguide, $t = 0.5$, $w_1 = 2.866$, $w_2 = 10.288$, $w_3 = 11.66$, $l_1 = 11.077$, $l_2 = 11.106$ – *all dimensions in mm*).

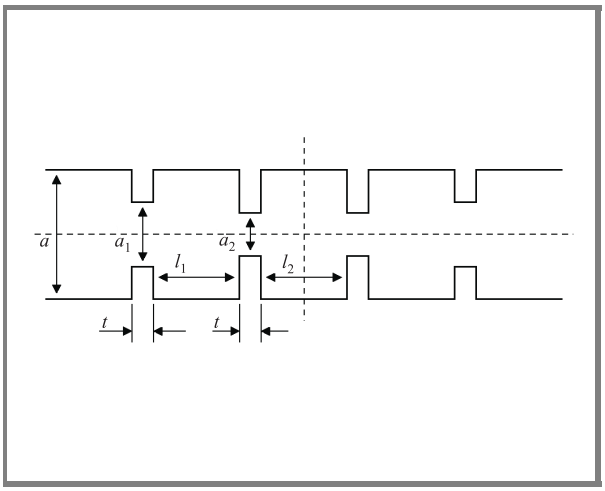

Fig. 2. Filter based on inductive irises in a rectangular waveguide (WR-75 waveguide, $a = 19.05$, $b = 9.525$, $t = 2$, $a_1 = 9.845$, $a_2 = 6.795$, $l_1 = 13.218$, $l_2 = 14.632$ – *all dimensions in mm*).

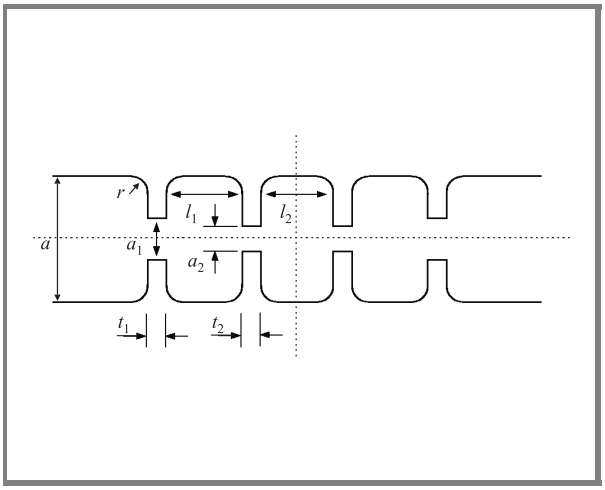

Fig. 3. Filter based on inductive irises in rectangular waveguide with rounded corners (WR-75 waveguide, $a = 19.05$, $b = 9.525$, $t_1 = 1.634$, $t_2 = 1.75$, $a_1 = 9.539$, $a_2 = 6.546$, $l_1 = 13.419$, $l_2 = 14.758$, $r = 1.5$ – *all dimensions in mm*).

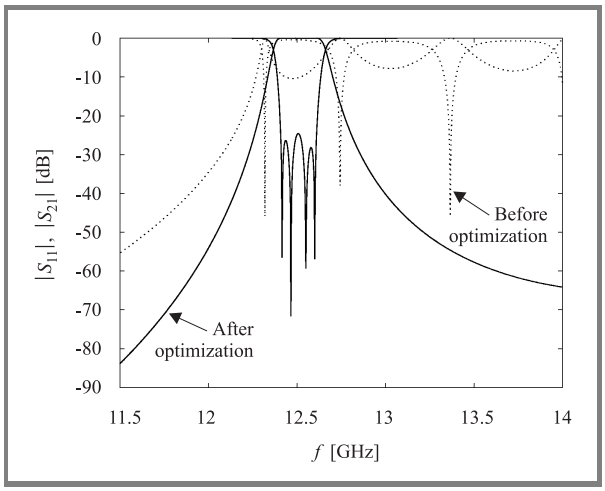

Fig. 4. Scattering parameters of E-plane metal insert filter.

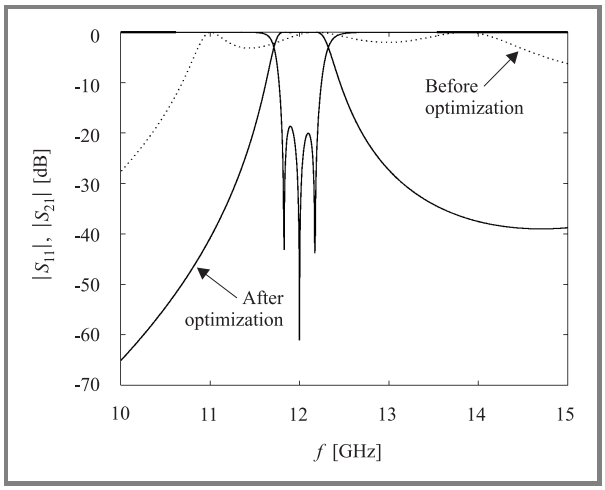

Fig. 5. Scattering parameters of filter based on inductive irises.

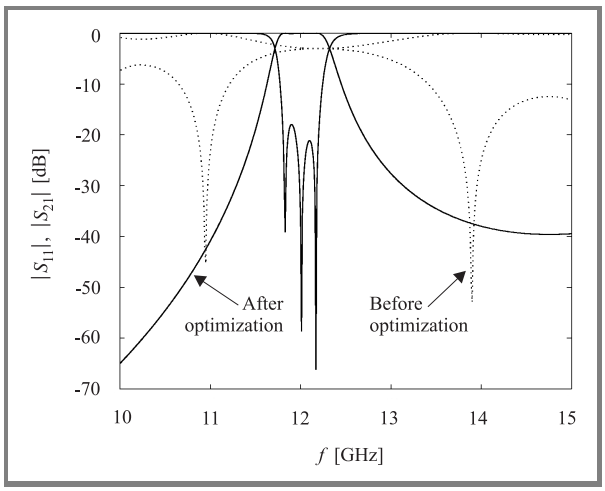

Fig. 6. Scattering parameters of inductive irises filter with rounded corners.

For the bandpass approximation the angular frequency ω is related to ω_0 and bandwidth

$$\Delta\omega \text{ by } \omega \to (\omega_0/\Delta\omega((\omega/\omega_0)-(\omega_0/\omega)).$$

Since F_N is a rational function so is S_{21} and up to the scaling factor they both are uniquely determined by the location of their poles and zeros. Calculating the poles (P_i) as roots of a denominator and zeros (Z_i) as roots of a numerator of the transfer function gives the cost function defined as follows:

$$C = \sum_{i=1}^{N} \left|Z'(i) - Z(i)\right|^2 + \sum_{i=1}^{N} \left|P'(i) - P(i)\right|^2, \qquad (7)$$

where (Z_i') and (P_i') are zeros and poles of a filter being optimized. The (Z_i') and (P_i') are calculated for every structure created by optimization procedure. For pure Chebyshev filters and other all-pole filters the cost function degenerates to the following form

$$C = \sum_{i=1}^{N} \left|P'(i) - P(i)\right|^2. \qquad (8)$$

To extract poles and zeros from the frequency response of the optimized filter the two procedures are possible depending on whether the time domain or the frequency domain software is used to calculate the electromagnetic response of the filter.

3. Pole extraction from time domain data for all-pole filters

Let us first deal with all-pole filters and the time domain techniques such as the Finite Difference-Time Domain method. Time domain techniques are in general ill-suited to repetitive analysis of filters required in optimization. This is because the simulation time for high-Q circuits can be too long. However, the analysis time can be substantially shortened and additionally for all-pole filters the poles required for forming the objective function can be extracted directly from time domain output transients without any need to compute frequency domain characteristics.

To this end we use the matrix pencil approach (MP) [4, 5]. In general, the MP technique builds a model of discrete time signal in the form of a superposition of $P/2$ damped sinusoids, where P is a model order. This can be written as

$$y(n\Delta t) \approx \sum_{i=1}^{P} A_i z_i^n, \qquad (9)$$

where $z_i = e^{p_i'\Delta t}$, Δt is the sampling time, n is the sample number, A_i is pole residue and p_i' is the location of pole in the complex plane. Hua and Sarkar [5] showed that poles of the model can be estimated by considering a matrix pencil

$$\underline{\underline{Y_1}} - \lambda \underline{\underline{Y_2}} \qquad (10)$$

with the following data matrices

$$\underline{\underline{Y_1}} = \begin{pmatrix} x(1) & x(2) & \cdots & x(L) \\ x(2) & x(3) & \cdots & x(L+1) \\ \vdots & \vdots & \ddots & \vdots \\ x(K-L) & x(K-L+1) & \cdots & x(K-1) \end{pmatrix} \qquad (11)$$

$$\underline{\underline{Y_2}} = \begin{pmatrix} x(0) & x(1) & \cdots & x(L-1) \\ x(1) & x(2) & \cdots & x(L) \\ \vdots & \vdots & \ddots & \vdots \\ x(K-L-1) & x(K-L) & \cdots & x(K-2) \end{pmatrix}, \qquad (12)$$

where K is the number of samples and L is the pencil parameter. The rank of matrix $\underline{\underline{Y_1}} - \lambda \underline{\underline{Y_2}}$ is P except when $\lambda = z_i = e^{p_i'\Delta T}$. Hence, the poles p_i' can be determined by finding the rank reducing values λ of matrix pencil. Technically, this is amounts to solving an ordinary eigenvalue problem

$$(\underline{\underline{Y_1}}^{\dagger} \underline{\underline{Y_2}} - \lambda \underline{\underline{I}})\underline{a} = 0, \qquad (13)$$

where $\underline{a}$ is the generalized eigenvector of (10) and $\underline{\underline{Y_1}}^{\dagger}$ is the Moore-Penrose pseudoinverse of $\underline{\underline{Y}}_1$, which can be found using the singular value decomposition.

Keeping in mind that the method is applied to filter design, selection of model order P is straightforward, namely the number of damped sinusoids should be twice as large as the number of filter cavities (poles appear in complex conjugate pairs) or, in other words it should be set to the number of poles in the filter prototype.

So the location of poles on the complex plane is determined for each trial filter by computing the eigenvalues of matrix $\underline{\underline{Y_1}}^{\dagger} \underline{\underline{Y_2}}$. These eigenvalues are used to evaluate the cost function later. Once the poles are known, one might proceed to find the amplitudes of each damped sinusoid. This would be required for obtaining the frequency domain characteristics. However, this step may be skipped in case of all-pole filter optimization as the amplitudes are not used in the definition of cost function.

Matrices $\underline{\underline{Y_1}}$ and $\underline{\underline{Y_2}}$ are assembled based on desampled FD-TD sequences of field recorded at the filter output. Selection of time segment to be used for extracting poles is based on the technique accounting for signal dynamics described in detail in [3]. In general, the recorded samples are divided into early and late time response. The first part is discarded. The other part, determining the late time behavior of output transients provides the samples for the MP method. The criterion for signal separation on early and late time responses is based on investigation of normalized average energy passing though output port of the filter.

Application of the MP technique for filter optimization, as proposed in this paper, requires an additional step whose incorporation guarantees correct extraction of poles. Before the data matrices $\underline{\underline{Y_1}}$ and $\underline{\underline{Y_2}}$ are assembled, the time-domain signal is passed through a cascade of digital filters.

The bandwidth of a single component of the cascade should be somehow greater than the bandwidth of filter being designed. In general, the cascade should consists of low-order Chebyshev or Butterworth filters whose poles shall not coincide with the poles of filter being the optimization target. This technique is called the Band-Pass Matrix Pencil (BPMP) method [5].

4. Extraction of zeros and poles from frequency domain characteristics

When the filtering function has zeros that affect the stop band behavior of a filter, the approach outlined above can not be used. Also, while theoretically possible, it does not make any practical sense to use BPMP operating on time domain data to optimize all-pole filter when the frequency characteristics are known (e.g. computed by the mode-matching method). For these cases we propose to use the Cauchy method [8]. The Cauchy method is an interpolation technique which assumes that the approximated function is expressed as ratio of two polynomials. Coefficients of these polynomials are found by applying the total least squares technique to solve a set of complex linear equations involving the values of function to be interpolated at few sampling points. To set up the equations one uses the filter's frequency characteristics obtained using the full wave method. The Cauchy method yields then the polynomials in numerator and denominator whose roots are zeros Z_i's and poles P_i's which are subsequently used to form the objective function. Note, that the order of the polynomials in numerator and denominator are known from filter specifications. This implies that provided the structure topology permits it, the Cauchy method combined with optimization procedure should find the filter dimensions which guarantee that transfer function of the optimal geometry reproduces as closely a possible, the distribution of zeros and poles of ideal electrical prototype. Obviously, the Cauchy method should be used also in conjunction with time domain analysis for filters whose transfer function contains zeros.

5. Results

The methods outlined above were verified by synthesizing the three previously mentioned filters. In all cases a starting guess for the optimization was chosen at random within the range of possible dimensions for a given topology. The first two filters were analyzed using mode matching techniques and the poles were found by means of Cauchy method. For the filter with the rounded corners, FD-TD QuickWave software was used and the poles extracted directly from transients with the MP technique described above. Regardless of the numerical tool used and the poles extraction technique applied the optimization converged to solution meeting electrical specifications (Figs. 4–6). The number of cost functions evaluations during the gradient based optimization (SQP method) ranged from 420 to 580 depending on number of independent variables. Finally, it has to be pointed out that while this paper presents only all-pole designs, pseudo-elliptic filters with finite transmission zeros have also been designed. The results are presented in [9].

6. Conclusions

Using a gradient based optimization technique along with a new definition of cost function it is now possible to design resonator filters based on given topology without any prior synthesis. Due to the judicious choice of goal function and robust post-processing techniques used to extract zeros on poles of the filter response, the new algorithm appears to converge globally from an arbitrarily selected starting dimensions.

References

[1] S. B. Cohn, "Direct-coupled resonator filters", *Proc. IRE*, vol. 45, pp. 187–196, 1957.

[2] R. Levy, "Theory of direct-coupled cavity filters", *IEEE Trans. Microw. Theory Techn.*, vol. 15, pp. 340–348, 1967.

[3] M. Mrozowski, "Criteria for building Prony models for time domain CAD", *IEEE AP-S Digest*, pp. 2306–2309, 1998.

[4] Y. Hua and T. K. Sarkar, "Generalized pencil-of-function method for extracting poles of an em system from its transient response", *IEEE Trans. Anten. Propagat.*, vol. AP-37, pp. 229–233, 1989.

[5] T. K. Sarkar and O. Pereira, "Using the matrix pencil method to estimate the parameters of a sum of complex exponentials", *IEEE Anten. Propagat. Magaz.*, vol. 37, pp. 48–55, 1995.

[6] S. Amari, "Synthesis of cross-coupled resonator filters using analytical gradient-based optimization technique", *IEEE Trans. Microw. Theory Techn.*, vol. 48, pp. 1559–1564, 2000.

[7] R. J. Cameron, "General coupling matrix synthesis methods for Chebyshev filtering functions", *IEEE Trans. Microw. Theory Techn.*, vol. 47, pp. 433–442, 1999.

[8] R. S. Adve, T. K. Sarkar, S. M. Rao, E. K. Miller, and D. R. Pflug, "Application of the Cauchy method for extrapolating/interpolating narrowband system responses", *IEEE Trans. Microw. Theory Techn.*, vol. 45, no. 5, pt. 2, pp. 837–845, 1997.

[9] P. Kozakowski and M. Mrozowski, "Automated CAD of coupled resonator filters", *IEEE Microw. Wirel. Compon. Lett.*, vol. 12, no. 12, pp. 470–472, 2002.

Piotr Kozakowski received the MSEE in microwave engineering from the Technical University of Gdańsk, Poland in 1997. His Master Thesis won a second prize at the Best M.Sc. Thesis Competition organized by Polish joint AES/AP/MTT Chapter in 1998. He is a co-author of four reviewed journal papers devoted to computer aided design of microwave filters and computational electromagnetics.

He is currently completing his work towards Ph.D. at the Technical University of Gdańsk.
e-mail: piotek@task.gda.pl
Department of Electronics, Telecommunications and Informatics
Technical University of Gdańsk
Narutowicza st 11/12
80-952 Gdańsk, Poland

Michał Mrozowski received his MSEE and Ph.D., D.Sc. degrees, all with honors, in microwave engineering from the Technical University of Gdańsk, Poland, in 1983, 1990 and 1994, respectively. He has been Professor at the Technical University of Gdańsk since 2001. His interests are with computational electromagnetics and filed theory. He published 47 reviewed journal papers and 2 monographs on computational electromagnetics and guided electromagnetic waves. He is a member of Electromagnetics Academy, MTT-1 Committee and served as a vice-chairman for MTT of the Polish joint AES/AP/MTT Chapter.
e-mail: mim@pg.gda.pl
Department of Electronics, Telecommunications and Informatics
Technical University of Gdańsk
Narutowicza st 11/12
80-952 Gdańsk, Poland

Paper

Modulator structures for radio-on-fiber applications

Sean V. Hum, Michał Okoniewski, and Robert J. Davies

Abstract — Traditional electro-optic modulators are not optimized for bandpass applications such as radio-on-fiber delivery systems due to their limited electro-optic response. This paper presents a resonant electrode structure that can be employed in optical modulator designs to enhance the electro-optic response of the modulator over a narrow frequency band, and improve the performance of optical radio systems. A simple model of the structure is developed, and experimental results validating the model and illustrating the effectiveness of the structure are presented.

Keywords — resonators, electro-optic modulators, microwave photonics, radio-on-fiber, optical modulation.

1. Introduction

Radio-on-fiber is an emerging and attractive architecture for optical distribution of radio signals in wireless delivery systems [1–3]. In traditional wireless delivery systems based on optical distribution networks, baseband signals are transported to base stations where they are upconverted to the operating radio frequency and transmitted to subscribers. In radio-on-fiber delivery systems, the actual radio signals are transported over the optical fiber network to the base stations on optical subcarriers, eliminating the need for costly RF conversion equipment at the remote sites and lowering overall system costs. A diagram of the downlink in a general radio-on-fiber system is shown in Fig. 1. Such systems have been proposed extensively for use in mobile communications systems and have most recently found applications in high capacity millimetre-wave transmission systems [4].

The electro-optic modulator at the transmitter, typically a Mach-Zehnder modulator (MZM), plays a crucial role in determining the performance of radio-on-fiber systems. The RF link gain between the input to the optical modulator and the output of the optical detector is largely determined by the depth of modulation that can be developed at the transmitter, which in turn depends on the V_π or switching voltage of the modulator. In fact, it can be easily shown that the link gain of the downlink is given by [5]

$$G = \frac{\mathscr{R}^2 G_o^2 P_{oin}^2 \pi^2 R_{MZM} R_{det}}{V_\pi^2}, \qquad (1)$$

where $\mathscr{R}$ is the responsivity of the photodetector in A/W, G_o is the gain of the optical link, P_{oin} is the optical source power, R_{MZM} is the termination resistance of the MZM electrode, and R_{det} is the termination resistance of the detector. Unfortunately, the RF link loss tends to be very large, on the order of 30 dB or greater, even if there is negligible optical loss in the fiber and the responsivity of the optical detector is very high (nearing the quantum limit). Therefore, efforts have focused on reducing the V_π of electro-optic modulators in order to address this problem.

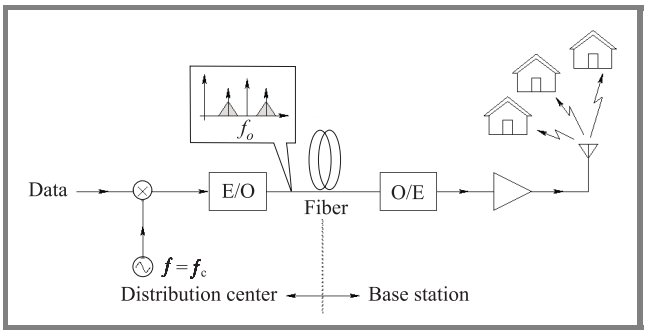

Fig. 1. The downlink of a general radio-on-fiber delivery system: E/O – electrical-to-optical conversion, O/E – optical-to-electrical conversion.

Traditional MZM designs have relatively high V_π values, due to the travelling-wave electrode structure used in each of the phase modulation arms of the MZM. One of these electrodes is shown schematically in Fig. 2a. The transmission line forming the electrode has a propagation constant $\gamma = \alpha + j\beta$ and characteristic impedance Z_0, and is terminated in matched load. This structure provides optical modulators with very high bandwidth capabilities to make them compatible with broadband digital systems such as OC-192, but develops relatively weak fields across the active region of the modulator, leading to a weak electro-optic effect and high V_π. Since broadband modulator performance is not a prerequisite for radio-on-fiber systems, it raises the possibility of optimizing the modulator for bandpass operation.

Resonant modulator electrode structures, first proposed for picosecond optical samplers [6], have emerged as a promising technique for reducing the switching voltage of electro-optic modulators. In these structures, the modulating electrode is transformed into a resonant cavity across which high electric field strength can be developed at the resonant frequency of the structure, lowering the V_π of the device. Hence, the bandwidth of the travelling-wave structure is sacrificed in order to yield a stronger electro-optic response. Resonant modulators have found application in op-

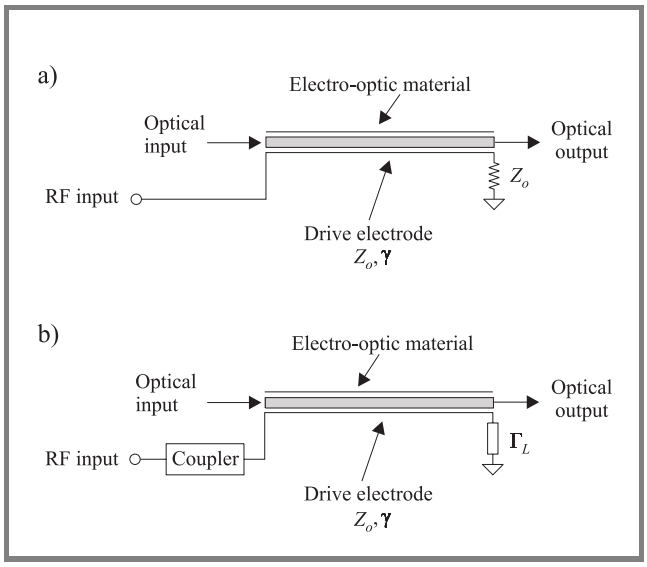

Fig. 2. Electrode structures for optical phase modulators in a MZM: (a) travelling-wave electrode structure; (b) resonant electrode structure.

tical phase modulators [7, 8], and have more recently been studied for use in analog and radio-on-fiber links [9–11]. This paper presents the design of several resonant electrode structures for optical modulators. A simple model for the structures is derived, and the model validated against experimental results. Experimental results also demonstrate the potential of resonant modulator designs in radio-on-fiber systems.

2. The resonant electrode structure

In a resonant electrode structure, shown in generalized form in Fig. 2b, the travelling-wave termination shown in Fig. 2a is removed and replaced with an electrical reflector with reflection coefficient Γ_L. A coupler is introduced at the input to the electrode, transforming the modulation arm into a resonant cavity whereby multiple reflections between the reflector and the coupler combine to produce a standing wave of increased amplitude relative to that achievable with the corresponding travelling-wave structure. This improves the electro-optic effect around the resonant frequency of the structure, lowering the V_π of the device.

The phase imparted to the optical wave depends on the field profile $E(z)$ seen by an optical wave as it travels through the modulator arm. If $\Delta\phi(t_0)$ denotes the phase imparted to an optical wave incident to the modulator arm at time t_0, the expression for $\Delta\phi(t_0)$ is given by [6]

$$\Delta\phi(t_0) = \int_{t_0}^{t_0+L/v_o} \frac{\pi r n^3 E[z = v_o(t-t_0), t] v_o dt}{\lambda_0}, \quad (2)$$

where L denotes the active region length, v_o is the optical phase velocity, n is the effective refractive index of the optical waveguide, r is Pockel's coefficient for the electro-optic material used, and λ_0 is the free space wavelength of the optical carrier. The field profile seen by the optical wave as a function of the position z along the modulator arm can be represented using a signal flow graph (SFG) with the electrode partitioned into two sections of length z and length $L-z$ and determining the amplitudes of the forward- and reverse-travelling waves within the cavity. The envelope $U(z)$ of the standing wave relative to the incident wave is then readily found as

$$U(z) = U_0\left(e^{-\gamma z} + \Gamma_L e^{-2\gamma L+\gamma z}\right), \quad (3)$$

where

$$U_0 = \frac{s_{21}}{1 - s_{22}e^{-2\gamma L}\Gamma_L} \quad (4)$$

and s_{ij} are the scattering parameters of the coupler. Generally, the reflector and coupler are chosen so that envelope of the field profile developed across the active region is symmetric with respect to the centre of the active region so that the expression (2) is maximized. For example, a mode which develops a field profile $|E(z)| \propto \sin(\beta z)$, $0 \le \beta z \le \pi$, is often employed. For simplicity, this mode will be considered in the analysis of the cavity. It is readily achieved using a short-circuited modulator electrode ($\Gamma_L = -1$) and a shunt-inductive coupler, as shown schematically in Fig. 3.

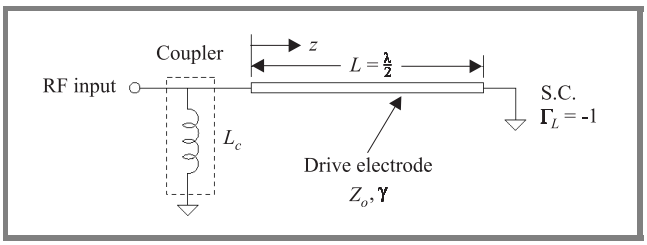

Fig. 3. Inductively-coupled half-wavelength resonator.

At resonance, the transmission coefficient of the coupling inductance is given by

$$|s_{21}| = \frac{2\omega_c L_c}{\sqrt{Z_0{}^2 + 4\omega_c^2 L_c^2}}, \quad (5)$$

where L_c denotes the coupling inductance and ω_c is the radian resonant frequency. For critical coupling into the cavity, which maximizes power transfer to the cavity and the corresponding electric field developed across the active region, the required coupling inductance can be found using a similar technique presented in [12] and is given by

$$L_c = \frac{Z_0}{\omega_c}\sqrt{\frac{\pi}{2Q_u}} \quad (6)$$

for a short-circuited $\lambda/2$ resonator. Q_u denotes the unloaded quality factor of the resonator. Substituting the

expression for the optimum coupling inductance given by Eq. (6) into Eq. (5) and simplifying yields

$$|s_{21}| = \sqrt{\frac{2\pi}{Q_u + 2\pi}}. \tag{7}$$

Next, consider the denominator of Eq. (4). At resonance, the denominator of this equation becomes an entirely real quantity because of the necessary condition for resonance that the loop gain $s_{22}e^{-2\gamma L}\Gamma_L$ be a real quantity. At resonance the loop gain is equal to $e^{-2\alpha_{eff}L}$, where α_{eff} is the apparent distributed attenuation factor of the cavity which accounts for any power lost from the reflector (if $|\Gamma_L| \neq 1$) and leakage back through the coupler. It is defined as

$$\alpha_{eff} = \alpha + \frac{1}{2L}\ln\left(\frac{1}{|\Gamma_L||s_{22}(\omega_c)|}\right). \tag{8}$$

Since the unloaded Q of the cavity Q_u is twice the loaded Q of the cavity $Q_l = \beta/2\alpha_{eff}$, and $2\beta L \approx 2\pi$ at resonance,

$$e^{-2\alpha_{eff}L} = e^{-2\beta L/Q_u} \approx e^{-2\pi/Q_u} \tag{9}$$

and the equation for U_0 can be written as

$$U_0 = \frac{\sqrt{2\pi/(Q_u + 2\pi)}}{1 - e^{-2\pi/Q_u}}. \tag{10}$$

The maximum field developed in the cavity is then given by

$$E_{max} = E_0 U_0 \left|e^{-\gamma z} + \Gamma_L e^{-2\gamma L + \gamma z}\right|, \tag{11}$$

where E_0 is the amplitude of the incident electric field. If $\alpha L \ll 1$, which is the case for any practical resonator, then the maximum value of $\left|e^{-\gamma z} + \Gamma_L e^{-2\gamma L + \gamma z}\right|$ is approximately 2. Hence, the peak field enhancement factor of the resonator is given by

$$F = \frac{E_{max}}{E_0} = \frac{2\sqrt{2\pi/(Q_u + 2\pi)}}{1 - e^{-2\pi/Q_u}}. \tag{12}$$

This equation relates the field enhancement factor offered by the resonator as a function of unloaded resonator Q. While it was derived for an inductively-coupled half-wave resonator, it can be shown this expression remains unchanged for other types of resonator configurations (for example, capacitively-coupled resonators or resonators employing higher order modes), provided that the critical coupling condition into the cavity is maintained.

If the shape of the standing-wave field envelope developed across the active region is known, then Eqs. (12) and (2) can be used to predict the overall phase imparted to the optical wave. For example, for the simple resonator case used in the development, $E(z) \approx FE_0 \sin(\beta z)$. However, in general passive sections of feedline may also form part of the resonant cavity, which causes a fraction of this field profile to be developed across the active region of the modulator. If the coupler and reflector are chosen to symmetrize the field profile developed across the active region, this feedline acts to flatten the electric field profile which improves the modulation response further at the expense of lowering the resonant frequency of the structure. While this feedline may be purposefully added to achieve this effect, generally it is desirable to minimize the cavity loss as much as possible. The analysis will consider the case of arbitrary feedline length.

To determine the optical modulation enhancement factor P over a travelling-wave modulator, the integration of Eq. (2) is carried out for a modulator arm with total electrode length L_t and active region length $L < L_t$, with the active region centred across the electrode. The resulting expression for P is

$$\begin{aligned} P &= \frac{\Delta\phi}{\Delta\phi_{TW}} \\ &= \frac{v_o F}{L}\left\{\frac{L_t}{\omega L_t - \pi v_o}\sin\left(\frac{\omega L}{2v_o} - \frac{\pi L}{2L_t}\right) + \right. \\ &\quad \left. + \frac{L_t}{\omega L_t + \pi v_o}\sin\left(\frac{\omega L}{2v_o} + \frac{\pi L}{2L_t}\right)\right\}, \end{aligned} \tag{13}$$

where $\Delta\phi_{TW}$ is the phase induced by a corresponding travelling-wave modulator with the same geometry. For more complicated resonator configurations, the exact modulation improvement can be determined by computing the exact standing-wave envelope using signal flow graph analysis of the structure, and using Eq. (2) to determine the phase imparted to the optical wave.

Converting a standard travelling-wave electrode design to a resonantly-enhanced electrode is an effective method for reducing the apparent V_π of the device over a narrow frequency range. It is important to realize that resonantly-enhanced modulators are not meant to replace other techniques for reducing the V_π of electro-optic modulators, but rather merged with these techniques to further lower V_π figures. The true value of a resonant-enhancement techniques lies in the fact that it can be integrated with almost any arbitrary electrode geometry, provided that the reduction in bandwidth is acceptable. Hence, recent advances in low-V_π travelling-wave modulators can be used in conjunction with a resonant electrode to achieve ultra-low V_π values.

3. Designs and results

Practically, resonantly-enhanced electrode structures can be realized in two ways. First, the coupler and reflector can be patterned directly with the modulator electrode to create a fully integrated resonant modulator electrode. The second approach is to use a packaged electro-optic modulator and attach the coupler and reflector externally, yielding a so-called externally-resonated design. Ultimately, the former method yields the best results since integrated designs achieve inherently L_t/L ratios close to unity, yielding devices with the highest resonant frequency and the lowest cavity losses. However, to validate the concepts presented

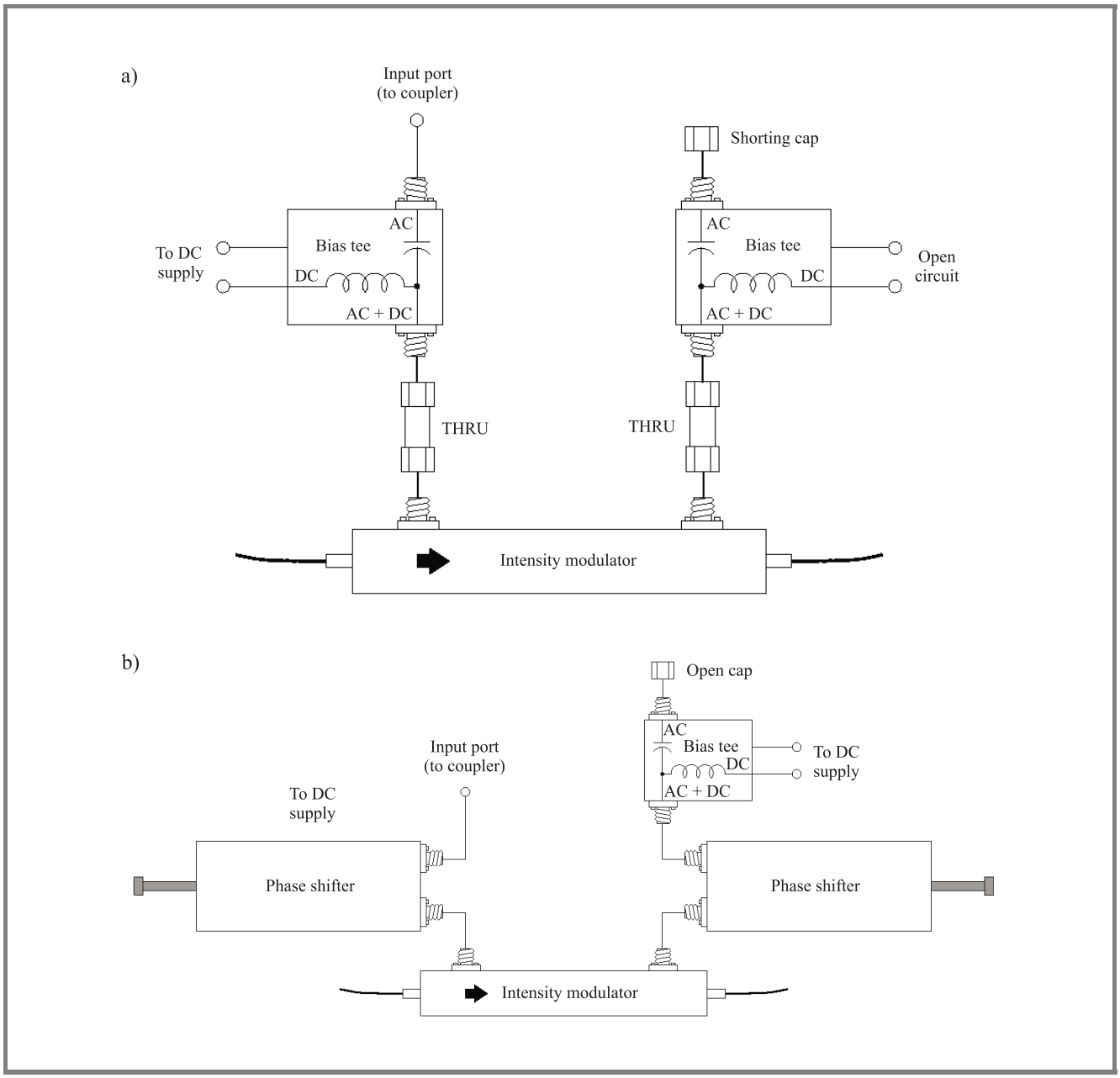

Fig. 4. Externally-resonated modulator designs: (a) basic design (I); (b) design with adjustable field confinement (III-IV).

in this paper, the latter approach was taken for ease of experimentation.

Several externally-resonated modulator structures were constructed using several off-the-shelf MZM's. Four designs were evaluated in all. The first design, shown in Fig. 4a, achieved minimal confinement of the half-wave field profile to the active region (i.e. a large L_t/L ratio) due to the large delay of the bias tees which increased the overall electrical cavity length. The second design (not shown) mitigated this problem to some extent through the use of an external DC bias electrode. Successive designs used higher-order resonant modes with the structure shown in Fig. 4 to achieve active region field profiles closer to the desired half-wavelength standing-wave shape. Phase shifters allowed both the resonant frequency of the device to be changed as well as the spatial position of the standing wave to be moved within the cavity. The ultimate goal of these designs was to emulate a fully-integrated resonant modulator with $L_t/L = 1$.

Resonator couplers were realized using CPW shunt stub circuits (for the inductively-coupled designs) and CPW series stub circuits (for the capacitively-coupled, higher-order mode resonator designs). All the couplers were designed to provide critical coupling into the cavity and to minimize the additional electrical length added to the cavity.

The resonant modulator designs were embedded in an experimental prototype of a radio-on-fiber delivery system and the RF link gain of the system characterized using

a standard network analyzer. Experimental results showing the link loss reduction and bandwidths achieved with the prototypes are summarized in Table 1. Theoretical reductions in link loss are shown in parentheses. Note that for the resonator configurations employing higher-order modes, the effective L_t/L ratio was computed using the known active region length L and $L_t = \lambda/2$ for the effective cavity length.

Table 1
Calculated and measured resonant modulator parameters

Parameter	I	II	III	IV
f_r [MHz]	462.5	780.0	1195.5	1499.2
L/L_t [%]	33	58	72	100
Link loss reduction [dB]	9.1 (8.6)	6.8 (7.1)	4.0 (4.4)	2.7 (2.1)
V_π reduction [%]	65	54	37	26
3 dB trans. bandwidth [%]	13.7	16.5	5.0 (30.1)	4.9 (38.8)
10 dB R.L. bandwidth [%]	4.2	5.5	1.7 (10.2)	1.6 (12.8)

All the modulators provided substantial gain over their travelling-wave counterparts, with link gain enhancement ranging from 2.7 dB for the highest frequency resonator to over 9 dB for the lowest frequency resonator. As expected, the link gain enhancement was reduced as the resonant frequency of the structures increased due to increasing cavity loss, and greater confinement of the half-wave profile to the active region (which reduces the L_t/L ratio, corresponding P/F ratio, and the modulation improvement). Nevertheless, significant reductions in V_π were achieved (26–65% depending on the resonator configuration), illustrating the effectiveness of the resonant enhancement technique.

The bandwidth offered by the resonator structures was excellent, around 15% for the first two designs. Designs employing higher-order mode resonators had correspondingly reduced bandwidths due to the narrowband nature of the resonators, but the bandwidth of an integrated modulator that achieves the same level of field confinement could be expected to be much greater (corresponding to the bandwidths in square parentheses in Table 1). The highest frequency tested was 1500 MHz, where the $n = 8$ resonant mode was employed to develop exactly half a wavelength across the active region across one of the arms in the packaged MZM.

The table also illustrates that the simple model used to predict the field enhancement of the structures was very accurate, with the maximum error in the predicted modulation enhancement less than 8%. Hence, the developed expressions can be used to approximate the performance of externally-resonated designs and should be equally applicable to integrated designs.

Graphs of the measured link gain improvement for all four designs are shown Fig. 5, plotted along a frequency-normalized abscissa. The curves for the higher-order resonant mode designs were also frequency scaled to illustrate potential operation for these devices if resonance had been achieved using the fundamental mode (corresponding to the situation in an integrated device) instead of a higher-order mode. The return loss for each of the structures is also plotted. The tradeoffs between the designs is immediately apparent, with low frequency designs offering the greatest gain due to lower cavity loss at those frequencies and maximum P/F values due to fairly large L_t/L ratios.

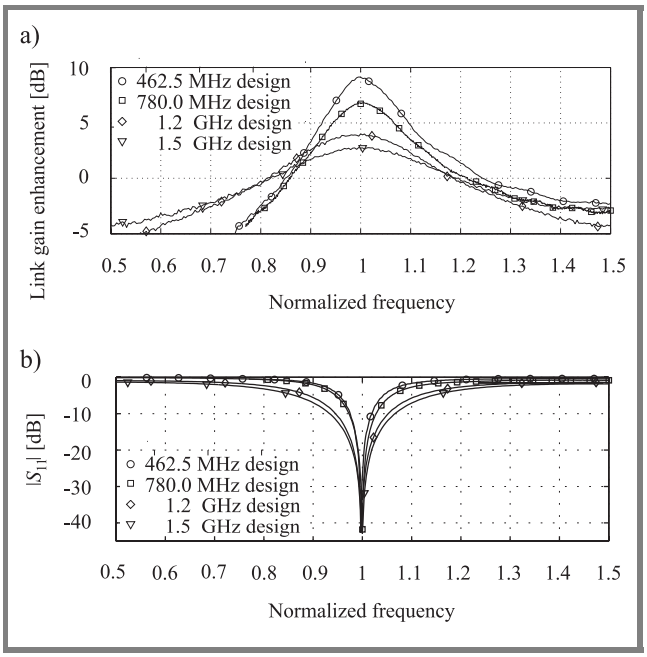

Fig. 5. Frequency-normalized link gain (a) and return loss (b).

As discussed earlier, signal flow graphs are useful for computing the exact field profile developed across the active region. This profile can then be used to accurately determine the improvement in modulation depth offered by an arbitrary resonator configuration. SFGs are also useful for characterizing the gain of a resonantly-enhanced modulator as a function of frequency. This study included an assessment of the accuracy of the SFG model used to derive expression (12). SFGs are well suited to analyzing the externally-resonated structures because the scattering parameters of the external components can be readily measured and integrated into the signal flow graph. Furthermore, it is anticipated that the SFG approach will be highly useful in developing more sophisticated resonator circuits, as well as analyzing integrated resonant modulator designs where more complicated circuit models of the electrode may be required.

Figure 6 illustrates the modulation improvement and input reflection coefficient predicted using the SFG model of two of the externally-resonated modulator structures. There is a clear correlation between measured and predicted results, and performing an SFG analysis of the structures actually resolved the small differences between the predictions of

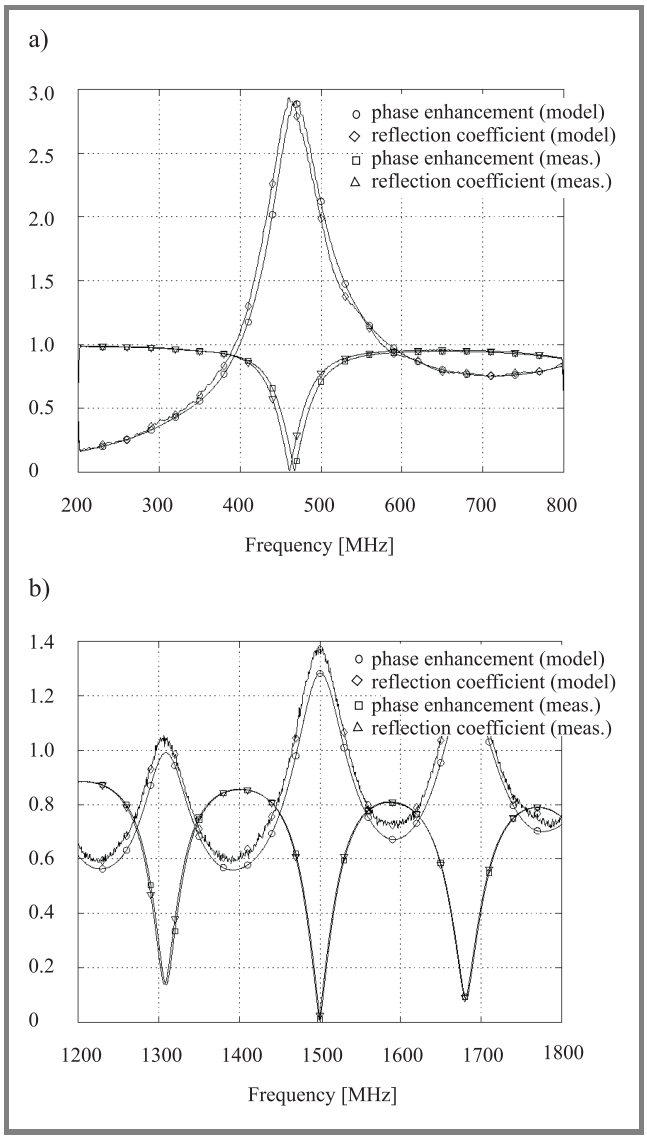

Fig. 6. Modeled and measured link parameters as a function of frequency for design I (a) and design IV (b).

Eq. (13) and the actual measured modulation improvement in Table 1. The slight differences in the predicted resonant frequency (most noticeable in the lowest frequency design) are attributed to extra delay introduced in the measurements when the resonator circuits were separated into components for *s*-parameter characterization. This error was much less pronounced for the higher frequency designs because the delay offset was a much smaller portion of the overall delay of the cavity. In either case, the delay can be easily characterized and removed.

4. Conclusions

Resonant electrode structures can significantly improve the response of travelling-wave electro-optic modulators over a narrow frequency range, reducing the link loss in radio-on-fiber systems. A simple model of a generic resonant electrode structure has been developed, and experimental results validate the model and show the potential of resonant electrode structures in improving the performance of radio-on-fiber systems.

It is anticipated that fully integrated resonant electrode designs will outperform the structures shown here since the cavity losses in such modulators would be much lower and the fundamental resonator mode could be utilized at high frequencies. Regardless, all the modulators provided bandwidths requisite of those required for radio-on-fiber systems.

Current work is focusing on designing a resonantly-enhanced modulator structure for millimetre-wave frequencies where the radio-on-fiber system prototype will be deployed. One of the major challenges with operating at these frequencies is that the active region of the modulator must be reduced substantially in order to support the fundamental resonator mode. Novel resonator structures are currently under development to relax this constraint.

Acknowledgements

The authors would like to thank the National Science and Engineering Research Council (NSERC) of Canada, the Alberta Informatics Circle of Research Excellence (iCORE), the University of Calgary, and TRLabs for their financial support of this project.

References

[1] A. J. Cooper, "Fibre/radio for the privison of cordless/mobile telephony services in access network," *Electron. Lett.*, vol. 26, no. 24, pp. 2054–1056, 1990.

[2] W. I. Way, "Optical fiber-based microcellular systems: an overview," *IEICE Trans. Commun.*, vol. E76-B, no. 9, pp. 1091–1102, 1993.

[3] M. Shibutani, T. Kanai, W. Domom, K. Emure, and J. Namiki, "Optical fiber feeder for microcelluar mobile communication systems," *IEEE J. Selec. Areas Commun.*, vol. 11, no. 7, pp. 1118–1126, 1993.

[4] L. Noel, D. Wake, D. G. Moodie, D. D. Marcenac, L. D. Westbrook, and D. Nesset, "Novel techniques for high-capacity 60-GHz fiber-radio transmission systems," *IEEE Trans. Microw. Theory Techn.*, vol. 45, no. 8, pp. 1416–1422, 1997.

[5] C. H. Cox III, G. E. Betts, and L. M. Johnson, "An analytic and experimental comparison of direct and external modulation in analog fiber-optic links," *IEEE Trans. Microw. Theory Techn.*, vol. 38, no. 5, pp. 501–509, 1990.

[6] L. A. Molter-Orr, H. A. Haus, and F. J. Leonberger, "20 GHz optical waveguide sampler," *IEEE J. Quant. Electron.*, vol. QE-19, no. 12, pp. 1877–1883, 1983.

[7] M. Izutsu, H. Murakami, and T. Sueta, "Standing-wave structure optical waveguide modulator using a resonant electrode at 10 GHz," in *Conf. Proc. OFC/IOOC '87*, 1987, p. TUQ32.

[8] M. Izutsu *et al.*, "Millimeter wave light modulator using $LiNbO_3$ waveguide with resonant electrode," in *Conf. Proc. CLEO*, 1988, pp. PD14–1.

[9] G. K. Gopalakrishnan and W. K. Burns, "Performance and modeling of resonantly enhanced $LiNbO_3$ modulators for low-loss analog fiber-optic links," *IEEE Trans. Microw. Theory Techn.*, vol. 42, no. 12, pp. 2650–2656, 1994.

[10] Y. S. Visagathilagar, A. Mitchell, and R. B. Waterhouse, "Resonantly enhanced Mach-Zehnder interferometer modulators," in *Conf. Proc. ACOFT/AOS'99*, 1999.

[11] Y. S. Visagathilagar, A. Mitchell, and R. B. Waterhouse, "Fabry-Perot type resonantly enhanced Mach-Zehnder modulator," in *MWP'99 Dig.*, 1999, pp. 17–20.

[12] D. M. Pozar, *Microwave Engineering*. 2nd ed. Wiley, 1998.

Sean Victor Hum was born in Calgary, Alberta, Canada in 1976. He received his bachelor's degree in 1999 and his master's degree in December 2001, both in electrical engineering from the University of Calgary. Since interning with TRLabs in 1997 he has been involved with various aspects of optical radio systems, with his master's research focusing on specialized devices for this application. Currently, he is pursuing his doctorate at the U of C in the area of reconfigurable antennas. His research interests lie in the area of reconfigurable RF systems and microwave photonics.

e-mail: svhum@cal.trlabs.ca
TRLabs
University of Calgary
(403) 210–3529 Street NW
Calgary, Alberta, T2L 2K7, Canada

Michał Okoniewski received his MSEE and Ph.D. (with distinction) degrees from the Technical University of Gdańsk, Gdańsk, Poland in 1984 and 1990, respectively. From 1984 to 1986 he was with the Institute of Fluid Flow Machinery, Polish Academy of Sciences, and since 1986 with the Technical University of Gdańsk as an Assistant Professor. From 1992 to 1994 he was with the University of Victoria, British Columbia, Canada, as an NSERC International Postdoctoral Fellow and later as a Reserach Fellow and an Adjunct Professor. Since 1998 he has been an Associate Professor at the University of Calgary and a scientist with TRLabs Calgary. In 2002 he was appointed a prestigious CRC Chair position in Applied Electromagnetics. Dr. Okoniewski's current research interests include applied and computational electromagnetics, antennas, passive componets, RF MEMS, microwave photonics, dielectric spectroscopy and confocal microwave microscopy for breast cancer detection. Dr. Okoniewski is a Senior Member of IEEE and an Associate Editor of IEEE Transactions of Antennas and Propagation.

e-mail: michal@enel.ucalgary.ca
Department of Electrical and Computer Engineering
University of Calgary
2500 University Drive NW
Calgary, Alberta, T2N 1N4, Canada

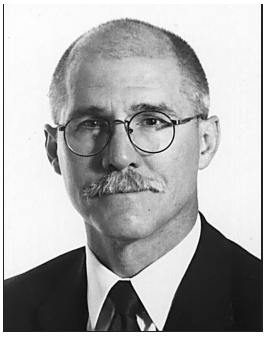

Robert J. Davies received his B.Sc. and M.Sc. degrees in electrical engineering from the University of Calgary, Canada, in 1987 and 1989, respectively. He received his Ph.D. in electrical and computer engineering from the University of Alberta, Canada in 1999. He was a researcher with TELUS Communications in Calgary from 1989 until 1997. He is currently a research scientist with TRLabs in Calgary and an Adjunct Professor at the University of Calgary. His research interests include radio systems, photonics and high speed signal processing. He has 2 patents granted, 4 others pending, and has authored or co-authored 30 papers.

e-mail: davies@cal.trlabs.ca
TRLabs
University of Calgary
280 3553–31 Street NW
Calgary, Alberta, T2L 2K7, Canada

Paper

A 24 GHz PHEMT-based oscillator

Arkadiusz Lewandowski, Günter Kompa, Wilfred Mwema, and Wojciech Wiatr

Abstract — We present a systematic nonlinear procedure for designing microwave oscillators utilising a nonlinear PHEMT model, the negative resistance approach and the describing function concept. The procedure is applied in the design of a 24 GHz oscillator, which is then realised in hybrid technology. Measurement results show −6% shift in the frequency but an acceptable agreement in the output power. A detailed analysis shows that the frequency shift arises mainly from inadequate CAD models in the *K* band, for the microstrip components employed in our design.

Keywords — microwave oscillator, oscillator design method, negative resistance, describing function, nonlinear PHEMT model, microstrip components models.

1. Introduction

The rapid growth of MMIC market calls for a continuous improvement in design techniques to facilitate a fast and inexpensive realisation of new circuits. While oscillators play a leading role in every radio communication system, their design at high operating frequencies is particularly difficult, mainly due to nonlinear properties of the active device. This implies that the nonlinear properties have to be not only correctly represented with an adequate transistor model [1], but also properly accounted for during circuit analysis and optimization. The complexity of these tasks is such that a simplified approach is often required to attain a reasonable solution effectively.

Various oscillator design approaches for microwave applications have been proposed. However there is still no clear optimal lane to follow. Simple design methods, based on small-signal scattering parameter description [2–4], allow estimating the oscillation frequency, but they fail in the prediction of the oscillator output power. Thus, experimental tuning is often needed. Moreover, thorough studies have recently shown that these methods may even lead to false judgments [5–7].

Superior results may be obtained using methods that combine small-signal analysis with some elements of nonlinear approach based on an analysis of the DC-characteristics of the active device [8]. However, the most accurate designs must involve large-signal design procedures that employ the harmonic balance method and optimization techniques implemented in majority of modern professional CAD programs [4, 9, 10]. Unfortunately, the use of these methods is not as easy as their simpler counterparts due to the problem of local minima arising during the optimization [10].

The aim of the work reported in this paper, was to develope a simplified, yet consistent nonlinear design procedure that improves the prediction of the output power and oscillation frequency in *K*-band GaAs FET-based oscillators. The procedure was developed on the basis of a wide review of various existing methods and applied in the design of a 24 GHz oscillator [7]. Measurement results for the oscillator realized will be presented and discussed.

2. Large-signal PHEMT model

For the design, a PHEMT chip transistor AFP02N3 from Alpha Industries was selected and a simplified large-signal model, based on the topology shown in Fig. 1, developed. In this model, the parasitic effects, related to the metalisation pattern, contact pads and bonding wires, are represented by capacitances C_{pgi}, C_{pdi}, C_{pga}, C_{pda} and inductances L_g, L_s, L_d. The only nonlinear elements are the controlled current source i_{DS} and the capacitance C_{gs}. The current source i_{DS} is described through formulae taken directly from the Chalmers FET model [11]. Unfortunately, this model describes both capacitances C_{gd} and C_{gs} using nonlinear formulae that do not meet simple physical rules [1]. To circumvent this problem, C_{gd} has been treated as linear and C_{gs} represented by a simplified relationship [12], valid in the i_{DS} saturation region.

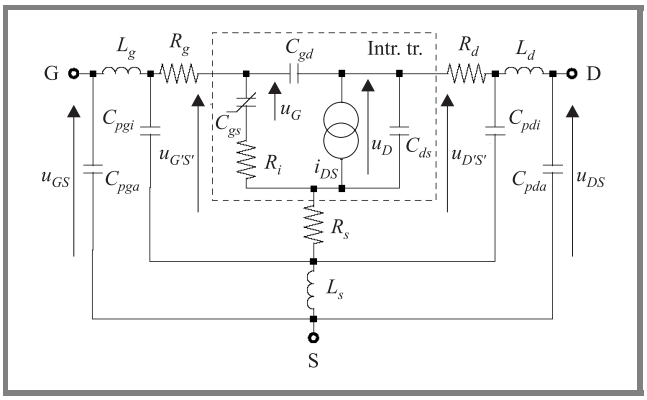

Fig. 1. Topology of large-signal PHEMT model.

The values of the equivalent circuit's elements were extracted from multi-bias small-signal S-parameter measurements of the transistor using the method presented in [13, 14]. The parameters of the function $C_{gs}(u_G)$ were then determined using a least-squares optimization. The results of the fit are shown in Fig. 2.

Using another least-squares optimization, the i_{DS} model parameters were extracted from the measured DC transistor characteristics. The fit obtained is shown in Fig. 3,

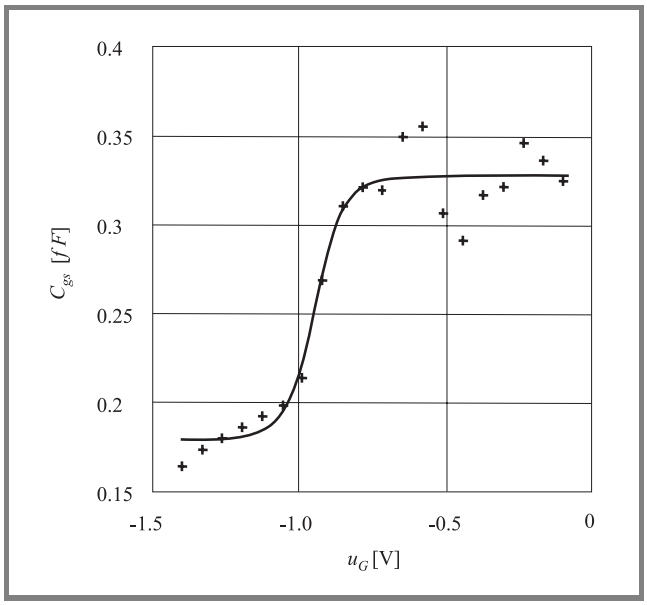

Fig. 2. Dependence of C_{gs} on u_G: measured (+) and fitted (-).

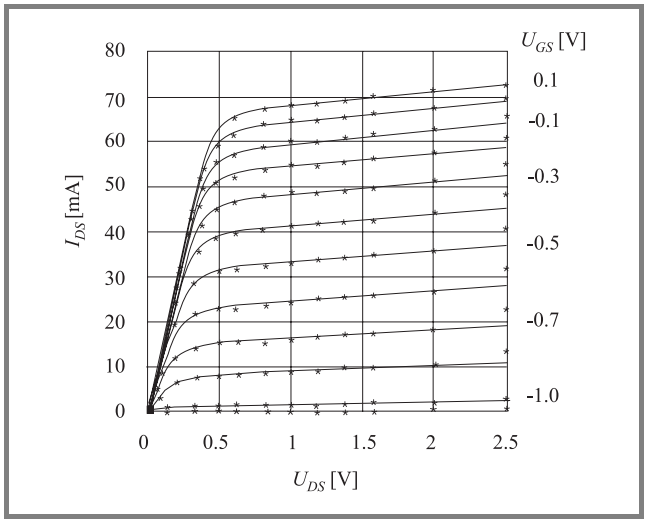

Fig. 3. PHEMT output characteristics: measured (x) and fitted (-).

which is in good agreement with the measurement for $U_{DS} < 2.0$ V. To avoid PHEMT operation in the ohmic region and soft-breakdown effects, not accounted for by the Chalmers model, the analyses were confined in the region bounded by $1.0\text{ V} < U_{DS} < 2.0\text{ V}$ and $-1\text{ V} < U_{GS} < 0.1\text{ V}$. Note that this model neglects the dispersion effects often noticed in microwave FETs [1]. This model was then employed in the oscillator design.

3. Oscillator design

A general oscillator configuration is shown in Fig. 4. The circuit can be split into an active and a load network along the dotted line as shown in this figure. The active network consists of the active device A with the feedback reactances jX_1 and jX_2. The load network is formed by a matching network MN, presumably lossless, terminated with $Z_0 = 50\ \Omega$. This circuit division corresponds with two relevant design steps.

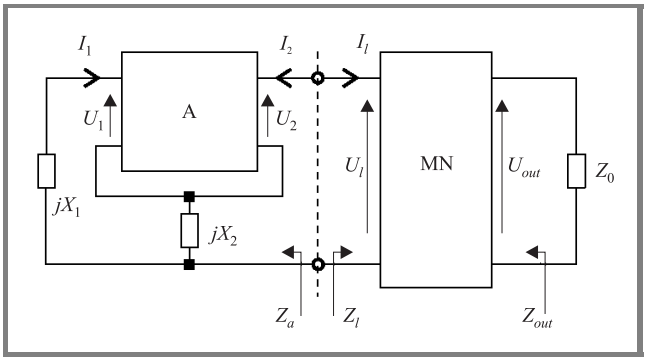

Fig. 4. General oscillator configuration.

3.1. Optimization of the active network

In this step, the optimal large-signal operating conditions and feedback reactances of the active network are sought for maximum power transfer and low harmonic content. To provide a good starting point for this optimization, we first evaluate the currents and voltages of the intrinsic transistor using the technique of Abe [8] based on the maximization of the power delivered by the active device, i.e. added power $P_{add} = -1/2\,\mathrm{Re}\,[U_1 I_1^* + U_2 I_2^*]$. To this end, the amplitudes U_g and U_d and their phase difference are adjusted keeping the intrinsic load cycle within the limits of the saturation region in the DC-characteristics specified earlier. These calculations utilise the small-signal transistor parameters and a linear analysis. Having determined U_1 and U_2, initial values for the reactances X_1 and X_2 are calculated using simple formula [8].

A large-signal optimization of the active device is then performed using the approach proposed by Andre *et. al.* [10]. An independent voltage source operating at a given frequency f_0 is attached to the network and the power dissipated in this source maximized through the harmonic balance method and a gradient optimization technique. Simultaneously, the harmonic content in the current is kept sufficiently low. In this way, the optimal voltage U_l^{opt} and current I_l^{opt} are determined and the reactances X_1 and X_2 are modified. Contrary to the technique in [10], no particular shape of the intrinsic load cycle is assumed during the optimization since this may lead to suboptimal results [7].

3.2. Design of the load network

This design aims at terminating the active network with the optimal impedance $Z_l^{opt} = U_l^{opt}/I_l^{opt}$ such that it operates at the steady-state voltage U_l^{opt} and current I_l^{opt} determined in the previous step. This goal is attained iteratively.

In the first step, the matching network MN, capable of transforming the standard matched load Z_0 into Z_l^{opt}, is defined. The oscillation start-up and build-up conditions and the equilibrium-state stability are then verified. The matching network and eventually the active one are continuously modified until all the conditions are met.

In verifying the fundamental oscillation start-up conditions at a frequency f_0', following general immitance terms are utilised:

$$\mathrm{Re}\,[W_{out}(f_0') + W_0] > 0; \quad \mathrm{Im}\,[W_{out}(f_0') + W_0] = 0, \qquad (1)$$

where W stands for immitance and indices *out* or 0 refer to the MN output or the matched load, respectively (see Fig. 4). Both the impedance and admittance forms of (1), corresponding with the relevant series or parallel resonant circuit representation, are considered. Only one of the two forms at a single frequency f_0', lying close enough to the required oscillator's frequency f_0, should be satisfied, to preclude any parasitic oscillation in the circuit.

The verification of the oscillations build-up conditions and the equilibrium-state stability is based on a describing function (DF) [15], which is the large-signal impedance Z_{out} for the fundamental Fourier component. The first verification lends itself to checking whether the inequality in (1) is satisfied for amplitudes $|U_{out}| < |U_{out}^{opt}|$, where U_{out}^{opt} corresponds with U_l^{opt}. As shown in Fig. 5, this inequality is satisfied for all intermediate states Q_0, Q_1 and Q_2 hence oscillations may build up from the initial state till the equilibrium state P. The oscillation frequency for each state is defined by Eq. (1) and marked on Fig. 5.

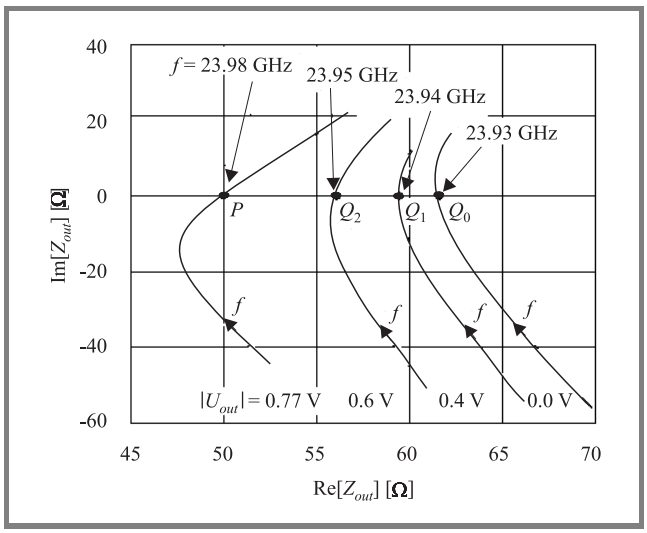

Fig. 5. Dependence of Z_{out} on frequency f for $|U_{out}| = \text{const}$.

In the steady-state, the stability of the oscillations, with regard to their frequency f and amplitude U_{out}, is examined. This involves checking a simple inequality, based on the DF, which is analogous to the well-known Kurokawa's stability condition [16].

4. Circuit realization

The oscillator was realised in hybrid technology using a 375 μm thick teflon laminate. The layout of the oscillator is shown in Fig. 6. The PHEMT chip is placed in the middle of the board marked and bonded using a 25 μm gold wire. The pair of identical shorted source stubs of a length greater than $\lambda/4$ constitutes a source capacitance, while the gate subcircuit acts as an inductance. The later comprises an open $\lambda/4$ stub, a main gate stub and a bias network. The drain subcircuit consists of a bias network, a matching network comprising a transmission line and an open stub, and a coupling capacitor to the output composed of two coupled $\lambda/4$ lines.

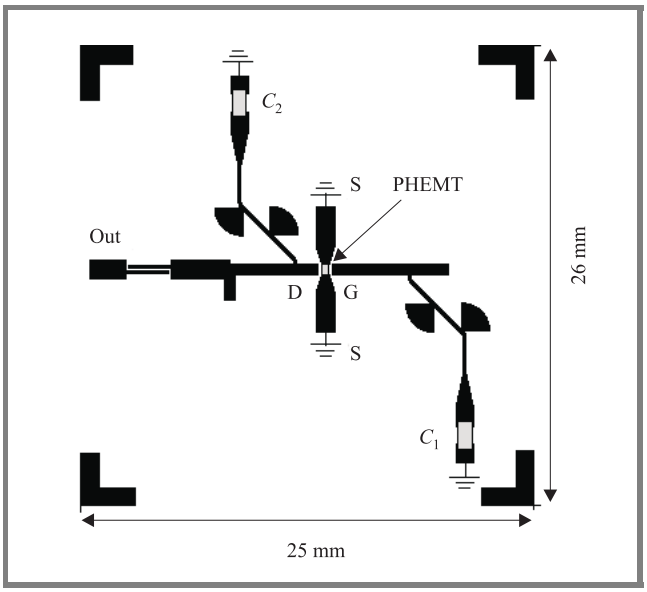

Fig. 6. The oscillator layout.

Two different PHEMT chips were successively bonded on the same PCB thus offering an opportunity to examine the effect of device variation. Both PHEMT chips exhibited a shift in their pinch-off voltage relative to the data sheet specification and their U_{GS} required individual correction, in order to obtain the design bias point $I_{DS} = 33$ mA and $U_{DS} = 1.6$ V. The output power was then measured and found to be in good agreement with the predicted value. However, the oscillation frequency was approximately 6% lower than the design frequency.

To study this problem more thoroughly, oscillator tuning characteristic versus U_{GS} was measured and depicted in Fig. 7 for both oscillator versions. The frequency shift may be attributed to the passive network, since only its slight dependence on U_{GS} can be noticed. Moreover, Fig. 7 reveals significant differences in the output power and efficiency traces obtained for each oscillator version. This may be caused partly by the nonrepeatability of the

bonding connections and partly by the variation in transistor characteristics across devices of the same type.

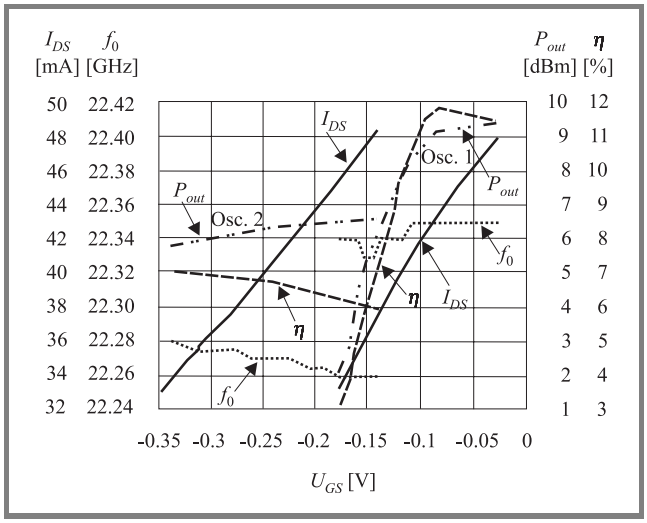

Fig. 7. Measurement results.

To check the above hypotheses, electromagnetic (EM) simulations of the layout and a sensitivity analysis of the oscillator circuit were performed. The EM simulations showed that the main contribution to the frequency shift comes from inadequacy of microstrip components models, we used for the designing, in the *K* band [17]. Moreover, a high sensitivity of the output resistance R_{out} and consequently the output power to the variation of the transconductance g_m and the source reactance was found. The analyses proved strong effects of the gate and source stub lengths, and bonding inductances on both the power and frequency.

5. Conclusions

A consistent nonlinear design procedure for microwave oscillators has been developed, utilising the Chalmers nonlinear HEMT model, the negative resistance approach and the describing function concept. The procedure has been applied in the design and realization of a 24 GHz PHEMT-based oscillator in hybrid technology. Measurements showed -6% shift in the frequency but an acceptable agreement in the predicted signal power. Further EM simulation of the oscillator layout explained this shift as mainly coming from inadequate CAD models of microstrip components used in the design. Sensitivity analysis performed on the circuit revealed the need for a more repeatable interconnect technology than wire bonding, e.g. flip-chip or quasi-monolitic [18] technology, for successful realization of such oscillators. This analysis emphasises the relevance of reliable CAD models of passive components for accurate nonlinear oscillator design, particularly at milimeter waves.

References

[1] I. Schmale, "Entwicklung eines konsistenten elektrothermischen Grosssignalmodells für Feldeffekttransistoren als Grundlage für den zuverlässigen Entwurf monolitischer Frequenzverdoppler". Ph.D. thesis, Univeristät Gesamthochschule Kassel, Kassel, 1999.

[2] E. Wasige, H. J. de la Torre, I. Ak-Layla, and G. Kompa, "An analytical design procedure for microwave oscillators based on S-parameters", in *Int. IEEE Worksh. Experim. Bas. FET Dev. Model. Relat. Nonlin. Circ. Des.*, Universität Gesamthochschule Kassel, Kassel, 1997, pp. 41.1–41.3.

[3] G. Gonzalez, *Microwave Transistor Amplifiers: Analysis and Design*. Englewood Cliffs, NJ: Prentice-Hall, 1997.

[4] R. Howald, "A 24 GHz HEMT microstrip oscillator using linear and nonlinear CAD techniques", *Microw. J.*, pp. 80–93, May 1994.

[5] S. Savaria and P. Champagne, "Linear simulators for use in oscillator design", *Microw. J.*, pp. 98–105, May 1995.

[6] M. Odyniec, "Oscillator stability analysis", *Microw. J.*, pp. 66–76, June 1999.

[7] A. Lewandowski, "Generator sygnału sinusoidalnego 24 GHz". Praca magisterska, Wydział Elektroniki i Technik Informacyjnych, Politechnika Warszawska, Warszawa, 2001 (M.Sc. thesis in Polish).

[8] H. Abe, "A GaAs MESFET oscillator quasi-linear design method", *IEEE Trans. Microw. Theory Techn.*, vol. MTT-34, pp. 19–25, 1986.

[9] A. V. Grebennikov, "Microwave transistor oscillators: an analytic approach to simplify computer-aided design", *Microw. J.*, pp. 292–300, May 1999.

[10] P. André, J. Dienot *et al.*, "Microwave oscillator design from load cycle optimisation – application to MMIC GaAs MESFET oscillator", in *Proc. 24th EuMC*, 1994, pp. 831–835.

[11] I. Angelov, H. Zirath, and N. Rorsman, "A new empirical model for HEMT and MESFET devices", *IEEE Trans. Microw. Theory Techn.*, vol. MTT-40, pp. 2258–2266, 1992.

[12] U. Schaper and A. Werthof, "Large-signal HEMT model for resitive mixer design", in *Int. IEEE Worksh. Experim. Bas. FET Dev. Model. Relat. Nonlin. Circ. Des.*, Universität Gesamthochschule Kassel, Kassel, 1997, pp. 26.1–26.5.

[13] F. Lin and G. Kompa, "FET model parameter extraction based on optimization with multiplane data-fitting and bidirectional search – a new concept", *IEEE Trans. Microw. Theory Techn.*, vol. MTT-42, pp. 1114–1120, 1994.

[14] W. Mwema and G. Kompa, "A new simplified and reliable HEMT modelling approach using pinched cold FET S-parameters", in *Proc. MTTS 2000*.

[15] A. Gelb and W. Vander Velde, *Multiple-Input Describing Functions and Nonlinear System Design*. New York: McGraw-Hill Book Company, 1968.

[16] K. Kurokawa, "Some basic characteristics of broadband negative resistance oscillator circuits", *Bell Syst. Tech. J.*, pp. 1937–1955, July-Aug. 1969.

[17] A. Lewandowski and W. Wiatr, "Verification of CAD models for microstrip components using FD-TD method", in *Proc. 14th Microw. Conf. MIKON-2002*, Gdańsk, Poland, May 2002, pp. 357–360.

[18] E. Wasige, G. Kompa, F. van Raay, W. Scholz, I. Rangelow, F. Shi, R. Kassing, R. Meyer, and M.-C. Amann, "A new technological concept for optimum circuit design at microwave and milimeter-wave frequencies", in *Int. IEEE Worksh. Experim. Bas. FET Dev. Model. Relat. Nonlin. Circ. Des.*, Universität Gesamthochschule Kassel, Kassel, 1997, pp. 23.1–23.5.

Arkadiusz Lewandowski received the M.Sc. degree in electronic engineering from Warsaw University of Technology, Poland, in 2001. Currently he is working towards Ph.D. degree at the Institute of Electronic Systems, Warsaw University of Technology. His main research interests include oscillator design and simulation methods, modelling of active microwave devices and microwave on-wafer measurements.
e-mail: A.Lewandowski@elka.pw.edu.pl
Institute of Electronic Systems
Warsaw University of Technology
Nowowiejska st 15/19
00-665 Warsaw, Poland

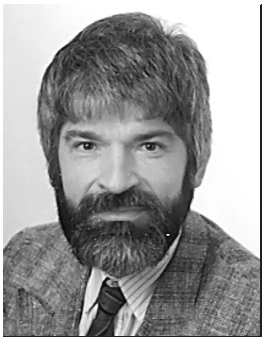

Günter Kompa was awarded the Dipl.-Ing. and the Dr.-Ing. degrees from the R.W.T.H., Aachen, Germany in 1970 and 1975, respectively. He joined Endress & Hauser, Germany in 1976 focusing on microwave and laser radar research and development. He won the 1978 Heinrich-Hertz Award from Institute of Radio and Electronic Engineers, London. Since 1984, he has been a Professor heading the Department of Microwave Technology at the University of Kassel, Germany. He is referee for the German Ministry of Research and Technology (BMBF) and the German Academic Exchange Service (DAAD) since 1990 and 1997, respectively. He established the masters course "Electrical Communication Engineering" at the University of Kassel, which is one of the first and only eight international postgraduate degree courses in Germany. His current research interests cover mainly circuit and system design of UWB microwave and laser radar, characterization and modelling of high power amplifiers both at device and system levels, and amplifier linearization algorithms. He has published over 150 technical papers and filed numerous patents.
e-mail: kompa@hfm.e-technik.uni-kassel.de
Fachgebiet Hochfrequenztechnik
University of Kassel
Wilhelmshöher Allee 73
D-34121 Kassel, Germany

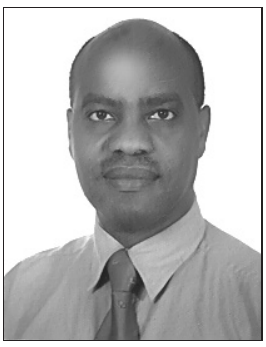

Wilfred Mwema obtained the B.T. degree in electrical and communication technology from Moi University and M.Sc. in electrical engineering from the University of Nairobi, Kenya, respectively. Since October 1997, has been pursuing Ph.D. degree in electrical engineering at the University of Kassel, Germany, where he has been working on microwave characterisation and modelling of GaAs-based field-effect transistors and just successfully completed his studies. His interests include microwave oscillator design, among other topics.
e-mail: mwema@hfm.e-technik.uni-kassel.de
Fachgebiet Hochfrequenztechnik
University of Kassel
Wilhelmshöher Allee 73
D-34121 Kassel, Germany

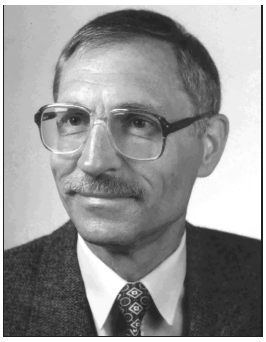

Wojciech Wiatr received the M.Sc., and Ph.D. degrees in electronic engineering from Warsaw University of Technology, Warsaw, Poland in 1970 and 1980, respectively. For 30 years he has been with the Institute of Electronic Systems at the Warsaw University of Technology. His main scientific interests are in the field of precision microwave measurements. He has been developing new techniques and instrumentation for broadband scattering and noise parameter measurements of microwave transistors and MMICs. He invented the RF multi-state total power radiometer for simultaneous noise and vector analysis of microwave networks using natural noise excitation. Dr. Wojciech Wiatr published 1 book, over 80 papers and holds two patents.
e-mail: Wiatr@ise.pw.edu.pl
Institute of Electronic Systems
Warsaw University of Technology
Nowowiejska st 15/19
00-665 Warsaw, Poland

Paper

Synthesis method for distributed amplifiers

Attila Zólomy

Abstract — New design method is presented for distributed amplifiers (DA). It is shown that by proper design of the applied transmission lines (TL) between the active devices the image impedance and the cut-off frequency (*COF*) of the input or output line of the DA can be independently tuned. As a consequence, the phase mismatch between the lines of the DA can be adjusted independently from the termination conditions and from the capacitances of the applied transistor and thus flat gain characteristic can be achieved. The method is well applicable for nearly unilateral devices like HBTs [1] and yields the highest gain-bandwidth product.

Keywords — distributed amplifier, gain-bandwidth products, phase synchronization, optical receivers.

1. Introduction

Distributed amplifiers have the widest bandwidth among the known gaining circuits. They are usually designed by computer optimization. However, in the presence of parasitics the error function has many local minima and thus it is difficult to find a global minimum. A better approach if the optimization is started from a simplified but almost perfect structure, which was generated by a systematic design procedure. However, huge amount of publications in the field [2] describes only analyses methods and just a very few gives direct synthesis methods.

An effective one was published by Beyer [3] for monolithic DAs comprised unilateral transistors. The method is valid if phase synchronization exists between the DA lines and if the applied TLs are short enough to be approximated by simple lumped Π network. Beside that, it manipulates the transistor losses to compensate the effect of the pole at the *COF*. However, as the input capacitance of the active device is usually much higher than the output one the phase synchronization can be difficult to achieve in a lumped element DA that works between fixed termination impedances. Other problem is that due to the required loss values, the other properties of the transistors (noise etc.) may be not optimal.

The method proposed by this paper tunes only the TLs between the active devices, thus the transistor's performance can be optimal. The design method is based on some important theoretical results, which were published in [4, 5]. They will be summarized as follows.

Considering the DA structure in Fig. 1 the closed formulas for the power-gain of a DA comprised TLs and unilateral active devices were derived. It was shown that the gain-bandwidth product (*GBP*) of the DA is proportional to the impedance-bandwidth product (*IBP*) of its input and output line. The *IBP* of a DA line is determined by the DA line impedance and by the *COF*.

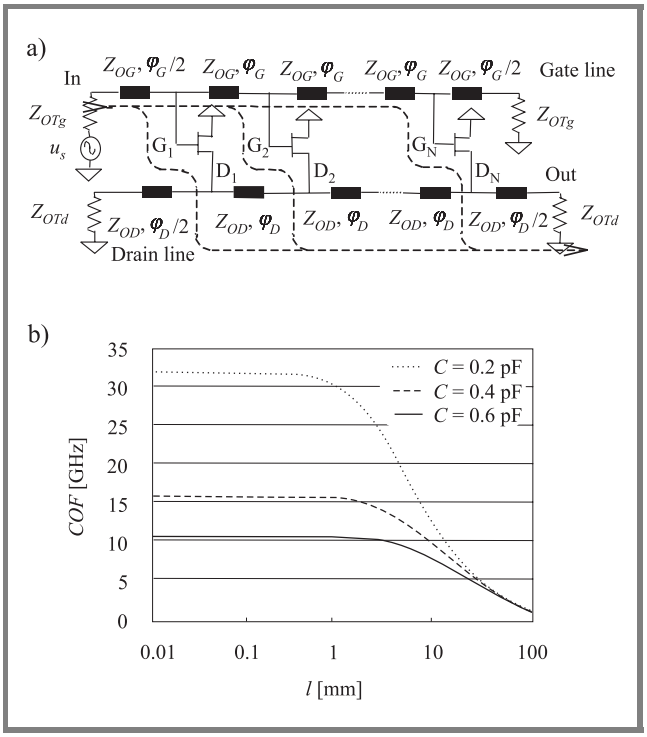

Fig. 1. (a) Model of an *N*-stage distributed element DA; (b) *COF* vs. TL's physical length *l* at different *C* values ($k = 50\ \Omega$, $v = c$).

In the case of a transistor which comprises only the input and output capacitances (C) and the transconductance the Z_{0T} and $Z_{0\Pi}$ image impedances of a line of the DA can be written as follows ($Y = j\omega C$):

$$Z_{0T} = Z_0\sqrt{\frac{2j\sin\varphi + Z_0 Y(\cos\varphi - 1)}{2j\sin\varphi + Z_0 Y(\cos\varphi + 1)}}, \quad Z_{0\Pi} = \frac{2Z_{0T}}{2 + jYZ_0\tan\frac{\varphi}{2}}. \tag{1}$$

The *COF* can be determined from the propagation factor per section, which is takes the form:

$$\theta = \operatorname{arcosh}\left(\cos\varphi + j\frac{YZ_0}{2}\sin\varphi\right); \quad \varphi = \omega\frac{l}{v}. \tag{2}$$

In the passband θ must be pure imaginary, i.e. the magnitude of the argument of the arcosh must be less than one. The *COF* can be calculated from this condition. However, it results a transcendental equation, which cannot be solved

in closed form, thus only approximate value for the *COF* (due to the TL, infinite number of upper passbands exists, but in this paper only the first one is applied) can be calculated. Conclusions are as follows:

- The *IBP* decreases as the capacitance increases.
- At a given capacitance and given TL characteristic impedance (Z_0) value, the image impedances are decreasing and the *COF* is increasing as the TL physical lengths (l) became shorter.

To maintain the image impedances on a k constant level the proper increase of the Z_0 value is necessary during the shortening of the TL lengths. The necessary Z_0 value can be computed from the DC limit of the image impedances:

$$Z_0(k, l, C) = \frac{1}{2l}\left(k^2 Cv + \sqrt{k^4 C^2 v^2 + 4l^2 k^2}\right). \qquad (3)$$

Substituting Eq. (3) into Eq. (2) and applying the condition mentioned there the *COF* can be calculated in the case of constant (k) low frequency image impedance (*LFI*) value at different TL lengths. The approximated *COF* are plotted in Fig. 1b as a function of the TL's physical length at different capacitance values. It can be seen, that the *COF* monotonically increases as the physical length of the TLs tends to zero. Because the image impedances are not changing we can conclude that the *IBP* is maximum at zero TL length. Simultaneously the characteristic impedance of the TLs must tend to infinity to satisfy Eq. (3). According to this it can be concluded that a DA line with lumped inductances has the highest *IBP*, i.e. a lumped element DA has the highest *GBP* with a given transistor and termination conditions.

The same behaviour was achieved in the presence of the series parasitic connection inductances (denoted by L_B) of the active device. It was also found that these inductances cause significant bandwidth degradation. In this case the formulas of image impedances and propagation factor remain valid if Y is replaced by Y^B ($Y^B = j\omega C/(1-\omega^2 C L_B)$). The required Z_0 value to get a constant line impedance can also be computed by Eq. (3). For this case the *COF* of a DA line vs. TL's physical length is plotted in Fig. 2a at different L_B values ($C = 0.4$ pF).

A third type of transistor connection is also proposed: the so-called V-shape connection which yields higher *COF* than the normal connection. The structure can be observed on the input line of he DA presented in Fig. 4a. The image impedances can be found in [5]. The propagation factor is given by Eq. (4). The necessary Z_0 value to maintain a constant (k) LFI can be computed by Eq. (5). The *COF* of a V-shape DA line vs. l is plotted in Fig. 2b ($L_B = 0.3$ nH).

An important conclusion of the above results is that in a DA applying TLs the *COF* as well as the θ of the DA lines can be varied independently from the line impedance value (usually it must be matched to the termination). Due to the variability of the phase mismatch between the gate and drain lines, this property gives an additional degree

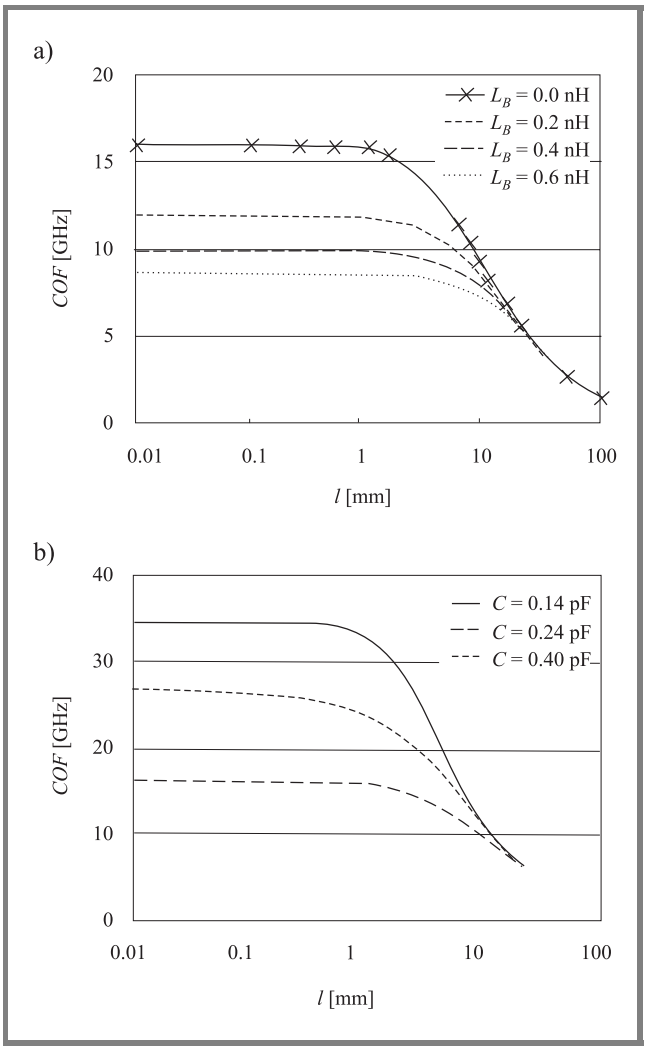

Fig. 2. (a) *COF* vs. l at different L_B values ($k = 50\ \Omega$, $v = c$); (b) *COF* vs. l at different C values ($k = 50\ \Omega$, $v = c$).

of freedom in the design. In contradiction, in a lumped element DA the θ yields from the capacitance and the image impedance value, hence cannot be varied [2]. In this paper the necessary phase mismatch between the DA lines are calculated to achieve a desired gain flatness. Next, a new hybrid structure is introduced for DAs using typical transistors. Finally, the design process is demonstrated on a design example, which gives the highest *GBP* with flat gain

$$\theta = \operatorname{arcosh}\left(\cos\theta(1 + YZ_B) + \right.$$
$$\left. + j\sin\theta\left(\left(2Z_B + Y\left(Z_0^2 + Z_B^2\right)\right)/2Z_0\right)\right); \qquad (4)$$
$$Z_B = j\omega L_B; \quad Y = j\omega C$$

$$Z_0(k, l, C, L_B) = \tfrac{1}{2l}\left(k^2 Cv - 2L_B v + \right.$$
$$\left. + \sqrt{k^4 C^2 v^2 + 4l^2 k^2 + 4L_B^2 v^2 - 4L_B v^2 k^2 C}\right). \qquad (5)$$

2. Effect of phase mismatch

The *GBP* is the highest if the physical lengths are minimal. Hence, during the design the TLs must keep as short as possible. Due to this reason, the effect of phase mismatch is analyzed only for lumped element DA. The phase mismatch can be described by the ratio of the drain and gate cut-off frequencies: $q = \omega_{CD}/\omega_{CG}$. The relative deviation of the power gain from its DC value as a function of the frequency is given by Eq. (6) for a DA comprised simplified transistors (only C_{GS}, C_{DS} and gm presents) the following equation:

$$\Delta P(\omega_{rel}) = \frac{1}{N^2} \frac{1}{\left(\sqrt{1-\omega_{rel}^2 \frac{1}{q^2}}\right)^* \sqrt{1-\omega_{rel}^2}} \left| \frac{\sin\left(\frac{N}{2}\Delta\theta\right)}{\sin\left(\frac{\Delta\theta}{2}\right)} \right|^2 . \tag{6}$$

In a real transistor the C_{GS} is bigger than C_{DS}, thus in Eq. (6) the frequency is related to the gate cut-off frequency, i.e. $\omega_{rel} = \omega/\omega_{CG}$.
As one can observe, at a given relative frequency the deviation depends on N (stage number) and q. By expanding the sin in Taylor series and neglecting the higher order parts an approximate analytical equation can be derived both of them. The N is given by Eq. (7) where ($\Delta\theta = \theta_D - \theta_G$)

$$N(\omega_{rel}, q, \Delta P) = \sqrt{\frac{40 - \sqrt{-320 + \left(1920 - 80\Delta\theta^2 + \Delta\theta^4\right)\left(1-\omega_{rel}^2\right)^{\frac{1}{4}}\left(1-\frac{\omega_{rel}^2}{q^2}\right)^{\frac{1}{4}}\sqrt{\Delta P}}}{\Delta\theta^2}} . \tag{7}$$

Similar equation can be derived for the presence of connection inductances:

$$N(\omega_{rel}, q, \Delta P) = \sqrt{\frac{40 - \sqrt{-320 + \left(1920 - 80\Delta\theta^2 + \Delta\theta^4\right)\left(1-\omega_{rel}^2\right)^{\frac{3}{4}}\left(1-\frac{\omega_{rel}^2}{q^2}\right)^{\frac{3}{4}}\frac{\sqrt{\Delta P}}{q}}}{\Delta\theta^2}} . \tag{8}$$

Due to the bigger gate capacitance, in real amplifiers the bandwidth of the drain line needs a significant reduction. According to this a DA with normal connection at the drain and V-shape connection at the gate may have practical importance. For this hybrid structure the N is described as follows

$$N(\omega_{rel}, q, \Delta P) = \sqrt{\frac{40 - \sqrt{-320 + \left(1920 - 80\Delta\theta^2 + \Delta\theta^4\right)\left(1-\omega_{rel}^2\right)^{\frac{1}{4}}\left(1-\frac{\omega_{rel}^2}{q^2}\right)^{\frac{3}{4}}\frac{\sqrt{\Delta P}}{q}}}{\Delta\theta^2}} \tag{9}$$

and is shown in Fig. 3a for $q = 1.55$. In the figure one can observe that at this q value a four stage DA has a flat gain response. If higher stage number is required, the value of the q should decrease. For lower stage numbers q must be increased.
If the flat response is required only up to 0.57 ω_{rel}, a six stage DA can produce a gain variation of less than 1 dB in the passband. It can be shown that up to 0.57 ω_{rel} the input and output matching of a DA is better than -20 dB,

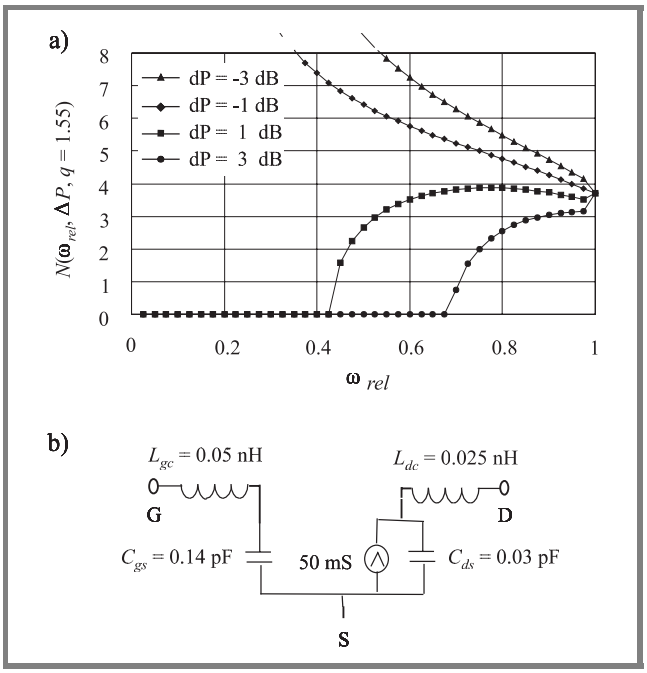

Fig. 3. (a) Number of stages to achieve a given gain deviation vs. relative frequency; (b) transistor model.

if the lines of the DA are ideal artificial transmission lines with *LFI* equal to the termination.

3. Design example

The method is demonstrated on a design example. The applied unilateral transistor model is shown in Fig. 3b. The inductances are the on-chip inductances. We assume that due to technological reasons the lowest value of the connection inductances (f.e. bonding inductance) is $L_B = 0.3$ nH. Due to the big difference between the transistor capacitances the application of the hybrid structure is practical. The gate is V-shape connected. If the only elements between the transistors are the two connection inductance ($2L_B$), the low frequency impedance (*LFI*) of the resulting gate artificial line is $LFI_G = (2L_B/C)^{0.5} = 65\ \Omega$ [4]. The cut-off frequency can be calculated by Eq. (10), due to the significant effect of the on-chip inductance on the bandwidth [4]

$$f_{cG} = \frac{1}{2\pi\sqrt{C_{gs}(L_{gc} + 2L_B/4)}} = 30.08\ \text{GHz}. \tag{10}$$

To achieve a matching better than -20 dB to 50 Ω, a *LFI* lower than 60 Ω is required. The gate line ends in a T-section, thus its characteristic impedance is monotonically decreased with frequency. Due to this property, a *LFI* level higher than the termination impedance results good matching in wider band. With 60 Ω *LFI* the matching is better than -20 dB up to 0.74 ω_{rel}. But to achieve 60 Ω *LFI* value, inserting of TLs is necessary. If we assume again that due to technological reasons at least $l = 0.5$ mm is needed, the resulting Z_0 is 38 Ω (from Eq. (5)). The degra-

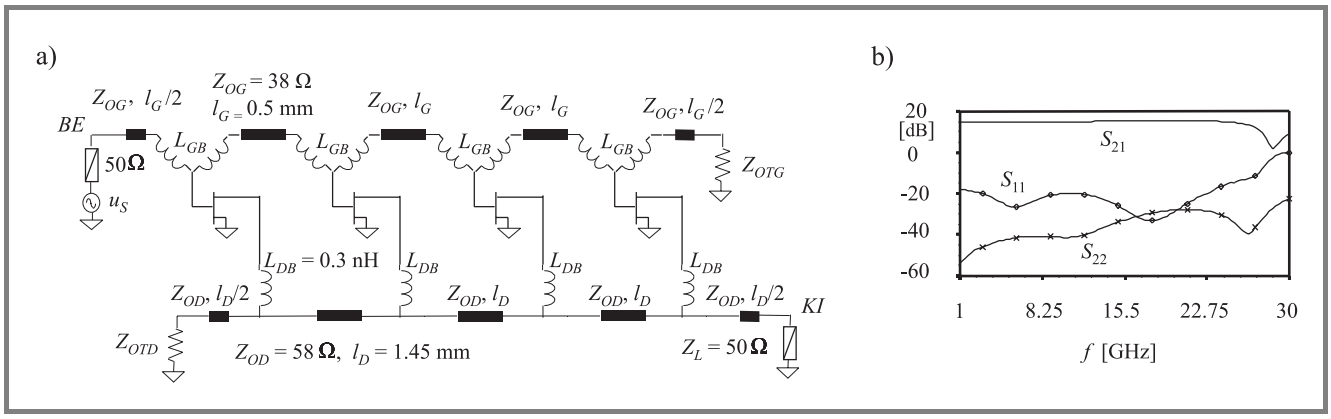

Fig. 4. (a) Hybrid DA structure with element values; (b) simulated results before optimization.

dation of the cut-off frequency is approx. 0.708 GHz (see Fig. 2b). Thus, up to $(30.08-0.708)*0.74=21.7$ GHz the matching of the gate line will be better than -20 dB.

In the drain line the transistors are connected by normal way, i.e the connection inductances are in series. If the line is designed for 50 Ω *LFI* the resulting interstage inductance value is $L_D = 0.075$ nH and the lumped element cut-off frequency is described as:

$$f_{cD} = \frac{1}{\pi\sqrt{C_{ds}\left(4(L_B+L_{dc})+L_D\right)}} = 49.56 \text{ GHz}. \quad (11)$$

However, in this case the q is 1.691, which is to big for a four stage amplifier. As it is shown in Fig. 3a the desired q value is 1.55, which corresponds to a drain cut-off frequency of 45.4 GHz. To achieve this, a proper TL must replace the L_D inductance. The necessary length can be read out from a figure similar to Fig. 2a, if a curve belong to $C = 0.03$ pF and $L_B = 0.3$ nH is drawn. The resulting l is 1.45 mm (in the case of $v = c$). The required drain TL Z_0 value to maintain a drain line *LFI* of 50 Ω is $Z_{0D} = 58$ Ω, which can be calculated from Eq. (3).

The final four stage amplifier structure is shown in Fig. 4a. The simulated results without optimization are shown in Fig. 4b (Aplac 7.5). They exactly follow the predicted properties. To a certain extent the effect of the losses and the source inductance can also be compensated by the decrease of q.

If the transistor is bilateral the value of the feedback capacitor (C_{GD}) is critical. If it is less than about 40% of C_{DS} its effect can be compensated by computer optimization applying the result of this method as a starting point.

References

[1] Bin Li and S. Prasad, "Harmonic and two-tone intermodulation distortion analyses of the inverted InGaAs/InAlAs/InP HBT", *IEEE Trans. Microw. Theory Techn.*, vol. 45, pp. 1135–1137, 1997.

[2] T. T. Y. Wong, *Fundamentals of Distributed Amplification*. Boston, London: Artech House, 1993.

[3] J. B. Beyer, S. M. Prasad, R. C. Becker, J. E. Nordman, and G. K. Hohenwarter, "MESFET distributed amplifier design guidelines", *IEEE Trans. Microw. Theory Techn.*, vol. 32 pp. 268–275, 1984.

[4] A. Zólomy, A. Hilt, G. Járó, and T. Berceli, "The effect of parasitic inductances in distributed amplifiers", in *Proc. 12th Int. Conf. MIKON'98*, Kraków, Poland, 1998, vol. 3, pp. 463–467.

[5] A. Zólomy, "Gain-bandwidth performance comparison of lumped and distributed element eistributed amplifiers", in *Proc. 13th Int. Conf. MIKON'2000*, Wrocław, Poland, 2000, vol. 1, pp. 101–104.

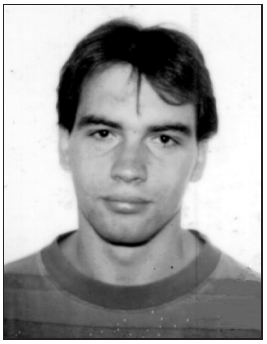

Attila Zólomy received the M.Sc. degree from the Technical University of Budapest, in 1994. Since 1994 he has worked on his Ph.D. thesis at the Department of Microwave Telecommunications as a Ph.D. student and since 1998 as an assistant lecturer. His thesis "New solutions for the circuits of high speed optical receivers" is now submitted for review. His main research interest are in the field of high speed optical receivers, wideband distributed amplifiers, optical generation of milimeter wave signals, harmonic MMW VCO-s. Presently, he is working in the group of Prof. Tibor Berceli on optical routers. He is a member of IEEE and author or co-author of 28 technical papers.

e-mail: zolomy@mht.bme.hu
BME-MHT
Technical University of Budapest
Goldmann György st 3
H-1111 Budapest, Hungary

Paper

Reliability and low-frequency noise measurements of InGaAsP MQW buried-heterostructure lasers

Sandra Pralgauskaitė, Jonas Matukas, Vilius Palenskis, Emilis Šermukšnis, Juozas Vyšniauskas, Gregory Letal, Robert Mallard, and Saulius Smetona

Abstract — A laser diode reliability test based on the measurements of the low-frequency optical and electrical noise, and their correlation factor changes during short-time ageing is presented. The noise characteristics reveal obvious differences between the stable and unreliable lasers operated near the threshold region. An excessive Lorentzian type noise with negative correlation factor at the threshold could be one of the criteria for identifying unreliable lasers. The behavior of unreliable lasers during ageing could be explained by migration of point recombination centres at the interface of an active layer, and by the formation of defect clusters.

Keywords — laser diode, low-frequency noise, optical noise, electrical noise, correlation factor, reliability.

Laser diodes (LDs) are extensively used as a signal source in fibre optical communication systems. High performance optical fibre systems need sources with a number of features: stable single-frequency output, gigabit/s modulation capability, stable operating lifetimes exceeding 10^8 hours at room temperature, and manufacturability. Buried heterostructure (BH) multiple-quantum-well (MQW) lasers possess performance characteristics that make them attractive for various applications. Optimization of the design parameters of the BH structure has led to a realization of very low threshold current, lower thermal resistance and stable transversal mode oscillation with nearly symmetric beam profile [1]. However, in the case of the BH laser, the complexity of the fabrication procedure (e.g. the requirement for additional growth steps as compared to a simple ridge-waveguide design) requires that rigorous attention be given to reliability concerns in order to meet product lifetime requirements. The degradation of BH structures is related to a decrease in the carrier lifetime or a decrease in non-radiative lifetime due to degradations of the edges of the active region [2, 3].

Product reliability is normally confirmed by accelerated ageing experiments, which take significant time and resources. As a result, there is a great demand for a simple, room-temperature device reliability screen to differentiate inherently reliable from unreliable production batches or devices. Low-frequency (LF) (usually $1/f$) noise is a typical excess noise that can be a very sensitive measure of the quality and reliability of optoelectronic devices [3–5]. Detection of LF noise can indicate the presence of imperfections. In addition, LF noise might be useful in providing insight into any changes observed during accelerated ageing experiments. In our preliminary work [6, 7] we have observed a correlation between the LD reliability and noise intensity. The LD reliability is also correlated to the degree of correlation between optical and electrical noise fluctuations. In this paper we report on the reliability test, that is based on the low-frequency optical and electrical noise, and how their correlation factor changes during short-time ageing at higher forward currents and at elevated temperatures.

The semiconductor lasers investigated in this paper are 1550 nm InGaAsP MQW BH gain-coupled, distributed-feedback (DFB) LDs with a thyristor-type p-n-blocking layer. Two experimental batches of LDs were chosen. The preliminary accelerated lifetime test (500 h, 150 mA, 100°C) showed that the threshold current degradation (increase by nearly a factor of 2 during the first 40 hours of operation) occurs during ageing for samples from one batch (these samples referred to as "unreliable devices" in this paper), while operation characteristics of samples from another batch were stable [6].

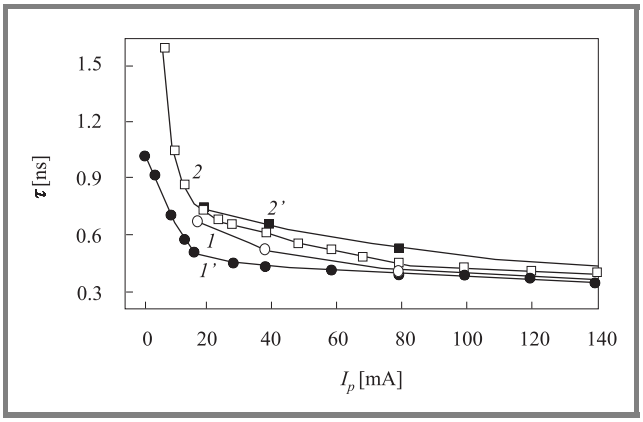

Fig. 1. The lasing delay time dependencies on pulse amplitude: *1* and *2* are respectively for stable and unreliable devices before ageing, *1'* and *2'* are respectively after 500 h ageing (measurement direct current is 5 mA, $T = 290$ K).

The voltage-current, optical output power and pulse characteristics were measured for all devices and then noise properties of a selected set of devices were analyzed. Threshold current for the stable devices was in the range of 6–8 mA, while for the unreliable ones ranged between 11–13 mA.

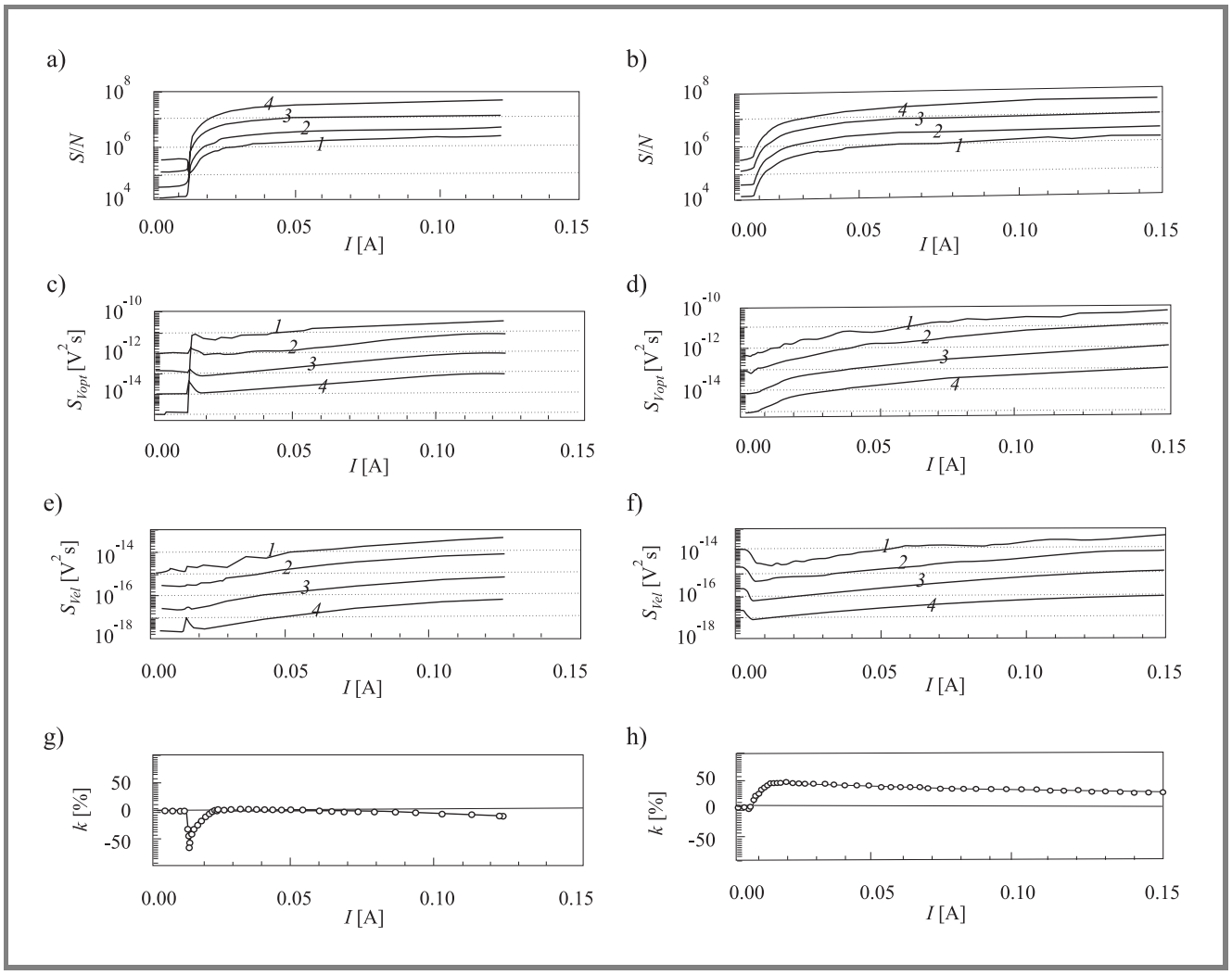

Fig. 2. (a, b) Signal-to-noise relation (S/N), (c, d) optical (S_{Vopt}) and (e), (f) electrical (S_{Vel}) fluctuation spectral density (*1* – 22 Hz, *2* – 108 Hz, *3* – 1.03 kHz, *4* – 10.7 kHz) and (g, h) correlation factor (k) (20 Hz–20 kHz) dependencies on laser current for unreliable (a, c, e, g) and stable (b, d, f, h) samples ($T = 290$ K; the devices were not aged).

Unreliable devices also have slower switching characteristics, too (Fig. 1): the lasing delay time for stable devices is in the range of 0.42–0.49 ns, while for unreliable ones is about 0.56–0.62 ns. In addition, a degradation of the switching characteristics during ageing for the unreliable devices was observed.

Noise characteristics (optical and electrical fluctuation spectral densities, optical signal-to-noise ratio and correlation factor between optical and electrical fluctuations) were measured at low frequencies (20 Hz–20 kHz). The noise measurement results for stable and unreliable LDs exhibited some differences in noise characteristics before ageing (Fig. 2). The noise intensity in the lasing operation region of samples from both batches was similar. However, the stable devices exhibit a strong positive correlation factor (30–60% for different samples) between the electrical and optical noises above threshold, while the unreliable devices exhibit a weak correlation. The reason for this difference is hypothesized to be due to defects in the semiconductor. The optical and electrical noise spectra are of $1/f$ type for all investigated LDs in the working current range. Various semiconductor growth and laser processing defects cause this noise. Positive correlation in the LDs operation shows that the devices contain defects that substantially modulate current flowing through the active region. However, the main differences were observed at the threshold region (transition from light emission diode to laser operation region): an increase of a high frequency component of the optical and electrical noise intensity (Fig. 2c and e, curve *4*) and negative correlation factor (30–70%) for different lasers (Fig. 2g) were observed for unreliable sample operation near the threshold. A high frequency component in stable samples has not been observed.

Further differences in the noise spectra of reliable and unreliable devices are observed close to threshold. Figures 3 and 4 present the optical and electrical noise spectra in the vicinity of the threshold current for the both types of devices before and after ageing. For unreliable samples (be-

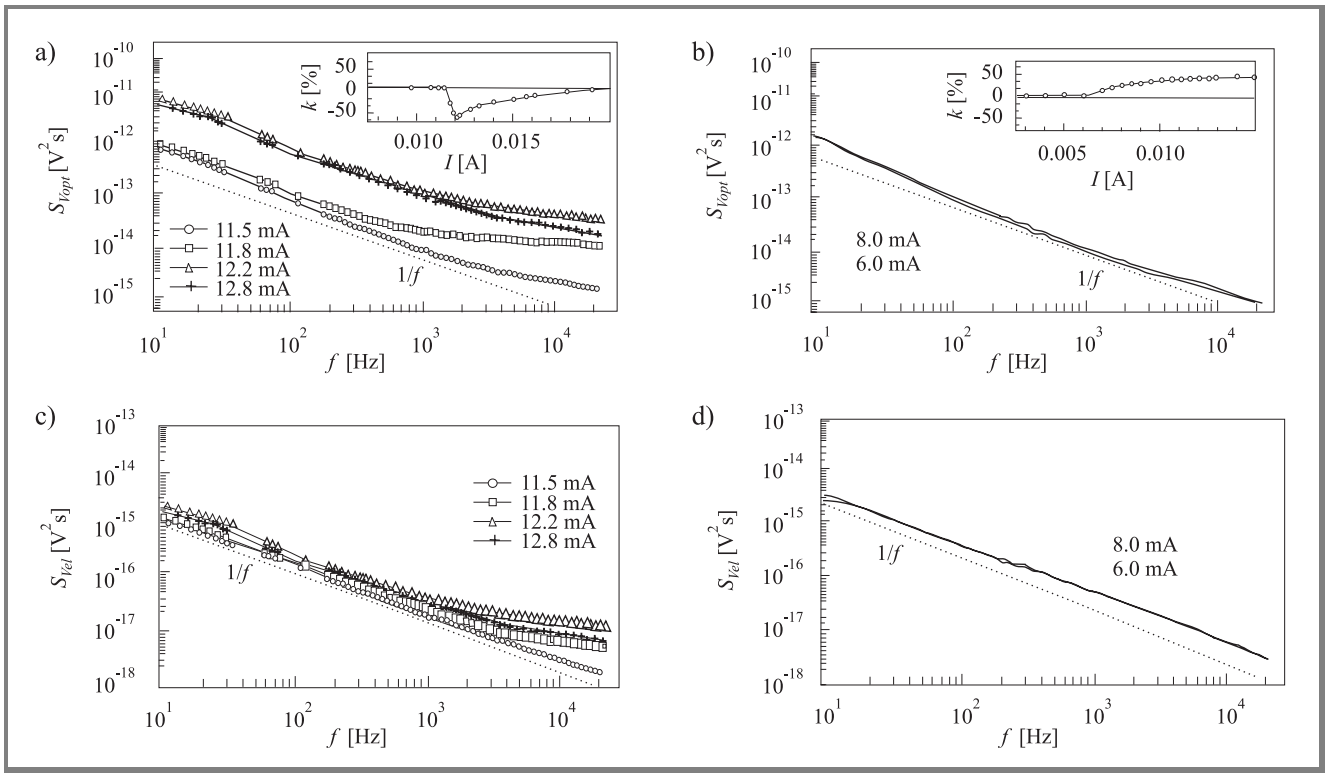

Fig. 3. Optical (a, b) and electrical (c, d) fluctuation spectra in the threshold region for unreliable (a, c) and stable (b, d) samples ($T = 290$ K; inclusion: correlation factor dependencies on laser current) (the devices were not aged).

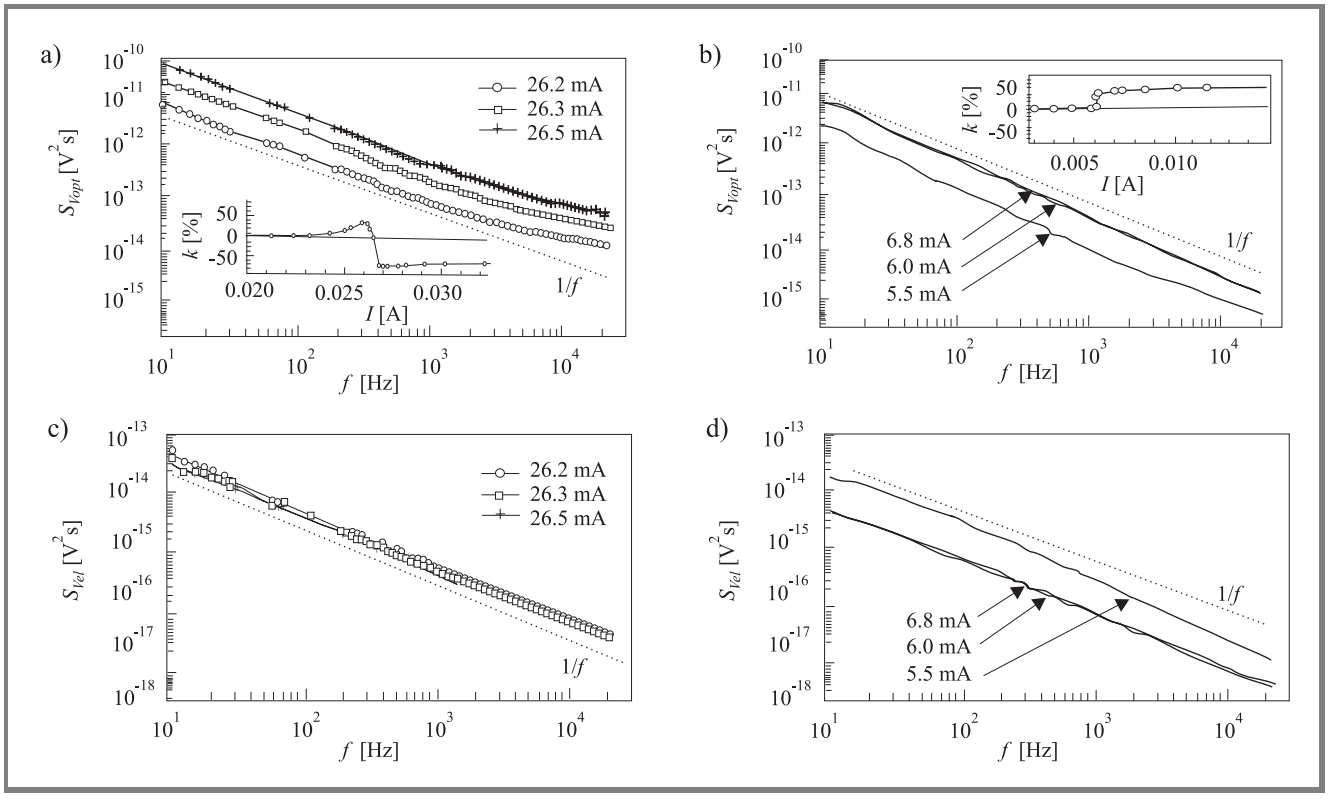

Fig. 4. Optical (a, b) and electrical (c, d) fluctuation spectra in the threshold region for unreliable (a, c) and stable (b, d) samples ($T = 290$ K; inclusion: correlation factor dependencies on laser current) (the devices were aged 500 h at 100°C and 150 mA).

fore ageing) excess high-frequency Lorentzian type (with the relaxation time of a few nanoseconds) electrical and optical noise component with negative correlation factor was observed (Fig. 3). A high frequency component for the stable samples has not been observed. The noise spectra for stable devices are approximately $1/f$ type. Furthermore, there is no correlation between optical and electrical fluctuations at the lasing threshold (Fig. 3). After ageing ($\sim$ 500 h) the unreliable devices exhibit a more intensive LF noise than before ageing (an optical noise spectral density increased by an order of magnitude) and the correlation factor at the threshold currents became positive (30–60%). There were no noticeable changes in the stable device noise intensity and other noise characteristics.

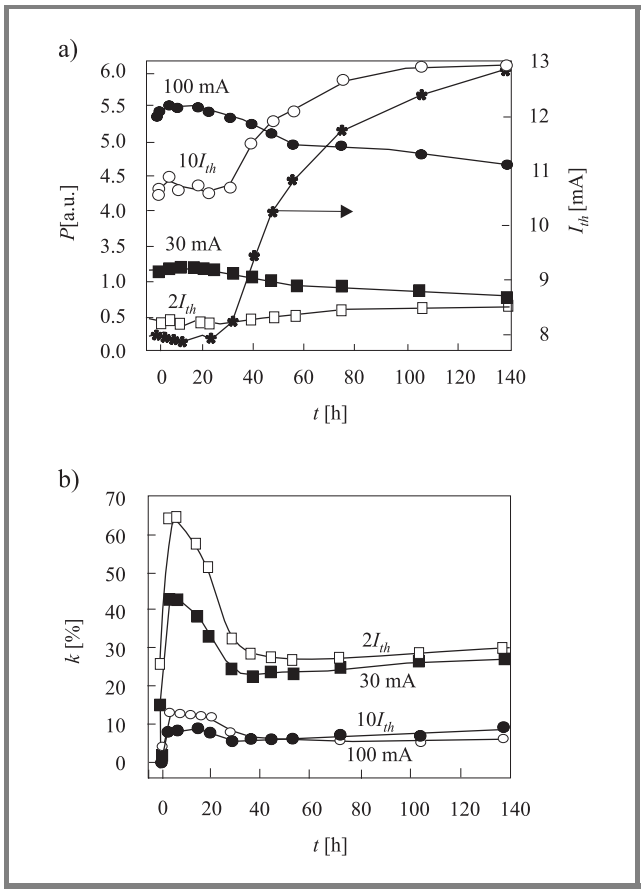

Fig. 5. Optical output power (P), threshold current (I_{th}) (a) and correlation factor (k) (b) dependencies on the ageing time for different laser currents of unreliable samples (ageing at 60°C and 150 mA, measurements at 290 K).

During ageing the high-frequency noise component of unreliable samples at the threshold decreased significantly (Fig. 4). This result can be explained by considering the noise sources of different origin. A recombination process that produces high-frequency fluctuations in both the laser resistance and the light output power commonly causes Lorentzian noise (i.e. the resistance and light output power fluctuate with opposite signs). On the other hand, cluster type defects are usually characterized by a wide distribution of relaxation times of charge carriers and, hence, produce a $1/f$ noise spectrum. It is hypothesized that during ageing at elevated temperature and high current densities the point (or other separated) defects responsible for Lorentzian noise migrate to form clusters (or macrodefects) at the active layer interfaces. Probably, the absence of such mobile defects in stable lasers can explain why the level and spectra of noises do not change during ageing for stable samples.

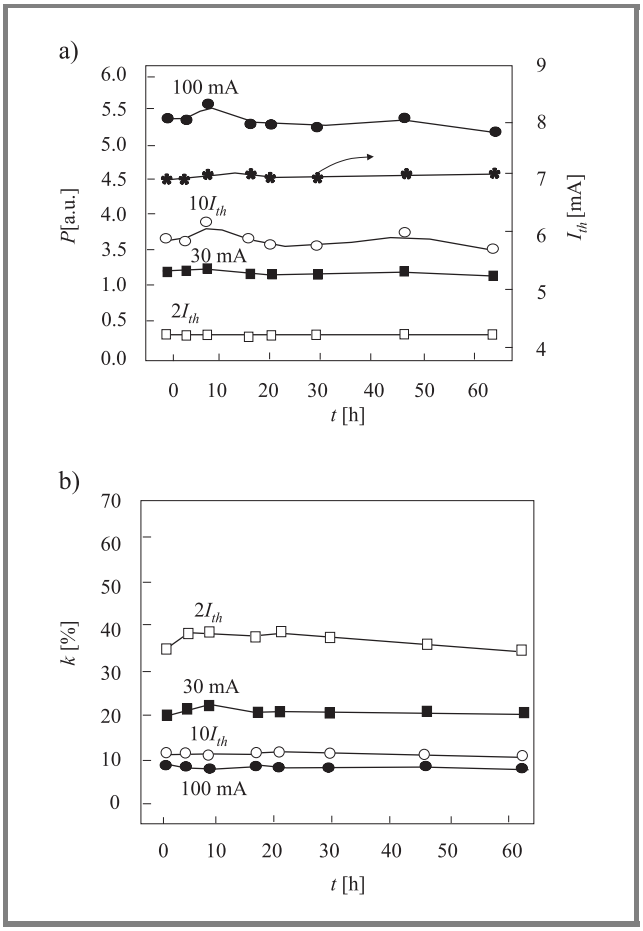

Fig. 6. Optical output power (P), threshold current (I_{th}) (a) and correlation factor (k) (b) dependencies on the ageing time for different laser currents of stable samples (ageing at 60°C and 150 mA, measurements at 290 K).

We have observed significant differences in noise characteristics at the vicinity of the threshold between LDs with good and poor reliability (Figs. 2 and 3). With that in mind, we conducted detailed short-time ageing experiments (ageing conditions: 60°C and 150 mA). Results of this experiment (Figs. 5 and 6) show that noise measurement method could be used as early LD reliability predictor. It could be seen that threshold current for unreliable devices does not increase in the initial phase of the ageing, while the noise characteristic changes are the largest in this phase: during the first 20 hours of ageing at comparatively low temperature optical noise spectral density increases by an order of magnitude and the correlation factor between optical and

electrical fluctuations changes from 0 to 68% ($I \approx 2I_{th}$, Fig. 5). There is enough just to increase operation current up to 100 mA for the short time (few minutes) in order to change the correlation factor at threshold from -20% to $+18\%$. After ageing at rigid conditions (100°C) the unreliable samples above threshold have negative correlation factor (see inclusion in Fig. 4a), while after ageing at moderate conditions (60°C) a negative correlation was not observed (Fig. 5). This shows that defects migration and clusters formation way depends on the ageing conditions.

These results show that noise characteristics (especially the electrical and optical noise correlation factor) are a very sensitive measure of the device quality. We observed significant changes in the correlation factor, while changes of the total output power remain comparatively small. Conversely, as can be seen in Fig. 6, the noise characteristics of the stable laser diodes do not change during the short-time ageing at elevated temperature.

Conclusions. Noise characteristics reveal obvious differences in the reliable and unreliable lasers operated near threshold. Large high-frequency components in both optical and electrical noise and negative correlation factor between these parameters were observed in the unreliable lasers operation at threshold. Conversely, the reliable lasers exhibit no noise correlation change in the transition from spontaneous to stimulated emission.

After 500 hours of ageing at 100°C, and forward bias of 150 mA, the stable devices exhibited no measurable change in the noise spectra. However, both the optical and electrical noise of the degrading devices increased by an order of magnitude after ageing. It is believed that the changes in the unreliable devices operation characteristics (threshold current, output power, and noise characteristics) during the ageing are due to the migration of point recombination centres (responsible for the Lorentzian noise before the ageing) and formation of electrically active defect clusters (macrodefects) with a wide distribution of relaxation times.

Noise characteristics, and especially correlation factor between optical and electrical fluctuations, are very sensitive to the laser degradation and could be used as a powerful early predictor of reliability. This technique is especially useful in the case where the lifetest is performed at low temperature, in which a long endurance test is needed for the BH laser reliability evaluation.

References

[1] K. Takemasa, M. Kubota, T. Munakata, and H. Wada, "1.3-μm AlGaInAs buried-heterostructure lasers", *IEEE Photon. Technol. Lett.*, vol. 11, no. 8, pp. 949–951, 1999.

[2] M. Fukuda and G. Iwane, "Degradation of active region in InGaAsP/InP buried heterostructure lasers", *J. Appl. Phys.*, vol. 58, no. 8, pp. 2932–2936, 1985.

[3] L. K. J. Vandamme, P. J. L. Herve, and R. Alabedra, "A decade of low frequency noise in optoelectronics and photonic component", in *Proc. 14th ICNF, Noise Phys. Syst. 1/f Fluct.* Eds. C. Claeys and E. Simoen, Lauven, Belgium, 1997, pp. 495–502.

[4] G. Hartler, U. Golze, and K. Paschke, "Extended noise analysis – a novel tool for reliability screening", *Microelectron. Reliab.*, vol. 38, pp. 1193–1198, 1998.

[5] L. K. J. Vandamme, "Noise as a diagnostic tool for quality and reliability of electron devices", *IEEE Trans. Electron. Dev.*, vol. 41, no. 11, pp. 2176–2187, 1994.

[6] G. Letal, S. Smetona, R. Mallard, J. Matukas, V. Palenskis, and S. Pralgauskaitė, "Reliability and low-frequency noise measurements of InGaAsP MQW buried-heterostructure lasers", in *Proc. 16th ICNF Noise Phys. Syst. 1/f Fluct.*, Ed. G. Bosman, New Jersey, 2001, pp. 743–746.

[7] S. Pralgauskaitė, V. Palenskis, J. Matukas, Č. Pavasaris, E. Šermukšnis, J. G. Simmons, R. Sobiestianskas, and S. Smetona, "Optical and electrical characteristics of DFB MQW laser diodes", *Mat. Sci.*, vol. 7, no. 2, pp. 80–86, 2001.

Sandra Pralgauskaitė was born in Kaunas, Lithuania, in 1975. She received B.S. degree in radiophysics and M.S. degree in telecommunication physics and electronics from the Vilnius University, Vilnius, Lithuania, in 1997 and 1999, respectively. Currently she is working towards Ph.D. degree in Semiconductors Physics Institute, Vilnius, Lithuania. Since 2001 she is a member of IEEE Lithuanian Section. Her main research interests are semiconductor lasers, low-frequency noise, quality and reliability of semiconductor devices.

e-mail: sanprl@uj.pfi.lt
Semiconductor Physics Institute
A. Goštauto 11
2600 Vilnius, Lithuania

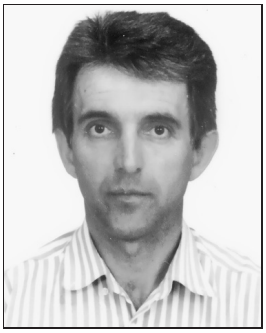

Jonas Matukas was born in Lithuania, in 1957. He graduated from Faculty of Physics at the Vilnius University, in 1980, and received the Ph.D. degree in 1993. Since 1993 he has been working as senior scientific researcher at Noise Research Laboratory, Vilnius University, and since 1998 he has been Associated Professor at Vilnius University. He works on low-frequency noise and other characteristics of electronic devices (Schottky diodes, semiconductor lasers, photodetectors).

e-mail: jonas.matukas@ff.vu.lt
Department of Radiophysics
Vilnius University
Sauletekio 9
Vilnius, Lithuania

Vilius Palenskis was born in Lithuania, in 1941. He graduated from Faculty of Physics at the Vilnius University, in 1965. He received the Ph.D. degree in 1977. Since 1980 he has been Associated Professor and head of the Noise Research Laboratory at the Vilnius University. His scientific research has been mostly on fundamental properties of low-frequency noise in materials (metals, thin films, semiconductors, superconductors, magnetics) and electronic devices (p-n, tunnel and Schottky diodes, bipolar and FET transistors, semiconductor lasers and others) and their applications.

e-mail: vilius.palenskis@ff.vu.lt
Department of Radiophysics
Vilnius University
Sauletekio 9
Vilnius, Lithuania

Emilis Šermukšnis received the B.S. and M.S. degrees in telecommunication physics and electronic from the Vilnius University, Vilnius, Lithuania, in 1999 and 2001, respectively, where he investigated semiconductor lasers pulse characteristics, optical and electrical low-frequency noise characteristics. He is currently working towards Ph.D. degree at the Noise Laboratory, Vilnius University, Lithuania. He is also active in Centre for Electrophotonic Materials and Devices at McMaster University and Nortel Networks, Canada, researching high frequency relative intensity noise, time resolved frequency chirp and their degradation during ageing of semiconductor lasers.

e-mail: esermuk@medbank.lt
Department of Radiophysics
Vilnius University
Sauletekio 9
Vilnius, Lithuania

Juozas Vyšniauskas was born in 1949, in Kybartai, Lithuania. He graduated from the Moscow Power Institute with a degree in radiophysics and electronics, in 1973. Immediately after, he started working as a scientific researcher at the Radiophysics Department, Vilnius University, Lithuania. He has been working in the field of experimental research and computer simulation of semiconductor diodes since 1975. He received the Ph.D. degree from the Vilnius University, Lithuania, in 1975. He has been working as a Professor at the Radiophysics Department, Vilnius University since 1989. He is currently working on computer simulation of semiconductor lasers.

e-mail: juozas.vysniauskas@ff.vu.lt
Department of Radiophysics
Vilnius University
Sauletekio 9
Vilnius, Lithuania

Gregory Letal
e-mail: saulius@bookham.com
Bookham Technologies
Ottawa, Ontario, Canada

Robert Mallard
e-mail: saulius@bookham.com
Bookham Technologies
Ottawa, Ontario, Canada

Saulius Smetona
e-mail: saulius@bookham.com
Bookham Technologies
Ottawa, Ontario, Canada

Paper

Optical control of semiconductor synchronized microwave oscillators in the power suppression mode

Dmitri A. Usanov, Alexander V. Skripal, and Anton V. Abramov

Abstract — The influence of optical radiation on the performance of the synchronized microwave Gunn-diode oscillator in the coherent signals subtraction mode has been described theoretically and investigated experimentally. The high sensitivity of the oscillator characteristics to the change of the optical intensity affecting the semiconductor diode structure has been shown. It is suggested to use this mode for the creation of optoelectronic microwave systems with the controlled amplitude and phase of the output signal and for the high-accuracy indication of optical radiation.

Keywords — optical control, synchronization, semiconductor microwave oscillator, Gunn diode.

1. Introduction

At present considerable attention is paid to the researches, devoted to the development of optically controlled microwave semiconductor elements on the basis of bipolar and field transistors, IMPATT and TRAPATT diodes, Gunn diodes [1–3].

A lot of publications are devoted to the investigations of the performance of semiconductor microwave oscillators in the lock mode under the influence of optical radiation [4–6]. Circuits for frequency stability increase, systems with controlled amplitude and phase of output signal, required for example for phased array, were developed on the basis of these oscillators [6, 7].

Despite the fact that the optical power level, used for control of microwave semiconductor devices, is low, and the range of the fundamental frequency and power tuning is not more than several percent, the phase shift of output signal of the locked oscillator can reach 180°. This allows us by selecting the optical power level to obtain the optimal value of the output signal or to obtain almost complete suppression of the signal and to increase significantly the sensitivity of optoelectronic schemes to the optical radiation.

In this work the synchronized oscillator on the Gunn diode with optical control in the comparison circuit operating in the coherent signals subtraction mode is investigated experimentally and theoretically.

2. Analytical model

Consider the model of the single-circuit diode locked oscillator (Fig. 1) with the resistive active semiconductor element, *IV*-curve of which has a section of negative differential conductivity $G(U)$, which depends on the amplitude of AC voltage:

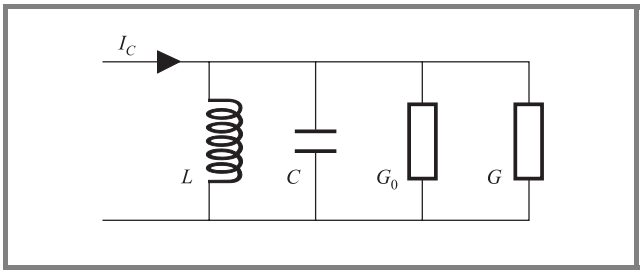

Fig. 1. Equivalent scheme of the single-circuit diode synchronized oscillator.

$$G(U) = -G_A + \alpha U^2 .$$

The gain-frequency characteristic $y(x)$ and the phase-frequency characteristic $\varphi(x)$ of such synchronized oscillator are described by the following equations [8]:

$$y\lfloor (y-1)^2 + x^2 \rfloor = F ,$$

$$\mathrm{tg}\varphi = \frac{x}{y-1} ,$$

and oscillations stability conditions in the steady-state mode are: $y > 0.5$ and $x^2 + (y-1)(3y-1) > 0$.

Variables describing frequency detuning, amplitude of oscillations and amplitude of an external influence are represented correspondingly:

$$x = \left(1 - \frac{\omega_0^2}{\omega^2}\right)\frac{q}{d_0}, \quad y = \frac{U^2}{U_0^2}, \quad F = \frac{q^2 E_C^2}{U_0^2} ,$$

where $q = \frac{G_0}{\alpha U_0^2}$, $d_0 = \frac{G_0}{\omega C}$, ω_0 and U_0 are the oscillations frequency of free-running oscillator and their amplitude, ω and $E_C = I_C/G_0$ are the frequency and amplitude of the external influence, C is the diode capacity, L is the inductance of diode holder, G_0 is the conductivity of load.

Since with the external synchronization in the steady-state mode the phase difference constancy between output signal of self-oscillator and synchrosignal is provided, then the investigation of the behaviour of the gain-frequency and phase-frequency characteristics of the signal in the load

G_L when subtraction of the output signal p_{out} of the self-oscillator and synchrosignal p_S is of interest.

The current in the load G_L can be represented as $I_L = I_{SL}\sin(\omega t + \alpha) + I_{out}\sin\big(\omega t + \beta - \varphi(x)\big)$, where I_{out} and I_{SL} are the amplitudes of currents, induced by the output signal of the synchronized oscillator on the load G_L and the synchrosignal on this load when conveying directly to the load G_L, $\varphi(x)$ is the phase difference which depends on the frequency detuning within the locking range, α and β are the initial phase difference.

The amplitudes of the currents I_{out} and I_{SL} in the load G_L, if load conduction equals oscillator's output conduction and internal conduction of the synchrosignal source, are defined from relations: $I_{out} = \sqrt{k_1 2P_{out}}G_L$, $I_{SL} = \sqrt{k_2 2P_{SL}G_L}$, where k_1 and k_2 are power-transfer coefficients of oscillator's output signal and synchrosignal to the common load defined by the power loss in transmission lines.

Under the coherent signals subtraction the phase ψ and the amplitude I_{L0} of the resulting current in the load $I_L = I_{L0}\sin(\omega t + \psi)$ are defined by expressions:

$$\psi = \operatorname{arctg}\left[\frac{I_{SL}\sin\alpha + I_{out}\sin(\beta-\varphi)}{I_{SL}\cos\alpha + I_{out}\cos(\beta-\varphi)}\right],$$

$$I_{L0} = \sqrt{I_{SL}^2 + I_{out}^2 + 2I_{SL}I_{out}\cos(\beta-\varphi-\alpha)}.$$

If amplitudes of currents I_{out} and I_{SL} are equal, and phase condition $\beta - \alpha - \varphi = \pi$ is fulfilled, almost complete suppression of the signal I_L is possible.

In the locking range the phase difference φ between oscillator's output signal and synchrosignal can vary from $-\pi/2$ to $\pi/2$. This allows us to achieve the antiphasing signals being added during the changing of frequency detuning x.

The power accepted in the load G_L is computed by formula: $P_L = I_{L0}^2/2G_L$.

The influence of optical radiation with quantum energy larger then the forbidden gap results in increasing the free charge carrier concentration in the semiconductor by the value of

$$\Delta n = \frac{\beta(1-R)IS_0\tau\alpha\left[\frac{\left[\alpha L_0^2 + S_p\tau\right]}{(L_0+S_p\tau)}L_0\left(1-e^{-\delta}\right) - \frac{1-e^{-\alpha d}}{\alpha}\right]}{h\nu\left(\alpha^2L_0^2-1\right)d}$$

taking into consideration the surface recombination [9].

If an oscillator is the Gunn oscillator then the free charge carrier concentration change in semiconductor results in changing the negative differential conduction and capacity of Gunn diode [10]:

$$G_A = G_{A0}\frac{n_0 + \Delta n(I)}{n_0},$$

$$C(I) = S\sqrt{\frac{q\left(n_0 + \Delta n(I)\right)\varepsilon\varepsilon_0}{2U_d}},$$

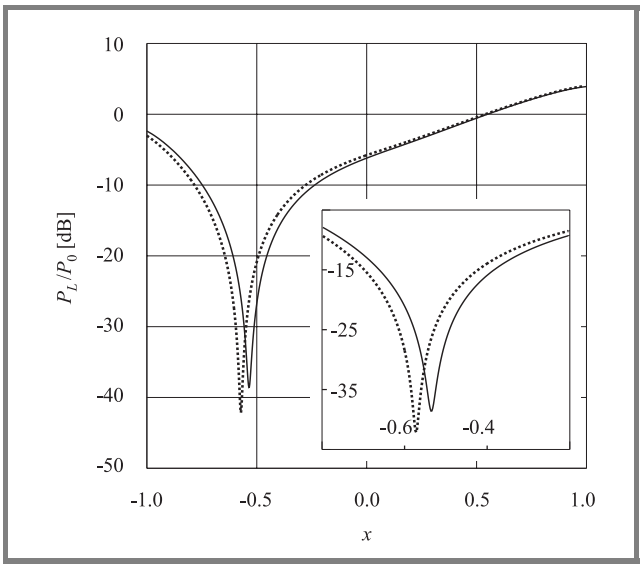

Fig. 2. The power-frequency characteristics of signal in the load.

where n_0 is the donor concentration, S is the diode area, U_d is the domain voltage.

The results of computation of synchronized Gunn-diode oscillator (SGDO) power-frequency characteristics at the constant synchrosignal power are shown in Fig. 2 (full curve). Computations show that the influence of the optical radiation of small intensity of 100 W/cm^2 results in changing the least value position on power-frequency characteristics (Fig. 2, dotted curve) and under the constant synchrosignal frequency – in considerable (up to 30 dB) changing the output power in the oscillator load (Fig. 3).

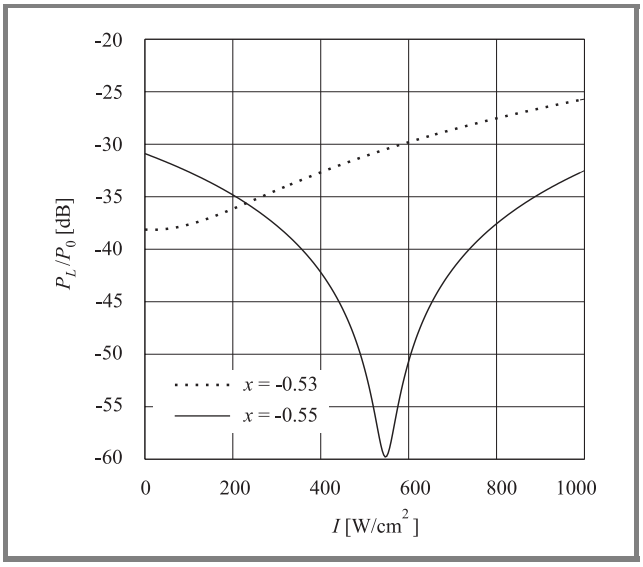

Fig. 3. The dependence of output signal from the optical intensity.

The phase-frequency characteristics $\psi(x)$ of the signal in the load G_L are shown in Fig. 4. On these characteristics at a point of minimum of power-frequency characteristics the

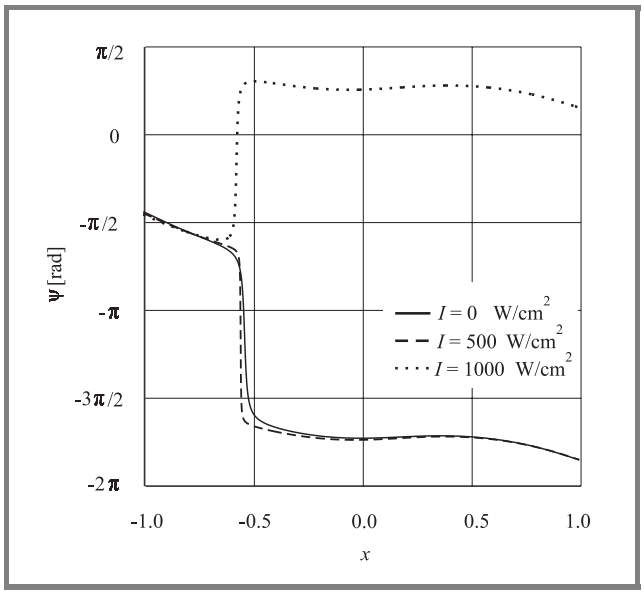

Fig. 4. The phase-frequency characteristics of signal in the load.

abrupt output signal phase ψ change up to π is observed. At the same time the slope of phase-frequency characteristic at a point of minimum of power-frequency characteristics under the influence of optical radiation can change its sign (Fig. 4, dotted curve).

The analysis of the obtained results shows that on the basis of the semiconductor oscillator synchronized by an external signal the microwave system realizing sufficiently great (up to 30 dB) levels of output signal change under the influence of optical radiation can be developed.

3. Experimental results

For the experimental investigations the setup shown in Fig. 5 was used. The semiconductor microwave oscillator of 3-centimeters region with Gunn diode 3A703 as active element was investigated. As a source of optical radiation the He-Ne laser was used. In one of the arms of circuit the synchrosignal source (microwave oscillator G4-83) was placed. In the other arm the Gunn oscillator was placed. At the output of the circuit the synchrosignal and Gunn oscillator output signal were summarized on the common load. The resultant signal was observed on the spectrum analyzer C4-27 and on the power meter M3-51.

By adjusting of Gunn diode bias, power level and frequency of synchrosignal and changing of the elements parameters the mode of coherent subtraction of both signals on common load has been implemented. While synchrosignal frequency change within the locking range the output power change up to 40 dB was observed.

The results of measurements of the dependence of the first harmonic power P_L/P_0 of the signal at the output of the bridge circuit in the load when oscillator operates in the

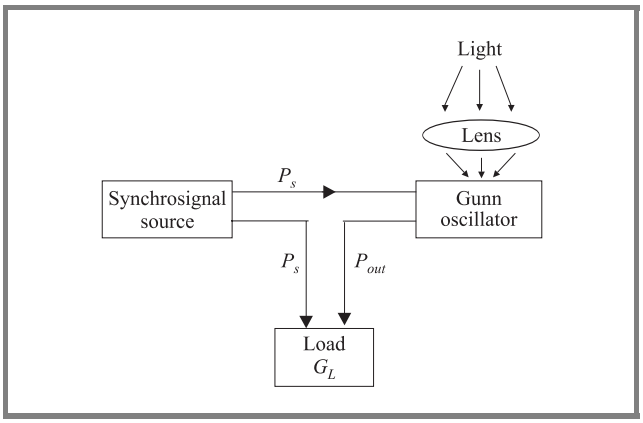

Fig. 5. The experimental setup.

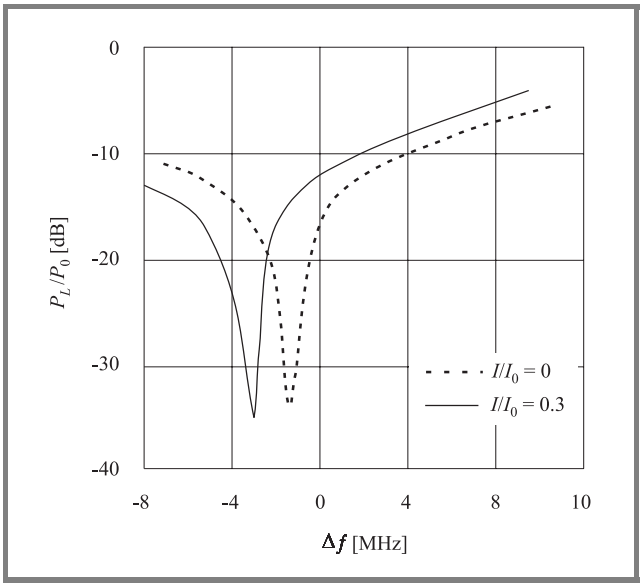

Fig. 6. The experimental power-frequency characteristics of the synchronized Gunn oscillator.

locking mode on the synchrosignal frequency (power frequency characteristic) with (solid curve) or without (dashed curve) an external optical radiation are shown in Fig. 6.

It follows from these results that at a point of minimum of power-frequency characteristic the scheme under investigation has extremely high sensitivity (about 20 dB/MHz) to the change of the Gunn oscillator fundamental frequency. Therefore the influence of optical radiation of 100 W/cm^2, which results in the insignificant changes of frequency (about 1–3 MHz) and power (about 0.01–0.1 mW) of Gunn diode output signal, results in changing the least value position on power-frequency characteristics (Fig. 6, solid curve). With the constant synchrosignal frequency the influence of optical radiation results in significant (up to 30 dB) change of the synchronized oscillator output power in the load (Fig. 7). The dependencies of the first harmonic power P_L/P_0 of the SGDO output signal on the reduced optical intensity I at the constant detun-

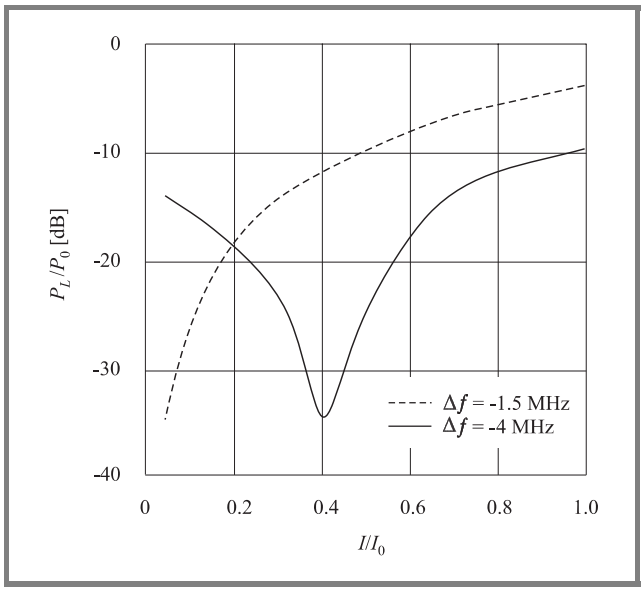

Fig. 7. Experimental dependencies of the SGDO output power on the intensity of the optical radiation.

ing Δf are shown in Fig. 7. By selecting detuning Δf both monotonous and non-monotone dependencies $P_L/P_0(I)$ can be obtained.

4. Computer simulation

For the description of the multicircuit SGDO in the bridge circuit in the mode of the coherent subtraction of the synchrosignal and the synchronized oscillator output signal on common load it is suggested to use the equivalent scheme shown in Fig. 8 [11].

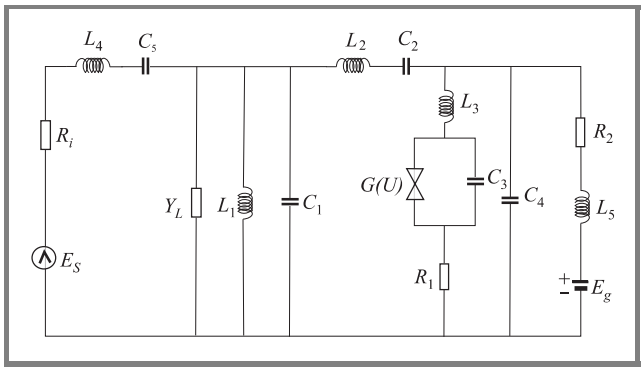

Fig. 8. The equivalent scheme of the SGDO.

Elements of this scheme simulate semiconductor structure of Gunn diode as connected in parallel capacity C_3, active nonlinear conduction $G(U)$ that is determined from *IV*-characteristic of the diode [11] and resistance R_1 connected in series; elements of diode body L_3 ,C_4, microwave circuit of diode presented as in-parallel L_1C_1, and in-series L_2C_2, circuits, equivalent conduction of load on the output of bridge scheme Y_L, Gunn diode feed circuit consisting of voltage source E_g, choke L_5, and resistance R_2; microwave circuit of synchrosignal generator containing source of alternating signal E_S, resistance R_i and in-series circuit L_4C_5.

This equivalent scheme is described by the system of ten first-order differential equations based on the Kirchhoff laws. The influence of the optical illumination was simulated, as in the analytical model, by the dependence of the Gunn diode negative differential conductance and capacity on the optical intensity.

As a result of numerical solution of the differential equations system the dependence of the instantaneous current in the load G_L as a function of time $i_L(t)$ was determined. By the Fourier transform of the $i_L(t)$ the harmonic components of the current in the load were calculated, their amplitudes were determined, and the powers of the harmonics at the output of the SGDO were calculated: $P_{kL} = i_{kL}^2/2Y_L$, where i_{kL} – the amplitude of the harmonic components of the current in the load, k – the number of a harmonic.

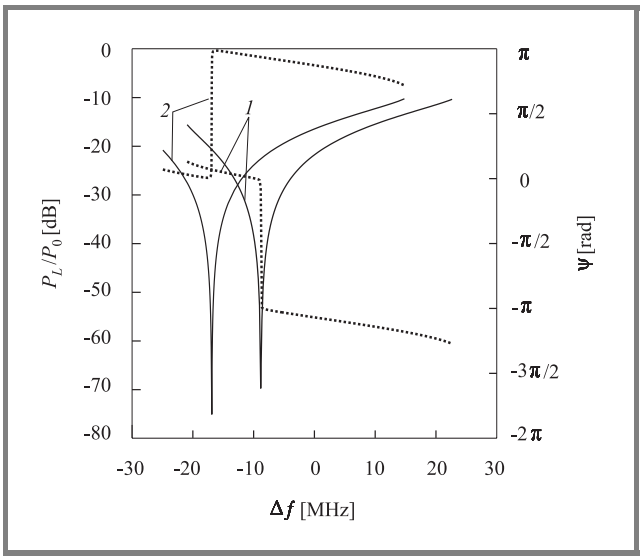

Fig. 9. Power-frequency (full curves) and phase-frequency (dotted curves) of the output signal first harmonic: *1*) $I = 0$, *2*) $I = 10^6$ W/m^2.

On the basis of the above mentioned model the calculations of the power-frequency characteristics of SGDO were carried out. The results of calculations of the SGDO power-frequency and phase-frequency characteristics at the constant synchrosignal power and the various values of optical intensity are shown in Fig. 9.

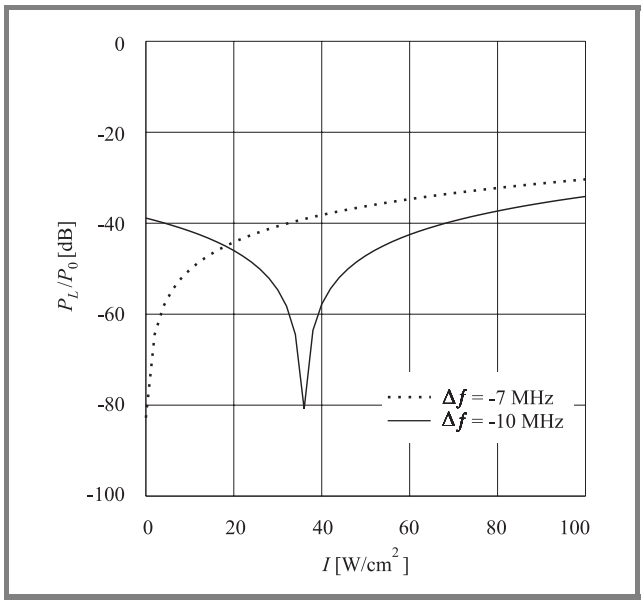

Fig. 10. The dependence of the output signal on the optical intensity.

The dependencies of the SGDO output power on the optical intensity for the various values of the detuning Δf are shown in Fig. 10. Depending on the detuning value the oscillator output power can be both monotone increasing (dotted curve) and having the minimum (solid curve). Here the changing of the output microwave signal power exceeded 40 dB. The steepness of the phase-frequency characteristic $\psi(x)$ at a point of minimum of the power-frequency characteristic is up to $\pi/$MHz.

5. Conclusion

In this work the influence of optical radiation on the performance of the synchronized microwave Gunn oscillator in the coherent signals subtraction mode has been described theoretically and investigated experimentally.

The experimental investigations and calculations show the high sensitivity of the oscillator characteristics to the change of the optical intensity affecting the semiconductor diode structure. This allows us to use the coherent signals subtraction mode in synchronized Gunn-diode oscillators for the creation of optoelectronic microwave systems with the controlled amplitude and phase of the output signal, for the high-accuracy indication of optical radiation and for the creation of the semiconductor microwave elements with extended functional possibilities.

Acknowledgment

The work was supported by the program of Russian Education Ministry code 208.02.02.040 and by the grant no. T00-2.2-2219 of the Russian Education Ministry in the fundamental researches in technical sciences.

References

[1] A. J. Seeds and A. A. Salles, "Optical control of microwave semiconductor devices", *IEEE Trans. Microw. Theory Techn.*, vol. MTT-38, no. 5, pp. 577–585, 1990.

[2] D. A. Usanov and A. V. Skripal, *The Physics of Semiconductor Devices Operation in Microwave Circuits*. Saratov: Saratov State University, 1999.

[3] S. J. Rossek and C. E. Free, "Optically controlled microwave switching and phase shifting using GaAs FET's", *IEEE Microw. Guid. Wave Lett.*, vol. 5, no. 3, pp. 81–83, 1995.

[4] R. D. Esman, L. Goldberg, and J. F. Weller, "Optical phase control of an optically injection-locked FET microwave oscillator", *IEEE Trans. Microw. Theory Techn.*, vol. MTT-37, no. 10, pp. 1512–1518, 1989.

[5] X. Zhang and A. S. Daryoush, "Full 360° phase shifting of injection-locked oscillators", *IEEE Microw. Guid. Wave Lett.*, vol. 3, no. 1, pp. 14–16, 1993.

[6] V. S. Andreev and N. V. Makarov, "Optical control of microwave semiconductor devices", *Radioelectron. Commun. Syst.*, vol. 38, no. 10, pp. 17–33, 1995.

[7] A. S. Daryoush, "Optical synchronization of millimeter-wave oscillators for distributed architectures", *IEEE Trans. Microw. Theory Techn.*, vol. MTT-38, no. 5, pp. 467–476, 1990.

[8] V. S. Andreev, "To the theory of synchronization of self-oscillators on the devices with negative resistance", *Radio Eng.*, no. 2, pp. 43–53, 1975.

[9] R. A. Smith, *Semiconductors*. Cambridge: Cambridge University Press, 1978.

[10] M. Shur, *GaAs Devices and Circuits*. New York, London: Plenum Press, 1987.

[11] D. A. Usanov, A. V. Skripal, and D. V. Ulyanov, "Power suppression mode in semiconductor synchronized microwave oscillators", in *Proc. 13th Int. Conf. MIKON-2000*, Wrocław, Poland, 2000, vol. 1, pp. 109–112.

Dmitri A. Usanov has graduated from Physics Faculty of Saratov State University, Russia, in 1965. He received Doctor's degree in physics and mathematics sciences, in 1989. Since 1990 he is the Professor of Solid State Physics Department and from 1985 till the present the head of Solid State Physics Department. He is an author of monographs, textbooks, more than 300 articles on solid state electronics, physics of semiconductors and radiophysics. He is the author of more then 90 inventions and patents, and member of the IEEE. In 1998 he received the title of Deserved Figure of Science of Russian Federation.

e-mail: UsanovDA@info.sgu.ru
Saratov State University
Moskovskaya 155
Saratov, Russia

Alexander V. Skripal has graduated from Physics Faculty of Saratov State University, Russia, in 1976. He received Doctor's degree in physics and mathematics, in 1998. Since 1998 till the present he is the Professor of Solid State Physics Department at Saratov State University. He is the author of more than 150 scientific publications, textbooks and inventions in area of solid state electronics, semiconductor physics and radiowave control, the member of the IEEE.
e-mail: SkripalA_V@info.sgu.ru
Saratov State University
Moskovskaya 155
Saratov, Russia

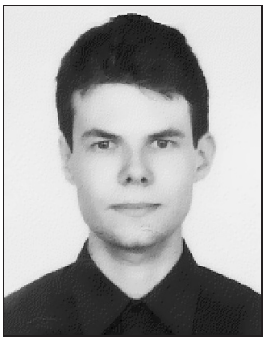

Anton V. Abramov has graduated from Physics Faculty of Saratov State University, Russia, in 2002. Since 2002 is the post-graduate student of Solid State Physics Department of Saratov State University. He is the author of 15 scientific publications. Field of scientific interests: semiconductor physics and solid state electronics. He is a Soros Foundation student.
e-mail: AbramovAV@info.sgu.ru
Saratov State University
Moskovskaya 155
Saratov, Russia

Paper

Vertical cavity surface emitting lasers in radio over fiber applications

Tamás Marozsák and Eszter Udvary

Abstract — Theoretical and experimental study of using direct modulated vertical cavity surface emitting lasers in radio over fiber applications is presented. The nonlinear distortion and signal to noise ratio are investigated and evaluated in case of short-range multi-carrier transmission. Nonlinear characterization and comparison of the different kind of semiconductor lasers are also presented.

Keywords — VCSEL, analog modulation, nonlinear distortion, radio over fiber.

1. Introduction

A modern communication system needs to be flexible, efficient, cheap, and should operate at high data rates. Such a system can use radio links between portable and mobile user equipment such as notebook computers and mobile telephones. This ensures flexibility and convenient services. For providing high capacity and for using the available frequency band efficiently the cell size should be small which requires many radio base stations or radio nodes as called in this paper. These radio nodes can be connected by optical fiber as a relatively cheap and high bandwidth solution. The optical fibers transmit the modulated radio carriers to the radio nodes allowing the radio node to be very simple. The optical fiber may transmit high data rate baseband digital signal as part of the local LAN at the same time.

For such a subcarrier multiplexed optical application great dynamic range and high linearity are required for the optical devices to have good system performance and avoid channel crosstalk. In the last few years the new generation of semiconductor lasers, the vertical cavity surface emitting lasers (VCSEL) proved to be competitive to the conventional, high performance edge emitting communication lasers [1]. In this paper some theoretical system considerations and the comparison of the different laser types based on spurious free dynamic range measurements are presented.

2. Signal to noise ratio

The figure of merit in a radio communication system is the signal to noise ratio (S/N) in the receiver. Because the radio nodes (RN) are fed by an optical link in the abovementioned radio over fiber system, the effect of the optical link should be considered. Figure 1 shows a simplified connection between a user and a radio node. The RN receives the optical signal by a high-speed photodetector (PD), it is amplified and transmitted by the antenna. In uplink direction the radio signal from the user is amplified by a low noise receiver, which directly modulates the laser source (LD).

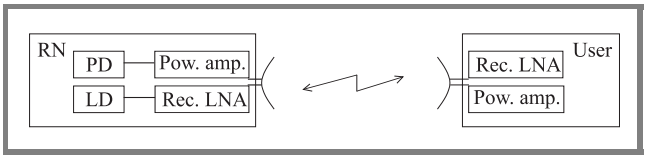

Fig. 1. Considering optical link noise in radio link.

The power amplifier in the RN will not degrade the signal to noise ratio coming from the PD. Because the signal and the transmitted noise are both attenuated in the radio channel, probably the receiver low noise amplifier (LNA) will determine the noise and hence, the S/N. In uplink direction the received signal is amplified by the RN LNA. The noise level after the LNA is probably higher than the relative intensity noise of the laser, which means that the noise of the optical link has no effect on the overall S/N, it will be determined by the radio link. More precisely this is the case if the S/N of the optical link is higher than the S/N of the radio link. To estimate the achievable signal to noise ratio in an optical link the nonlinearity and the noise of the optical link should be considered.

The laser relative intensity noise (RIN) and the receiver noise are the main noise sources in an optical link. It is a good assumption that the noise is determined by the laser if the optical attenuation is not high and this way the detected laser noise power is higher than the thermal noise of the receiver (the shot noise is usually smaller).

This is true if the fiber attenuation is less then

$$a = \frac{I_{ne}}{P_{LD} \cdot R_{PD} \cdot \sqrt{RIN}}, \tag{1}$$

where I_{ne} is the equivalent noise current density of the optical receiver, RIN is the laser intensity noise, P_{LD} is

the output power of the laser, R_{PD} is the photodiode responsivity. This gives $a = 10$ dB maximum fiber attenuation if $P_{LD} = 1$ mW, $RIN = 10^{-14}$ 1/Hz, $R_{PD} = = 1$ A/W and $I_{ne} = 10$ pA/Hz$^{1/2}$ which are practical device values. 10 dB attenuation is more than 30 km optical fiber, which is usually more than the distance range of microwave analog fiber optic links. This yields that the laser noise will determine the optical link performance.

The frequency dependence of the *RIN* can be rather high, especially when the optical back-reflection (BR) into the laser is high. Typical measured *RIN* spectra can be seen in Fig. 2 where a Ø14 μm multimode 850 nm VCSEL was measured at different bias currents. Above 5 mA bias the measurement was limited by the measurement setup. The highest relaxation oscillation frequency was around 7 GHz when 10 mA bias was applied than the optical power in the multimode fiber was 2 mW.

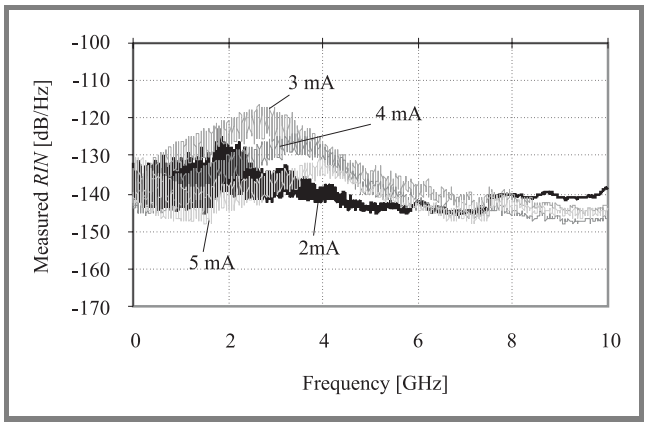

Fig. 2. Measured VCSEL relative intensity noise. Ripples caused by optical reflection.

From Fig. 2 it can be seen that $RIN = -140$ dB/Hz in average. Applying $m = 25\%$ modulation depth, which is a practical value with direct modulation, the S/N of the optical link:

$$\frac{\frac{1}{2}m^2}{RIN} = 125\frac{\text{dB}}{\text{Hz}}. \qquad (2)$$

This is usually much higher than the signal to noise ratio in radio links, but it must be noted, that linearity was not considered here (m should be lower if good linearity is required).

3. Nonlinear distortion

Linearity is especially important in subcarrier multiplexed systems. As the number of carriers increases the linearity problem become more and more serious because many odd (mainly third) order mixing products appear in the used band. The main source of intermodulation distortion in optical links is always the optical transmitter.

The figure of merit when the nonlinearity is investigated together with noise is the spurious free dynamic range (*SFDR*) defined as [2]:

$$SFDR = \frac{P_{in}(P_T = P_{noise})}{P_{in}(P_1 = P_{noise})} = \left[\frac{IP_3}{P_{noise}}\right]^{\frac{2}{3}}, \qquad (3)$$

where P_1 and P_T is the power of the detected fundamental and the third order mixing product, respectively, IP_3 is the third harmonic intercept point, P_{noise} is the detected noise power. This number is good figure of merit in performance characterization of an optical transmitter. Figure 3 compares the DFB, Fabry-Perot and VCSEL lasers in their *SFDR* measured as a function of the frequency and modulating signal power. The lasers were biased to 1 mW optical power. The curves show that the VCSEL exhibit the lowest *SFDR* and its curve is not that smooth as the others. This is mainly because the VCSEL was operated at 850 nm and the photodetector for that wavelength had high optical reflection. Still, the measured *SFDR* make this laser suitable for radio over fiber applications.

It can be seen that the *SFDR* decreases as the frequency increases. This is because the IP_3 decreases as the frequency approaches the laser relaxation oscillation frequency. It should be also noted that the *SFDR* should not change with the input power, but when P_{gen} is high the power of the higher order mixing products starts to be in the range of the main signal and the linear and cubic growth is not fulfilled for the fundamental and third harmonic mixing products respectively.

When the laser simultaneously transmits data in the baseband and on radio channels at RF as this possibility was mentioned in Section I, the second order nonlinearity also gets an important role. The baseband signal is mixed with the RF carriers causing distortions. This is shown in Fig. 4, where the laser was modulated with two RF carriers at 2 GHz (Fig. 4a) and than a 500 kHz baseband signal was added to them (Fig. 4b).

In Fig. 4 the laser was biased to 0.8 mW optical power in fiber, the modulation depth $m_{\text{BB}} = 2.7\%$ was for the base band and $m_{\text{RF}} = 11.4\%$ was for the RF signal. Increasing the laser power to 1.2 mW, and hence decreasing the modulation depths, the 3rd order product improved 15 dB, while the second order 9 dB. This yields that very low modulation depth has to be used to avoid distortions to degrade BER seriously. This could be avoided by up-converting the baseband signal into the RF also.

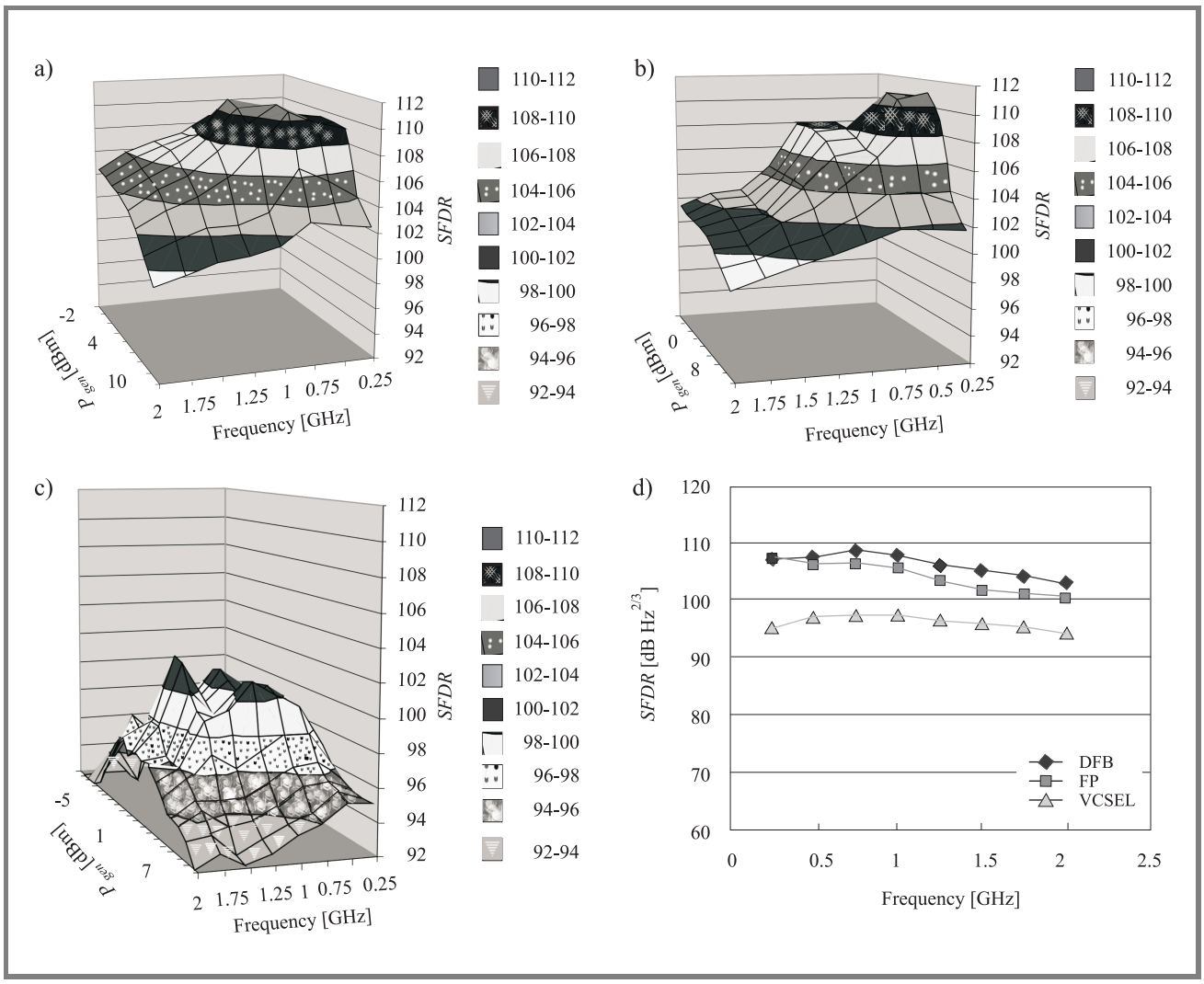

Fig. 3. *SFDR* versus frequency and modulating power for DFB (a), FP (b) and VCSEL (c) lasers. Comparison of *SFDR* as a function of the frequency for different laser types (d).

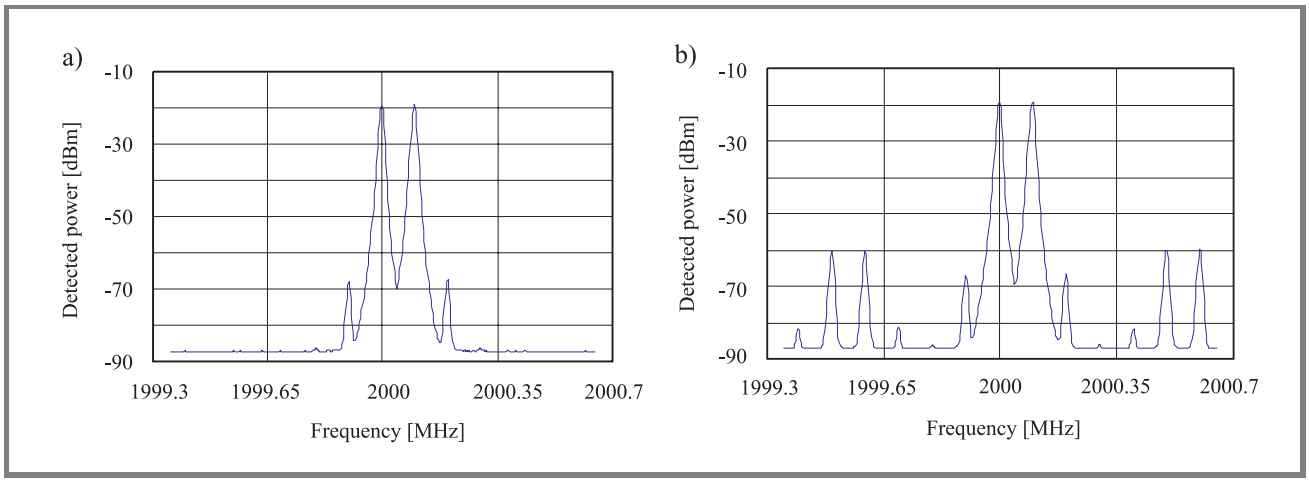

Fig. 4. Two tone intermodulation measurement (a) when a baseband signal was also added (b).

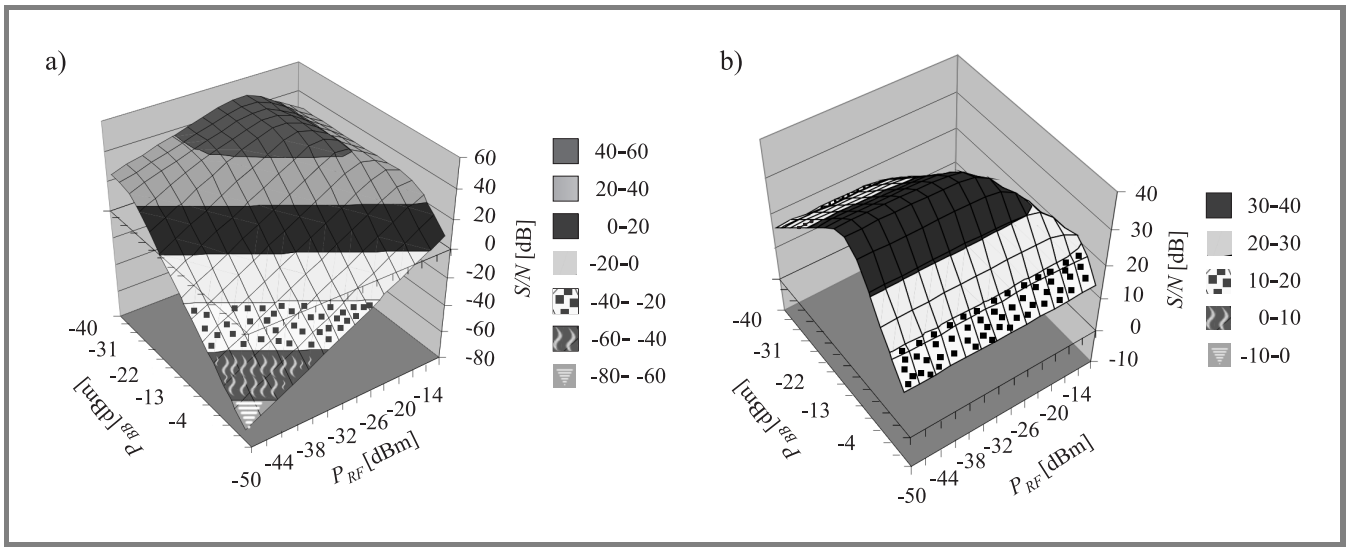

Fig. 5. Calculated signal to noise ratio in a radio channel (a) and in the baseband (b) as a function of modulating power in the baseband (P_{BB}) and in the radio band (P_{RF}).

4. System evaluation

The system described in the first section was evaluated by approximate calculations. The achievable signal to noise ratio was determined for the baseband signal and for a radio channel in the RF band. In the calculation the second and third order frequency conversions were considered. 10 equally spaced radio channels were supposed having 1 MHz modulation bandwidth each. The bandwidth of the baseband digital signal was 100 MHz representing a relatively high bit rate local area network. The parameters are summarized in Table 1. The IP_2, IP_3, *RIN* and slope efficiency parameters of the laser source are typical values coming from the measurements.

Table 1
Calculation parameters

Parametr	Value
Optical power	1 mW
RIN	−135 dB/Hz
Slope efficiency of laser source	0.3 W/A
IP_3 of laser source	−5 dBm
IP_2 of laser source	15 dBm
Photodetector responsivity	1 A/W
System impedance	50 Ω
Baseband bandwidth	100 MHz
RF bandwidth (1 channel)	1 MHz
Number of RF channels	10

The surface in Fig. 5a shows that if $P_{BB} > -19$ dBm the radio channel S/N start to decrease quickly and the same is true for the baseband if $P_{RF} > -20$ dBm (Fig. 5b). Choosing $P_{BB} = -22$ dBm and $P_{RF} = -20$ dBm seems to be good compromise, in that case $S/N_{RF} = 41$ dB, $S/N_{BB} = 21$ dB which are very good values.

5. Conclusion

The vertical cavity surface emitting lasers were compared to the popular FP and DFB lasers based on nonlinear dynamic measurements. Its spurious free dynamic range was less than the other candidates but the 95 dB $Hz^{2/3}$ value, measured in higher optical reflection environment, is still appropriate for radio over fiber applications. The measured values were used in a simple system performance calculation where radio carriers and digital signal in the baseband were transmitted at the same time. It was proved that high signal to noise ratio can be achieved with these lasers.

Acknowledgment

The authors acknowledge the Hungarian Scientific Research Fund (under the projects of OTKA no. F024113, T030148, T026557) and the COST 268 action of the European Union for their support.

References

[1] Ch. Carlsson, H. Martinsson, J. Vukusic, J. Halonen, and A. Larsson, "Nonlinear distortion reduction in transverse mode stabilized oxide-confined VCSELs", *Photon. Technol. Lett.*, vol. 13, no. 5, pp. 520–522, 2001.

[2] J. C. Fan *et. al.*, "Dynamic range requirements for microcellular personal communication systems using analog fiber-optic links", *IEEE-MTT*, vol. 45, p. 1390, Aug. 1997.

Tamás Marozsák received the M.Sc. degree in electrical engineering from the Technical University of Budapest (TUB), Hungary in 1995. Than became Ph.D. student at Department of Microwave Telecommunications in the field of optical communication. His main interest is microwave photonics, the application and modeling of semiconductor lasers, especially vertical cavity surface emitting lasers. He is author or co-author more than 30 technical papers.
e-mail: marozsak@mht.bme.hu
Department of Microwave Telecommunications
Budapest University of Technology and Economics
1111 Budapest, Goldmann Gy. ter 3
Hungary

Eszter Udvary received the M.Sc. degree in electrical engineering from the Technical University of Budapest (TUB), Hungary in 1997. Her M.Sc. thesis was on the design, fabrication and testing of microwave oscillators. Later she began Ph.D. study at the TUB, Department of Microwave Telecommunications. Her research interest includes optical and microwave communication systems, optical and microwave interactions and applications of special electro-optical devices. Her present field of interest is the application of semiconductor optical amplifier (SOA) in optical systems as amplifier, modulator and detector. She published more than 20 technical papers in these fields. She was awarded the Nokia MICROCOLL'99 young researcher conference prize and the URSI Young Scientist Award 2002.
e-mail: eszter.udvary@mht.bme.hu
Department of Microwave Telecommunications
Budapest University of Technology and Economics
1111 Budapest, Goldmann Gy. ter 3
Hungary

Paper

Evaluation of near field of the GSM base station antennas in urban environment

Dariusz Wójcik

Abstract — A simple and efficient method for evaluation of near field of the GSM base station antennas in urban environment is presented in this paper. The method is based on the replacement of panel antenna with a discrette linear array. Moreover, the geometrical optics approach is used to consider the influence of environment. The approximate results are found to be in excellent agreement with the results obtained by using the method of moments (MoM). Presented method can be successfully used for fast evaluation of exposure to electromagnetic fields emitted by the GSM base station antennas in urban environment.

Keywords — RF dosimetries, human exposure, radio base station, ray tracing.

1. Introduction

The rapid diffusion of wireless communication systems, specifically in cellular technology, has caused an increased concern for the potential detrimental effects on human health resulting from exposure to electromagnetic fields radiated by the antennas of these systems. This problem should be considered in two different aspects. The first one contains possible health hazards due to handheld phone devices. The second aspect, which this paper is devoted to, relates to EM fields emitted by the base station antennas.

Up to now, the exposure to the base station antennas has been studied in free space [6–9] and in urban environment in far field [10] only. Thus, the problem of exposure evaluation in near field in urban environment is still to be solved.

In the far-field region, which is defined as "the region of the field of an antenna where the angular field distribution is essentially independent of the distance from the antenna" [1], the EM field can be relatively easily calculated, since all required information is the gain pattern of antenna and the radiated power. If the antenna has a maximum overall dimension D, the far field region is commonly taken to exist at radial distances from the source grater then $R = 2D^2/\lambda$, with λ denoting the wavelength. At distances less then R, in the near-field region, the EM fields usually have very complicated morphology, which is difficult to evaluate. For the typical GSM base station panel antennas ($D \approx 1.3$ m) the boundary between near- and far-field is located at the distance ~ 10 m and ~ 20 m for GSM 900 MHz and GSM 1800 MHz, respectively. Additionally, in urban environment the exposure conditions are quite different from those for free space, due to many scattering objects which are usually present in vicinity of antennas (trees, buildings, etc.).

The techniques of "rigorous" numerical modelling, as moment method (MoM) or Finite Differences Time-Domain method, are mostly used for studying the near field of antennas. The most common problem connected with application of these methods is knowledge of geometry of the base station antennas. Additionally, when exposure in urban environment is modelled, dimensions of the region to be studied can be huge compared with the wavelength, and consequently the time needed for analysis is unacceptably long. Thus, a simple and reliable calculation method for prediction of exposure to electromagnetic fields in urban environment is needed.

In this paper, a simple, accurate and computationally efficient method for evaluation of near field of the GSM base station antennas in urban environment is presented. The method is based on the replacement of panel antenna with a linear discrete array. Moreover, the geometrical optics approach is used to evaluate the influence of environment. In order to use geometrical optics the two-dimensional ray-tracing algorithm is employed. The approximate results are compared with those obtained by using the method of moments. Proposed method can be successfully used for fast evaluation of exposure to electromagnetic fields emitted by the GSM base station antennas.

2. Geometry of the base station antennas

Panel antennas seem to be the most popular for GSM 900 MHz as well as for GSM 1800 MHz base stations. The typical panel GSM 900 MHz antenna geometry is shown in Fig. 1. The geometry of the model is reasonably close to that of the 730370 antenna [12]. The antenna consists of an array of four collinear dipoles with horizontal separators placed in front of a reflector having the dimensions (height $\times$ width) 1280×240 mm. As it can be observed in Fig. 1 the antenna is made up of four identical "cells".

For this antenna, its catalogue data are as follows: $G = 14$ dBi (25.1 W/W), half power beamwidth in principal E- and H-plane 90° and 13°, respectively. The antenna is representative for the "Eurocell Panels" family of base station antennas for vertical polarization, commercially available in the frequency range from 870 to 960 MHz.

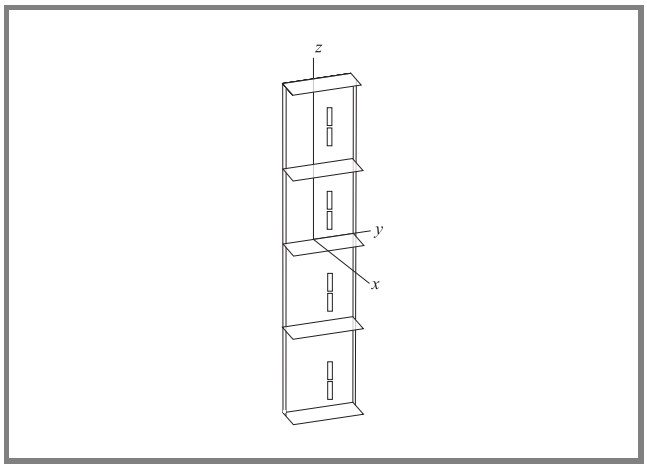

Fig. 1. Typical GSM base station panel antenna.

3. Near field of isolated antenna

A simple and effective method for evaluation of the near field of the GSM base station antennas is presented in [3, 9]. The method is based on the replacement of antenna with a linear discrete array. Every single "cell" of the original panel antenna is modelled by one source of the array.
Consider the array of N sources, as shown in Fig. 2. The fields emitted by every single source are calculated using far-field equations. The total EM fields in a particular observation point are obtained as a sum of the fields radiated by individual sources. The phase shifts arisen from

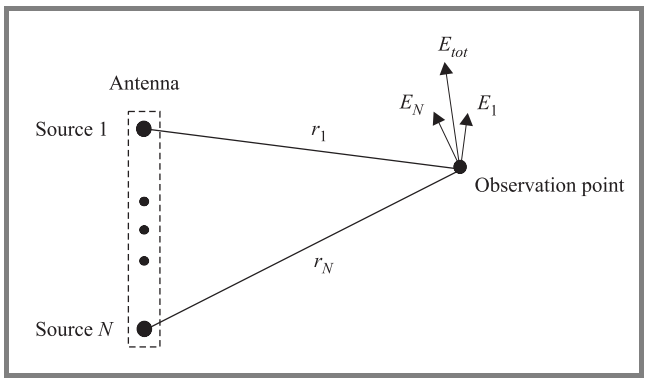

Fig. 2. Linear array as a model of base station antenna.

different distances between particular sources and the observation point are also included. Therefore, for a vertical polarization antenna, the total electric field is described by the following equation

$$\boldsymbol{E}_{tot}(\boldsymbol{r}) = \sqrt{\frac{30P}{N}} \sum_{i=1}^{N} \frac{\sqrt{G_s(\theta_i,\phi_i)}}{r_i} e^{-jkr_i} \mathbf{1}_{\theta_i}\,, \qquad (1)$$

where N is the number of "cells" of the antenna under investigation and at the same time it is the number of sources in its model; P is the radiated power and G_s is the gain pattern of unit cell. Distance between the source and the observation point is denoted as r_i, and $\boldsymbol{r}$ is a position vector associated with an observation point in the global coordinate system.
To apply Eq. (1), knowledge of the gain pattern of the unit cell of the antenna is necessary. It was found [9] that for the typical base station panel antennas sufficient approach of the gain pattern of the unit "cell" is function as follows

$$G_s(\theta,\phi) = \begin{cases} G_{\max} \sin^m(\theta) \cos^n(\frac{\phi}{2}) & -90 < \phi < 90 \\ 0 & \text{elsewhere.} \end{cases} \qquad (2)$$

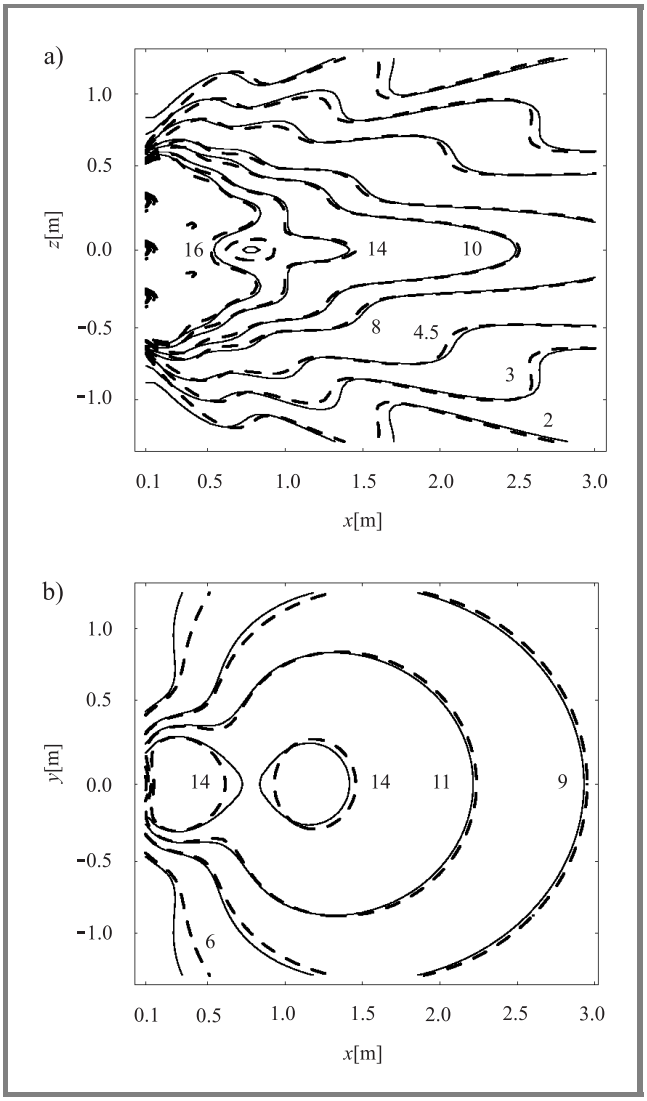

Fig. 3. Isolines of the electric field [V/m] in vicinity of 730370 antenna (radiated power 1 W) in principle E-plane (a) and H-plane (b), which were carried out using MoM (solid lines) and presented approach (dashed lines).

To obtain the appropriate half beamwidth of the antenna in principle E- and H-plain, values of respectively n and m should be calculated properly.
In order to examine the accuracy of presented calculating method, the approximated results are compared with the

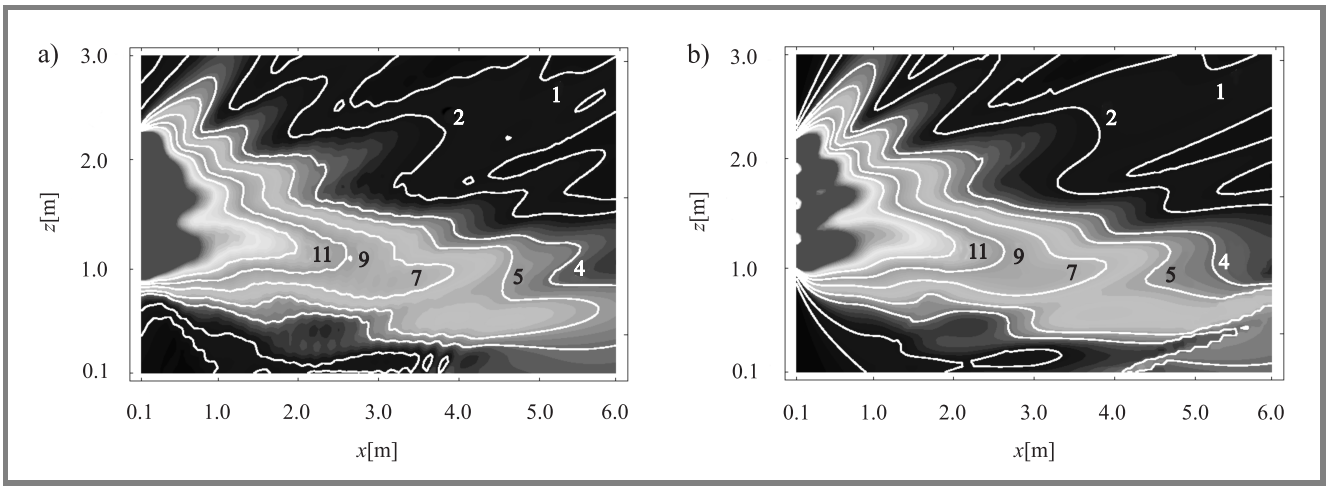

Fig. 4. Electric field [V/m] in vicinity of 730370 antenna (radiated power 1 W) placed 1m above and 1m in front of perfectly conducting plain, which were carried out using MoM (a) and ray-tracing approach (b).

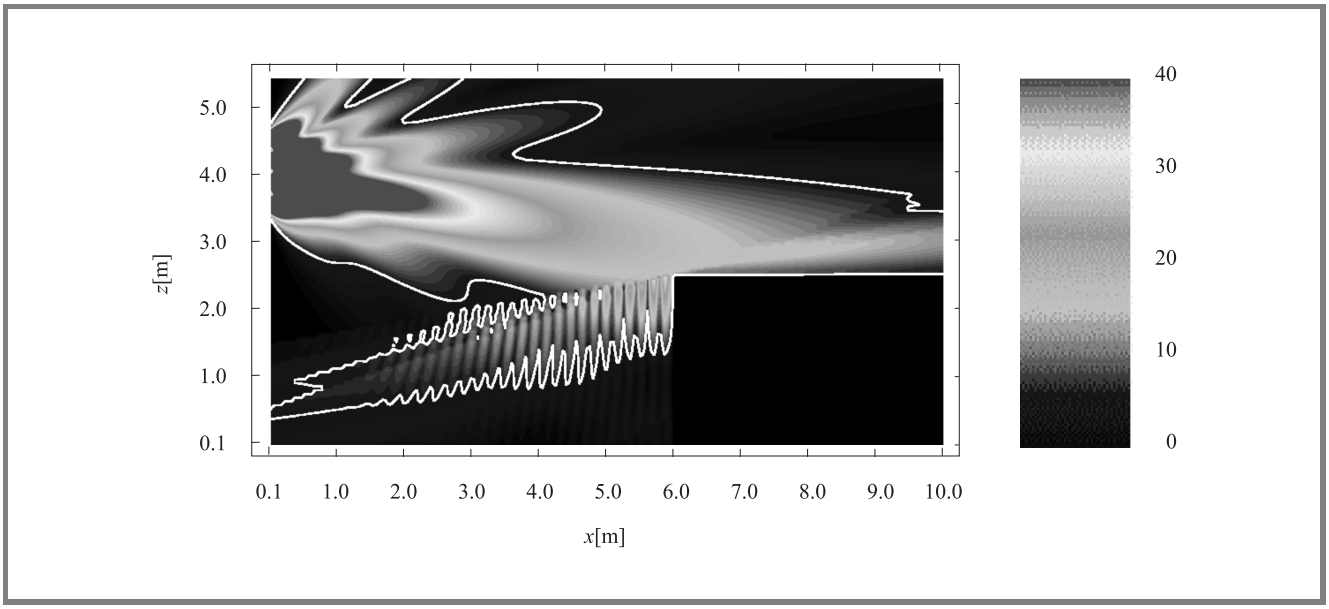

Fig. 5. The electric field [V/m] in vicinity of 730370 antenna (radiated power 15 W) placed in neighbourhood of a building.

results of numerical simulations, which were carried out using a customised, extended version of moment method based code MOMIC [2], which is specialized to wires and wire-grid structures. Isolines of the electric field in vicinity of 730370 antenna are shown in Fig. 3. One may notice that the approximated results are in excellent agreement with the full-wave analysis results.

4. Influence of the urban environment

To take under consideration the influence of scattering objects present in vicinity of antenna the geometrical optics approach has been used. Geometrical optics is a high-frequency asymptotic technique, which can be used to analyze objects large in comparison with the wavelength. Geometrical optics takes into consideration reflection and refraction mechanisms. Obviously, the edge diffraction mechanism also can play an important role in this case, which is omitted in presented approximations.

In order to use geometrical optics two-dimensional ray-tracing algorithm is employed. Recently, ray-tracing techniques have been widely used to predict radio propagation in indoor and outdoor environments [4, 5]. This approach has been also used to evaluate EM exposure level in the far field of the antenna in urban environment [10]. Ray-tracing gives reliable predictions of the EM field values only in the far-field region, where the antenna can be represented by the source point. However, if base station antenna can be

replaced with linear array, ray-tracing approach will be reliable for calculating field close to antenna as well.
In Fig. 4, the electric field in vicinity of the antenna placed 1 m above and 1 m in front of the perfectly electrically conducting rectangular plane is shown. The dimensions of the plane are $(x \times y)$ 3 m $\times 1$ m. The antenna has 11° electric down-tilt and emits power of 1 W. However, practically such analysis is not very valuable, it allows to validate the presented method because this case can be easily analyzed using the moment method as well. As it can be easily seen the proposed approach shows a good accuracy. Figure 5 describes the electric field morphology which appears in the surrounding of a building placed in vicinity of GSM base station antenna. The roof of the building is represented by perfectly conducting plane and the walls electrical parameters are $\varepsilon_r = 5$ and $\sigma = 0$ [4]. The building is located 1.5 m below antenna and 6 m in front of it. The antenna has 11° electric down-tilt and emits power of 15 W. As can be observed the field morphology is deformed by the building. There are reflections from the roof and wall, which causes the standing-wave in front of the building. In Fig. 5, an isoline of electric field intensity of 6.14 V/m is also marked. This value of electric field intensity corresponds in free space with power density of 0.1 W/m^2, which is maximum EM fields intensity permitted for general public by polish national recommendation on limitation of exposure to electromagnetic fields [11]. It is clearly seen that the shape of this isoline is quite different from the shape of appropriate isoline occurred in free space.

5. Conclusions

In this paper, a simple, accurate and computationally effective method for evaluation of near field of the GSM base station antennas in urban environment is presented. The method is based on the replacement of panel antenna with linear discrete array. Moreover, geometrical optics approach is used to evaluate the influence of environment. A number of comparisons between approximate results and full-wave analysis results carried out by author have proved that the proposed approach method is possible to estimate exposure to the near field of the GSM base station antenna in urban environment accurately.

References

[1] C. A. Balanis, *Antenna Theory: Analysis and Design*. New York: Wiley, 1997.

[2] A. Karwowski, "MOMIC – a computer program for analysis of wire antennas and scatterers", in *Proc. Nat. Telecommun. Symp. KST'97*, Bydgoszcz, Poland, 1997, vol. D, pp. 395–404 (in Polish) (also http://emlib.jpl.nasa.gov/EMLIB/MOMIC/).

[3] R. Mawrey, T. Riley, J. Higgins, and S. Slayden, "Predicting power density near antennas to met FCC RF safety regulation", *Mob. Radio Technol.*, pp. 36–47, Sept. 1997.

[4] Zhong Ji, Bin-Hong Li, Hsing-Yi Chen, and T. K. Sarkar, "Effective ray-tracing methods for propagation prediction for indoor wireless comunications", *IEEE Anten. Propagat. Magaz.*, no. 2, pp. 41–19, 2001.

[5] D. Ericolo and P. Uslenghi, "Two-dimensional simulator for propagation in urban environment", *IEEE Trans. Veh. Technol.*, vol. 50, no. 4, pp. 1158–1168, 2001.

[6] Z. Altman, A. Karwowski, M. Wong, J. Wiart, and L. Gattoufi, "Dosimetric analysis of base station antennas via simulation and measurements", in *15th Int. Wrocław Symp. Electromagn. Compab. EMC'2000*, Wrocław, Poland, 2000, part 1, pp. 240–244.

[7] A. Karwowski, "Comparision of simple models for predicting radiofrequency fields in vicinity of base station antennas", *Electron. Lett.*, vol. 36, no. 10, pp. 859–861, 2000.

[8] A. Karwowski and D. Wójcik, "Near field of the GSM base station antennas", in *Proc. Nat. Telecommun. Symp. KST'2000*, Bydgoszcz, Poland, 2000, vol. B, pp. 123–132 (in Polish).

[9] D. Wójcik, "Near field of the GSM base station antennas array", in *Proc. VIII Nat. Conf. KOWBAN'2001*, Świeradów-Zdrój, Poland, 2001, pp. 123–132 (in Polish).

[10] P. Bernardi, M. Cavagnaro, S. Pisa, and E. Piuzzi, "Human exposure to radio base-station antennas in urban environment", *IEEE Trans. Microw. Theory Techn.*, vol. 48, no. 11, pp. 1996–2001, 2000.

[11] "Rozporządzenie MOŚZNiL z dnia 11 sierpnia 1998 r. w sprawie szczegółowych zasad ochrony przed promieniowaniem szkodliwym dla ludzi i środowiska, dopuszczalnych poziomów promieniowania, jakie mogą występować w środowisku, oraz wymagań obowiązujących przy wykonywaniu pomiarów kontrolnych promieniowania", *Dz. U. RP*, 1998, nr 107, poz. 676 (in Polish).

[12] *Kathrein – Antennas for Mobile Communications*. Version 4, Edition 05/00.

Dariusz Wójcik was born in Czeladź, Poland, on January 10, 1974. He received M.Sc. degree in the field of electronics and telecommunications from Silesian University of Technology, Gliwice, Poland, in 1999. He is currently working towards Ph.D. degree in computational electromagnetics (MoM, FDTD) and issues of human exposure to EM field, particularly those emitted by radio base stations.
e-mail: dwojcik@polsl.gliwice.pl
Institute of Electronics
Silesian University of Technology
ul. Akademicka 16
44-100 Gliwice, Poland

Paper

Integration of home digital network and Bluetooth wireless communication system

Tomasz Keller and Józef Modelski

Abstract — The paper presents new method of integration home digital network with Bluetooth wireless communication system. In this new application Bluetooth is used as one of the main ways of communication and information exchange between elements of the system for integrated, centralized control of the digital devices in the multimedia home platform. Bluetooth enables communication between multimedia gateway with the HTTP server inside and personal communication assistants (PCA), special kind of the remote control. The aim of the system is centralization of services in the multimedia gateway and integration of different services using only one control device.

Keywords — wireless communications, multimedia systems, multimedia services, multimedia home platform, digital network.

1. Introduction

With the very fast growth of the modern transmission techniques there are also quite different requests of the potential subscribers for the integration of the services from different media. Good example of this situation is our house's environment. Nowadays subscribers have a lot of services from different devices and it is very hard to control all of them using only one device. It is not good time for using varied control system for different devices. That is the reason why one of the main features of the future house will be complex system for the integrated control of the home digital network. After that, users receive a huge amount of data transmitted from the digital television operators to home set-top boxes (STB). So, it is necessary to prepare the real system for the integrated control of the home digital network devices.

In this paper authors would like to introduce a new system for integrated control of home digital network devices, which was prepared in the Institute of Radioelectronics, Warsaw University of Technology. One of the main purposes for this kind of system was to use efficient way of communication between user's control devices (PCA) and multimedia gateway. According to its obvious limitations it was impossible to use infrared communication protocol. Authors decided that the best solution would be using Bluetooth radio communication interface. The reasons for this decision and main features of Bluetooth communication interface will be described in the next sections. During creating the system authors had to create new language of the device's communication connected with the services and devices description. This special language will be described in the next sections.

System is divided into three parts. The central part of the system is the multimedia gateway with a HTTP server inside. Multimedia gateway receives requests and sends responses to the control devices. The second part of the system is Bluetooth/HTTP bridge. The bridge creates HTTP connection with multimedia gateway every time document arrives, sends and receives documents and searches the environment for new Bluetooth devices. The last part of the system is a specially designed PCA. In fact it is an advanced remote controller with the keyboard and graphics display.

2. Bluetooth radio interface

The first problem during creating system for integrated control of home digital network devices was choosing special protocol for communication between system elements. From the beginning of creating the system it was obvious, that for the communication between user's control devices and multimedia gateway should be used one of the wireless communication protocol. The protocol used in the system should be cheap, effective and secure solution. There were two choices – infrared protocol (IrDA) and Bluetooth communication interface.

Nowadays the most popular system is the infrared data communication protocol. It enables effective and secure data transfer with direct connection point – point [1]. Another features of the IrDA is low power consumption and simple cheap implementation. However, for this kind of system IrDA has some limitations and it was impossible to use this interface. First of all, IrDA enables only point – point communication, so with using IrDA there should be only one control device controlling each of home devices. This obvious limitation excludes utilization of this protocol in the system. Another disadvantage of the infrared communication protocol is line-of-sight feature and very narrow (30 degree) angle of proper functionality. One of the objectives of the system is the possibility of controlling all home devices from any place in the house and the features of infrared communication does not allow to this. Mentioned features caused that it was impossible to use IrDA in the system. In this case authors decided that better solution would be using Bluetooth wireless communication interface.

Initially Bluetooth wireless technology was created to solve a problem of replacing cables used for communication between such devices as: laptops, palmtops, personal digital assistant (PDA), cellular phones and other mobile devices [2]. Now Bluetooth enables users to connect to a wide range of computing and telecommunications devices without any need of connecting cables to the devices. Bluetooth is a radio frequency specification for short range, point-to-multipoint voice and data transfer. It operates in the 2.4 GHz ISM (Industrial-Scientific-Medical) band. This band is free for use, so it is not necessary to have special license for communicating in this frequency range. Of course this range is full of other signals from different devices, so it should have special methods of preventing interference with other signal. Bluetooth uses the frequency hopping (FH) technology and it avoids from the interference. It is also the reason, why Bluetooth is very secure protocol. Bluetooth is based on a low-cost, short-range radio link and enables communication via ad hoc networks. Main features of the Bluetooth communication protocol are [3]:

– nominal link range is 10 m, it can be extended to 100 m by increasing transmit power;

– connection is created every time, it is needed by using the ad hoc networks;

– basic unit in Bluetooth networks is a piconet, it supports up to 8 devices (1 master device and up to 7 slave devices);

– one Bluetooth device can be a part of different piconets, they can exist simultaneously;

– possible transmission through solid, non-metal objects;

– built-in methods of security and preventing interferences;

– Bluetooth allows easy integration of TCP/IP for networking;

– there are two types of possible transmission: synchronous and asynchronous.

Despite of the short range, Bluetooth protocol has also a lot of advantages that are very important in designed type of system [4]. These are:

– it is not necessary for the devices communicating using this protocol to directly see each other;

– very easy network creation and configuration (very efficient methods of looking for devices in the neighbourhood);

– possibilities of moving devices in the neighbourhood, not required line-of-sight.

All the presented features of Bluetooth wireless communication protocol and very rapid growth of the standard confirm, that Bluetooth is suitable solution for using in a system for integrated control of home digital network devices.

3. System architecture

As it was mentioned in an introduction, the whole system is divided into three main parts: PCA, Bluetooth/HTTP bridge and multimedia gateway. The general concept of the system architecture is presented in Fig. 1.

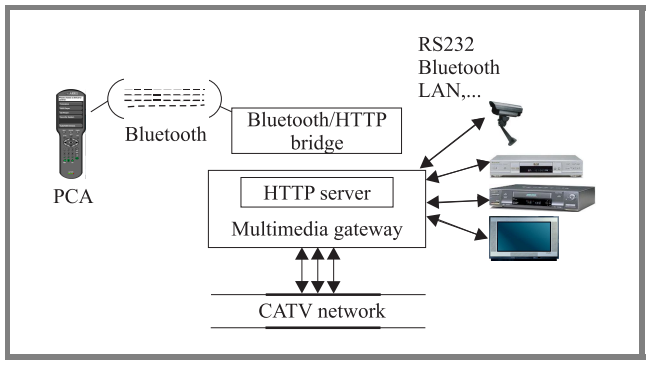

Fig. 1. General system architecture.

3.1. Personal communication assistant

The first part of the system is specially designed PCA. In fact it is an advanced remote controller with the keyboard and graphics display. One of the main objectives of the system is to enable the use of different services from the number of devices via the multimedia gateway and PCA from any place in the house, so for the communication between PCA and multimedia gateway, Bluetooth wireless protocol is used.

To extend the Java platform to consumer and embedded devices, Sun Microsystems developed special platform – J2ME (Java 2 Microedition). This platform is specially designed for programming such devices like: mobile phones, pagers, PDA, set-top boxes and others. This type of devices require special type of smaller Java virtual machine (VM), which is optimized for this environment. The core component of the J2ME platform is a special type of virtual machine called K-virtual machine (KVM). KVM is a Java virtual machine implementation designed specifically for small, resource-limited devices, it is based on the Spotless system developed originally at Sun Labs. KVM requires small computing resources (16-bits RISC or CISC processors) and small memory resources (160 – 512 kbit). There are two different configurations defined in the J2ME platform [5]:

– CLDC: designed for low-end consumer devices which have at least 160 kB available for the Java platform, processor speed starting from 16 MHz, limited power with usually battery operation and low-bandwidth connectivity and static size of the Java platform (VM + libraries);

– CDC: designed for high-end consumer devices with at least 2 MB available for the Java platform TCP/IP connectivity available.

Except these two different configurations there are different profiles in J2ME designed to accommodate the needs of a specific mobile consumer device market. Particularly, the mobile information device profile (MIDP) defines the architecture and API required to create applications for small, low-power mobile information devices like cell phones, pagers or PDA.

For the simulation of PCA authors used complete development environment which can help in creating and testing applications for mobile devices. Authors had at disposal also two Bluetooth communication modules with the programming interface and the programming simulation of the communication devices. The configuration of the modules was connected limited device configuration (CLDC) with the profile MIDP implemented. This configuration of the application platform enabled running applications with the KVM [6]. It was very good, because the PCA should be very cheap, effective solution with the minimum costs of production. Of course in these modules only basic Java classes from the main Java packages (java.lang, java.io, java.util) were implemented. There were also some classes for the creating user interfaces with the basic components for the small displays with limited number of buttons.

3.2. Bluetooth/HTTP bridge

Because Bluetooth modules were prepared to work with simulation environment in J2ME platform, it was not possible to use it in J2SE (Java 2 Standard Edition) platform. J2SE was necessary for using HTTP server in the main part of the system – multimedia gateway. That is the reason, why the third element of the system – Bluetooth/HTTP bridge was created. Bluetooth modules and API used in the system were not dedicated for Java 2 Standard Edition. They were designed for Java 2 Microedition, so it was necessary to create the bridge that would enable to convert the documents between Java 2 Microedition in PCA and Java 2 Standard Edition in multimedia gateway. Of course it is not the only objective of the bridge.

All the data exchange between PCA and multimedia gateway is done by using XML transaction documents. The first step of any action in the system is sending by the PCA transaction document with the service request. After finishing the action gateway sends to PCA transaction document with the service response. All ways of information exchange will be introduced in the next section. The main problem is that service request from the PCA is in a format not recognized by HTTP server. There has to be done conversion from Bluetooth data to HTTP request. Also in the return way, HTTP response document from server has to be converted to Bluetooth data message. All these conversions are done in the Bluetooth/HTTP bridge. After conversion the bridge sends request to multimedia gateway and response to PCA.

Every time transaction document from PCA arrives, the bridge creates the HTTP connection with multimedia gateway. There is no need of keeping this connection all the time, so it is created only if it is necessary. On the other hand, there is no constant connection between the bridge and PCA. One of the main features of Bluetooth protocol is that there is a possibility of creating ad hoc networks always, when Bluetooth device appears in the neighbourhood of other Bluetooth device. So, the bridge must search the neighbourhood and always when other Bluetooth device appears create the connection and assign them individual threads.

3.3. Multimedia gateway

The main part of the system is multimedia gateway, which is the communication node of the system. Multimedia gateway has a direct connection to all devices in home digital network. The gateway enables also the contact with the outside environment. The system of the integrated control of the home digital network (HDN) is based on the client – server architecture, where the clients are PCA and the server for the services concentrating is the multimedia gateway, which works as a HTTP server. There is also Java servlet technology in the gateway implemented.

According to the memory limitations of the PCA, it was necessary to treat PCA only as a navigation device, a kind of terminal for the multimedia gateway. In the multimedia gateway all services were centralized. Using HTTP server allows easier implementation of multi-access and multithread services. There is also the possibility to recall gateway using WWW, with very easy Internet based control. Multimedia gateway with the HTTP server can be used as a stand-alone device in the home neighbourhood. It can be also part of the advanced set-top box and can be at the subscriber's house or in the head-end as well.

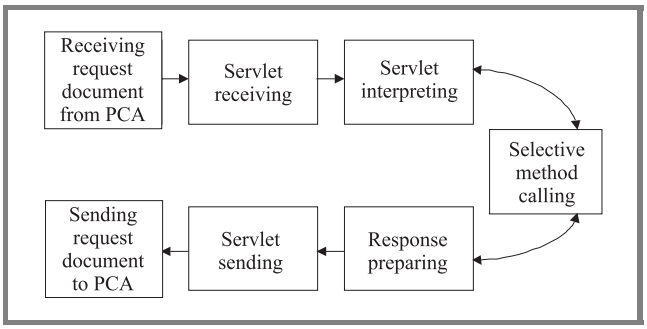

Fig. 2. Information flow at the multimedia gateway side diagram.

The protocol of the information between gateway and PCA is based on the exchange of the XML transaction documents. The diagram of the information flow in the system is presented in Fig. 2. The fundamental of any action in the system is sending by the PCA transaction document with the service request. This document is sent as a text stream to the Bluetooth/HTTP bridge, where it is changed

to the parameter of the servlet in the HTTP server. Multimedia gateway sends its response to the output stream of the HTTP server, then it is sending via the Bluetooth/HTTP bridge to the PCA.
First step of the session is a logging procedure – PCA sends to the gateway transaction document with user authentication information. As a response for correct logging procedure gateway sends to PCA main document with a set of services, ways of presentation services at the PCA's side and the action joined with the elements. Based on the main document PCA lists all available services on its screen. Choosing one of the menu element causes either execution of the action (sending proper transaction document) or entering to the next level of menu. After receiving request transaction document multimedia gateway executes actions and sends as fast as it is possible response document which is displayed on the PCA. After the user action PCA returns to the last menu, after executing all the needed services user do the logging out procedure and the session is closed.
Although to the most of the services this schema is good, there are a number of services with another way of the information flow. First of all these are notification services with the information about incoming new e-mail or caller identification of the new telephone call. It is well known, that in this case the initiative should not be from PCA but from the multimedia gateway.
Of course all data exchange between gateway and PCA is done with use of the Bluetooth/HTTP bridge. The bridge transforms Bluetooth data streams to HTTP requests and the other way round. Bridge is fully transparent for the documents.

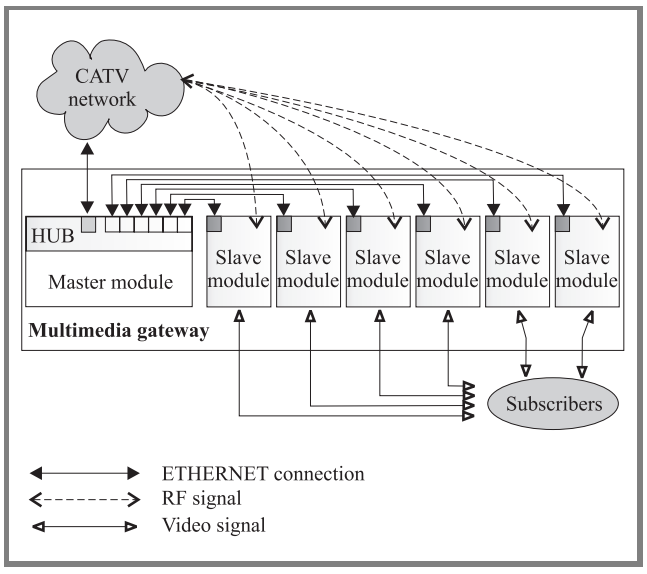

Fig. 3. The concept of multimedia gateway.

As it was mentioned before, using Bluetooth wireless communication protocol it is possible to use ad-hoc network, creating at the moment when it is necessary. Of course there is a possibility for multiple users to connecting to multimedia gateway simultaneously. If there are more than one PCA, Bluetooth master device can assign them individual threads and create special piconet. HTTP server inside multimedia gateway is also designed for multi-user operations. All this features make it possible to create one gateway designed for more than one user. This kind of multi-user multimedia gateway is presented in Fig. 3.
Designed multimedia gateway consists of one master module and number of slave modules. User's personal control devices communicate with master module via Bluetooth communication protocol. For connection between master and slave modules Ethernet cards are used. Multimedia gateway is connected to CATV network and have all possible input and output interfaces.

4. Types of transaction documents

There are three different types of XML transaction documents in the system: request document, response document and system main document. All of the types are described below.

4.1. Request document

Request document is sent by the PCA every time any service execution is needed. XML transaction request document contains all necessary information about desired service. In Fig. 4 is an example of request document.

```
<REQUEST>
    <CLIENT bda=„fff1" devicename=„PCA1"
        devicetype=„PCA"username=„Jerzy"/>
    <GATEWAY httphost=„localhost"
        servicename=„STBNavigator"
        serviceclass=„STBEngine"/>
    <PARAMname=„command" value=„channelup"/>
    <PARAMname=„execmode" value=„immediate"/>
</REQUEST>
```

Fig. 4. Example of request document.

Request document contains description of the client sending request, address of the target multimedia gateway, name of the required service, name of the class (driver) servicing the request and other parameters required to execute the service.

4.2. Response main document

There are two types of response documents: response main document and response simple document. Response main document is sent by the gateway to PCA as a response of logging procedure. In Fig. 5 is an example of this kind of document.
Response main document contains description of the menu tree, description of all user interface components and description of actions assigned to user interface components.

```
<RESPONSE type=„main”>
  <GATEWAY httphost=„localhost”
           servicename=„SystemLogin”
           serviceclass=„UserManager”/>
    <CLIENT bda=„fff1” devicename=„PCA1”
            devicetype=„PCA” username=„Jerzy”/>
    <CONTENT>
      <DISPLAY type=„menuset”>
        <MENUITEM caption=„ChannelDown”>
          <ACTION type=„GatewayRequest”>
            <GATEWAY httphost-„localhost”
                     servicename=„STBNavigator”
                     serviceclass=„STBEngine”/>
            <PARAM name=„command”
                   value=„channeldown”/>
            <PARAM name=„execmode”
                   value=„immediate”/>
          </ACTION>
        </MENUITEM>
      </DISPLAY>
    </CONTENT>
  </PARAM name=„execmode” value=„immediate”/>
</RESPONSE>
```

Fig. 5. Example of response main document.

4.3. Response simple document

Response simple document is sent by the gateway to PCA as a response for all client requests. In Fig. 6 is an example of this kind of document.

```
<RESPONSE type=„simple”>
    <GATEWAY httphost=„localhost”
             servicename=„STBNavigator”
             serviceclass=„STBEngine”/>
    <CLIENT bda=„fff1” devicename=„PCA1”
             devicetype=„PCA” username=„Jerzy”/
><CONTENT>
    <DISPLAY type=„none”/>
    <HIDDEN
      <DATAITEM name=„status” value=„ok.”/>
    </HIDDEN>
  </CONTENT></RESPONSE>
```

Fig. 6. Example of response simple document.

Response simple document contains description of the client sending the request, description of gateway from which response arrives and all the data as a result of command execution.

5. Conclusions

Authors proposed new architecture of the integration of home digital network with Bluetooth communication network. As an example of this application system for integrated control of home digital network devices was presented. Author's decision was to place central part of the system in the multimedia gateway and to use a HTTP server in the system. All services are centralized in multimedia gateway, user's control devices (PCA) are only terminals transmitting to gateway XML transactions documents.
Using all the features of Bluetooth communication interface it was possible to create efficient way of communication between devices, gateway and PCA. To enable this, authors have also created new language of the device's communication connected with the services and devices description. Using XML transaction documents made the system very flexible. Developing of the system and adding new services is also very easy – there is no need to modify the whole system but only one service module.
One of the other advantages of this system architecture is the fact, that the gateway need not be placed at the user's house – it can be placed at the cable television operator's side or completely different place in Internet.

References

[1] D. Suvak, "IrDA and Bluetooth: a complementary comparison", Extended Systems Inc., 2000.
[2] "Bluetooth protocol architecture", White Paper, Bluetooth SIG, 1999.
[3] "Bluetooth technology", White Paper, Compaq Computer Corporation, Nov. 2000.
[4] B. A. Miller and Ch. Bisdikian, *Bluetooth Revealed: The Insider's Guide to an Open Specification for Global Wireless Communications*. Prentice Hall PTR, 2002.
[5] "Java 2 Microedition technology", White Paper, Sun Microsystems, 2000.
[6] E. Giguere, *Java2 Microedition: Professional Developer's Guide*. Wiley, Nov. 2000.

Tomasz Keller was born in Warsaw, Poland, in 1975. He received the M.Sc. degree in electronics engineering from Warsaw University of Technology, Institute of Radioelectronics, Television Division in 1999. Since 1999 he is a Ph.D. student at Television Division, Institute of Radioelectronics, Warsaw University of Technology. His research is focused on multimedia and television systems and wireless communication protocols in ISM band. During his Ph.D. studies he worked on several projects related to multimedia systems: "Modification to Power TV and Broadcast Software for WCS to Achieve Demo Quality" in 2000, "Home Multimedia Platform" in 2001. He is an author or co-author of 10 technical papers printed in journals and presented at scientific conferences, including 4 papers presented at international conferences.
e-mail: t.keller@ire.pw.edu.pl
Institute of Radioelectronics
Warsaw University of Technology
Nowowiejska st 15/19
00-665 Warsaw, Poland

Józef Modelski received the M.Sc., Ph.D. and D.Sc. (habilitation) degrees in electronics from Warsaw University of Technology in 1973, 1978, and 1987, respectively. In 1994 he obtained the State title of Professor. Since 1973 he has been with the Institute of Radioelectronics, Warsaw University of Technology (WUT) holding in sequence all academic positions from teaching/research assistant to tenured professor (1991). In 1976/77 he spent 13 months in U.S. as a Fulbright grantee working with the microwave laboratories: at the Texas University at Austin, Cornell University, and Communication Satellite Corporation COMSAT. In 1986 he joined for two years the Braunschweig Technical University (Germany) as a senior scientist. His research interests are in the areas of microwave phase modulators and shifters with semiconductor and ferrite elements, dielectric resonators and their applications, integrating waveguide technology for mass-production components, and design of communications antennas. He has published over 120 technical papers and 4 books, obtained 8 patents and many awards. Since 1996 J. Modelski has been Director of the Institute of Radioelectronics, WUT. He is chairing scientific boards in two research centers and International Microwave Conference MIKON, is a member of the TPCs of MTTS International Microwave Symposium, European Microwave Conference and many local conferences. He is IEEE Fellow Member.

e-mail: j.modelski@ire.pw.edu.pl
Institute of Radioelectronics
Warsaw University of Technology
Nowowiejska st 15/19
00-655 Warsaw, Poland

Paper

Applying the relational modelling and knowledge-based techniques to the emitter database design

Janusz Dudczyk, Jan Matuszewski, and Marian Wnuk

Abstract — The appropriate emitter database is one of the most important elements in the present electronic intelligence (ELINT) system. This paper provides an overview of the relational modelling, which is used to construct the emitter database for current ELINT systems. The method described, delivers the entities' relational diagram that is independent from the manner of the data storage in further process of implementation. This approach ensures the integrity of the measured data. The process of final emitter identification is based on "the knowledge-based approach" which was implemented during the process of constructing the database.

Keywords — emitter database, relational modelling, knowledge-based-techniques, semantic networks, confidence factor.

1. Introduction

The last local military conflicts show that success on the modern battlefield depends on the following aspects ([6]):

- detecting electromagnetic emissions and finding the direction of incoming signals;
- gathering basic information about an enemy's situation and his capabilities;
- analysing the emitter's characteristics such as technical parameters, operating role and geographic location;
- providing current and real-time information about hostile activities in the areas of interest and warn of threats;
- monitoring any changes of situation and target parameters;
- communicating the most important data as soon as possible (task, report, exchange information);
- providing the control, command and supporting of the forces on the electronic battlefield.

The present electronic intelligence system must be able to protect specific requirements. In this case, ELINT system ought to include correctly designed database. The process of designing the optimal structure of emitter database is a very complicated and sophisticated task. The main problem that appears during the process of constructing the database is the difficulty with correct selection of the features. The relational modelling (*tool of information engineering, used to construct the high quality entities' relational diagram*) is an essential element in forming the examined system.
The method of relational modelling delivers the "notional model" that is independent from the manner of the data storage in further process of implementation. The integrity of the measured data is an advantage of this approach.

2. The process of designing database, the entities' relational diagram

The emitter database is designed according to the following stages, illustrated in Fig. 1:

- notional model – in the form of entities' relational diagram;
- logical model – specific form of database (definite type of database);
- physical model – implemented according to the selection of physical organization.

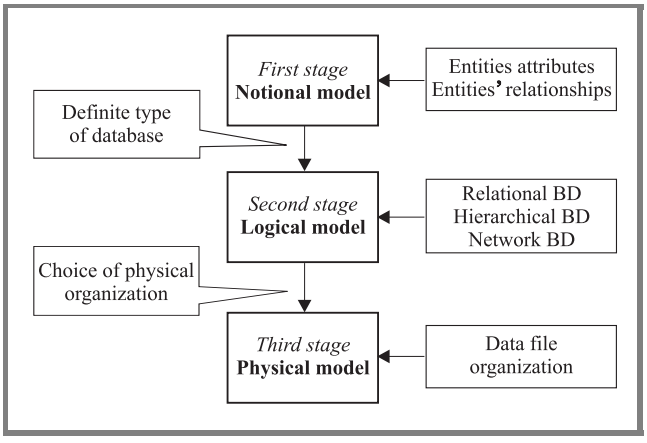

Fig. 1. The three – stage structure of designing database.

Principal aspects of relational modelling shown in Fig. 2, are the following [1, 2]:

- identification of important things in ELINT system /entities/;

- qualification of the properties of these things /attributes /;
- qualification of the kind of relationships between entities /entities' relationships/.

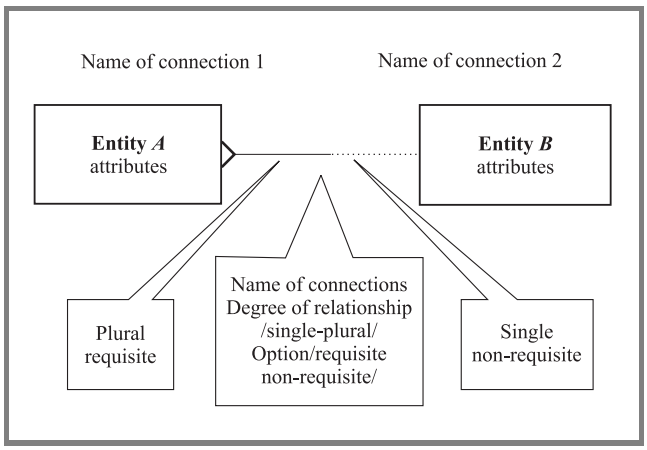

Fig. 2. Example of relationship between entity *A* and entity *B*.

An entity – can be defined as a thing or object, real or non-real. All information about it must be well known and stored.
Entity's relationship – can be defined as an essential connection between two entities.
It is advisable to add, the process of database designing based on relational modelling is accurately defined. Every entity must be univocally identified. Also every relationship must be determined. An entity should be described by its attributes.
As shown in Fig. 3, the relational diagram is the first stage of database designing [3, 4]. An entity is illustrated by a frame. An entity's name is located in the middle of the frame, for example: **Technical parameters**, **Radar platform**. The line-connected two entities' frames together illustrate the relationship between entities. Every relationship must be defined by the degree of relationship (it can be single or plural), the option (option defines the type of connection: requisite or non-requisite) and the name of connection (Figs. 2, 3). The conception of creation "notional model" should take into account "radar signature" in database. The "radar signature" in database includes all available data about radar signals. The main problem is to decide which information should be stored in database and correlate it with data types. In this case every entity should have a substitute in earlier prepared "radar signature".

3. Applying the knowledge-based techniques to emitter database

Now in ELINT systems knowledge-based techniques are widely examined [5, 7]. They may be applied to merge information and emitter identification. Usually information concerning the radar platforms known to be present, their locations, their intentions, their history of recent operational use, behaviour and their expected actions is not used. This is the kind of knowledge that is currently possessed only by the ESM operator and his supervisor. Usually part knowledge available to the knowledge-based ESM systems takes the form of individual radar details, their platforms and relationships between them. Knowledge-based techniques provide a means of studying this kind of knowledge and, ultimately, a means of representing it in a coherent manner.
The knowledge-base employs a declarative, rule-based representation of facts about the radar domain. The most important characteristics, which are related to each other in a specific type of radar and permit to recognize its application, are following:

- the principal parameters of radar signal that correspond to technical characteristics of the radiating set are: pulse width, carrier frequency, pulse shape, pulse repetition frequency, type of scan, beam width;
- carrier frequency is related to: antenna dimension, beam width, maximum range of radar;
- pulse width affects: range resolution and minimum range of radar;
- pulse repetition frequency limits the maximum unambiguous range of a pulse radar;
- pulse shape shows the range measurement accuracy;
- type of scanning (circular, sector, conical, helical, spiral, raster, etc.) is related to the application of radar;
- beam width affects the angular resolution.

Generally, a scheme of emitter identification may be based on rules or semantic networks. The simplest way of knowledge representation by rules is as follows:

IF *fact A is true* **AND** *fact B is true* **THEN** *conclude X*
ELSE *conclude Y*.

For example:

IF (pulse width is less than 0.5 μs) **AND** (type of scan is circular – sector)
THEN (the radar of battlefield surveillance was detected).

In real EW expert systems such procedures are much more sophisticated. Searching for the best solution needs other more complicated strategies (Fig. 4).
In order to make a decision in case of uncertainty, the probability theory or confidence factors (*CF*) may be used. The rules are activated in the moment when the values of this *CF* exceed the calculated thresholds, e.g.

IF *fact* (*CF* = 0,3) **THEN** *conclusion*.

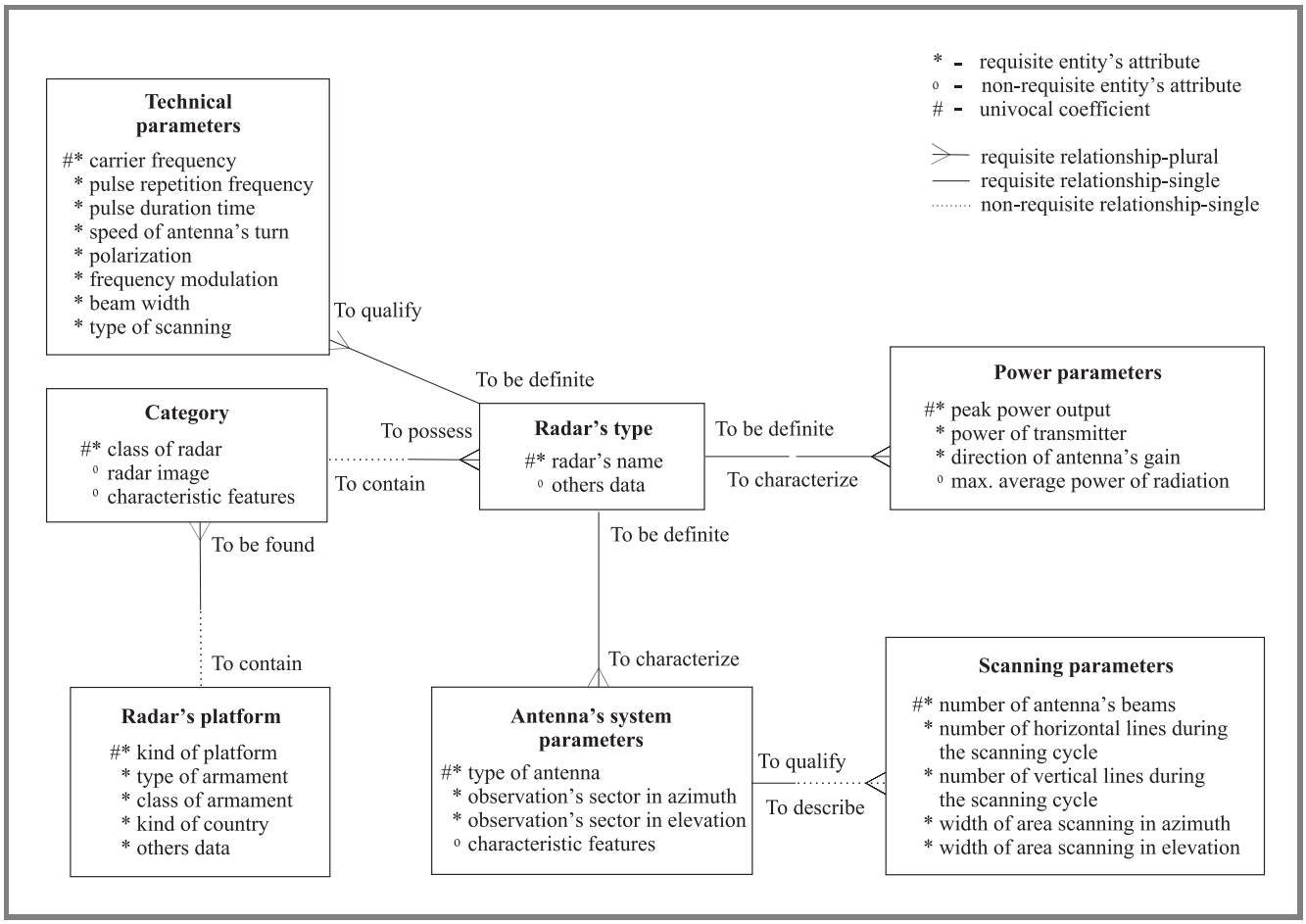

Fig. 3. The entities' relational diagram of ELINT system's database.

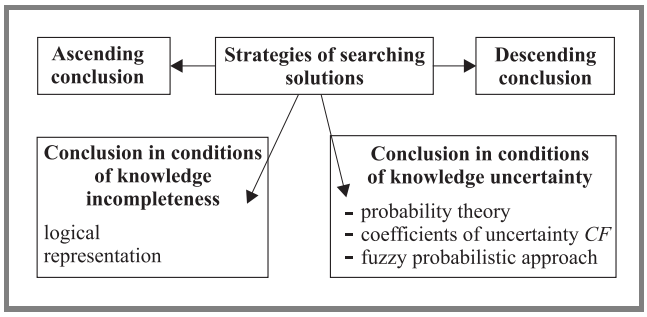

Fig. 4. Strategies of searching solutions.

In a fuzzy probabilistic approach, the classical two-values function f of membership of the object x to set A, is replaced by a "fuzzy" function:

$$f(x) = 1, \quad \text{if } x \in A$$
$$f(x) = 0, \quad \text{if } x \notin A$$
$$\downarrow$$
$$f : A \to \{0,1\}.$$

In the description of a real situation the following concepts: "nearly", "enough", "a little" which depict the surrounding reality very well, are often used.

4. Conclusion

Designing an optimal structure of ELINT system's database is a very sophisticated task. The database described in this paper was designed by using the relational modelling. The diagram of entities' relational-the most important stage during the process of designing was illustrated in Fig. 3. The database was estimated in size of the hard disc memory, taking into account the size of fields' types, the quantity and the character of tables. The process of final emitter identification based on "the knowledge-based approach" was implemented during the database constructing. Furthermore, entities' relational diagram deprives database of redundancy features and can be used in the electronic intelligence system or another military application.

References

[1] R. Barker, *Modelowanie funkcji procesów*. Warszawa: WNT, 2001.
[2] R. Barker, *Relatoinship Modelling*. Wokingham: Addison-Wesley Publisher, 1989.
[3] J. Dudczyk, "Applaying the relational modelling to design ELINT system's database", in *Proc. 4th Int. Electron. Telecommun. Conf. Stud. Young Sci. Work., SECON'01*, Warsaw, Poland, 2001.
[4] J. Dudczyk and J. Matuszewski, "Modern methods of database designing", in *Proc. XII Conf. "Contr. Regul. Radioloc. Flying Veh."*, Jelenia Góra, Poland, 2001 (in Polish).

[5] J. Matuszewski, "Some aspects of forming class metrics of objects for the expert system of electromagnetic emissions recognition", in *Proc. VIII Nat. Sem. "Artif. Intellig. Inform. Struct."*, Siedlce, Poland, 1995, pp. 205–214 (in Polish).
[6] J. Matuszewski and L. Paradowski, "The knowledge based approach for emitter identification", in *Proc. 12th Int. Conf. Microw. Radar, MIKON'98*, Kraków, Poland, 1998, vol. 3, pp. 810–814.
[7] J. Roe, S. Cussons, and A. Felthman, "Knowledge-based signal processing for radar ESM systems", *IEEE Proc.*, vol. 137, part F, no. 5, pp. 293–301, 1990.

Janusz Dudczyk received the M.Sc. degree in electronics engineering from the Military University of Technology, Warsaw, Poland with honours. He studied at the Electronics and Cybernetics Faculties (1992–1997). He is currently pursuing his Ph.D. degree in electronics engineering at the Military University of Technology, at the Institute of Telecommunication Systems. His primary research interests include electronic warfare, radar signal processing, emitter classification and identification, application of expert systems to radar signal recognition. His research activity and interests are focused on areas of electromagnetic compatibility, EMC chambers and utilising relational modelling to emitter database design.

e-mail: jdudczyk@wp.pl
Military Unit 4159
Kilińskiego st 27
96-100 Skierniewice, Poland

Jan Matuszewski was born in Cekcyn, Poland, in 1948. He received the M.Sc. degree from the Military University of Technology in 1972, where he studied at the Cybernetics Faculty (1967–1972). He obtained a Ph.D. degree in 1984. He has been working at the Military University of Technology for 30 years, where he is a lecturer of electronic warfare. His subject of interests is everything related to electronic warfare, especially radar signal processing, emitter classification and identification, designing emitter data base, application of neural network and expert systems to radar signal recognition. He has published 55 papers in the proceedings of conferences which were held in different towns in Poland and abroad. He completed the "Overseas Officers Electronic Warfare Course" at Royal School of Signals, Blandford Camp, U.K., in 1996. Since 1999 he has taken part in EW conferences organised by EW Section of SHAPE. He is also a member of NEDBAG (NATO Emitter Data Base Advisory Group).

e-mail: jmatuszewski@wel.wat.waw.pl
The Institute of Radar Technology
Military University of Technology
Gen. S. Kaliskiego st 2
00-908 Warsaw 49, Box 61, Poland

Marian Wnuk was born in Lublin, Poland, in 1943. He studied measuring systems at Technical University in Warsaw, Poland, where he received the M.Sc. degree in 1968. In 1987 and 1999, he received respectively Ph.D. and D.Sc. degrees from Military University of Technology (MUT), both in communication systems. Dr. Wnuk is a Professor at the Military University of Technology, and specialises in problem of concentration of the antenna field, analyses and construction of the antenna and dielectric layer. He has received Minister of National Defence awards for his outstanding scientific achievements and their practical applications. He is a member of many Polish research councils and industrial institutes. He published 137 papers.

e-mail: MWnuk@wel.wat.waw.pl
The Institute of Telecommunication Systems
Military University of Technology
Gen. S. Kaliskiego st 2
00-908 Warsaw 49, Box 50, Poland

Paper

Optimal site and antenna location for UMTS – output results of 3G network simulation software

Maciej J. Nawrocki and Tadeusz W. Więckowski

Abstract — The paper presents output results of 3G network simulation software in the area of optimal site location as well as finding optimal values of antenna tilt. The loss of capacity is shown for a wide range of tilts and different antenna directions. Nonuniform distribution of base stations has been also included in the simulation scenarios influencing system performance. All of the described parameters are especially significant to CDMA systems network planning.

Keywords — UMTS, 3G, CDMA, antenna tilt, site location.

1. Introduction

Soft-like behavior of 3G systems based on coded multiple access technique requires extensive analysis and optimisation related to WCDMA network planning. It becomes increasingly complex and sophisticated. An intuitive approach to solving CDMA related problems often leads to results inconsistent with reality. In TDMA/FDMA systems each of the planning stages can be treated independently, whilst the specificity of WCDMA radio interface causes all of the process elements to be interdependent.

The Institute of Telecommunications and Acoustics of the Wrocław University of Technology, Poland is conducting intensive research pertaining to CDMA cellular network modeling with special attention to the UMTS system.

Finding parameter values required to achieve a given network capacity is the main purpose of these analysis. The parameters modifiable by the operator include site locations, antenna directions and down-tilt values. Having appropriate control over these factors allows for the system capacity to be increased without any additional financial investments in new equipment.

2. Basic capacity calculations

The main term used to define the preliminary rough estimate of the system capacity is *pole capacity* [4, 5]. It states the maximum theoretical number of channels available in an ideal system with unlimited power resources. This number of channels for a multicell system and both link directions is determined through the following relation:

$$n = \frac{R_c}{R_b \cdot \frac{E_b}{N_0+I_0} \cdot (O_f + F)} + 1, \qquad (1)$$

where: n – the number of subscribers in a cell, R_c – the chip rate, R_b – the service bit rate, $E_b/(N_0+I_0)$ – the required energy per bit to noise and interference power spectral density at the receiver input, O_f – the orthogonality factor, F – the ratio between received intercell and intracell power. For a downlink O_f varies from 0.05 to 0.5 depending on the propagation environment. For an uplink it is assumed at $O_f = 1$. Considering that the F downlink value can vary for various distances between MS and BS, an averaged value should be used.

Unfortunately, the *pole equation* can only be used to roughly estimate the system capacity. Because the intercell and intracell interference are related to each other it is very difficult in practice to determine the F value using analytical methods even for an uniform distribution of subscribers at the given area.

The *pole equation* does not provide any information about the power emitted by the base stations and terminals. It is extremely important especially in the cases of nonuniform distribution of subscribers or base stations within a given area. The predicted power characteristics of network elements are the most important factors in the network planning process. This allows for example for a conclusion about the optimal antenna location.

The pole capacity in the same terms as (1) does not depend on the thermal noise and existence of control channels in the system, whilst the actual system capacity depends on these parameters.

A proper model of CDMA networks should include all or "almost all" of the intrasystem interference. More detailed description can be found in [3]. The main characteristic for a downlink is the total base station TX power as a function of the system load and active subscriber distance to the base station. For an uplink the system capacity is limited by an interference level measured at the base station. All results presented in the paper pertain to a system with the parameters shown in Table 1.

A non-heterogeneous propagation environment impacts the simulation results. The shadowing effect causes degradation of the system capacity. In order to simplify the calculations it is a common practice to assume a model, where the path loss is assumed as a sum of attenuation values resulting from the close to 4th power rule and of a random variable with a log-normal distribution. The standard deviation of this variable for an urban area can be stated between 4 to 12 dB. It also seems to be important

to take into account the correlation factors between different MS locations.

Table 1
Assumed parameters values

Parameter	Value
Carrier frequency	2 GHz
User bit-rate (voice)	12.2 kbit/s
Chip rate	3.84 Mchip/s
Orthogonality factor	DL: 0.4, UL: 1
Voice activity factor	100%
Required $E_b/(N_0+I_0)$	DL: 7.9 dB, UL: 6.1 dB
Maximum TX power per TCH channel	DL: 30 dBm, UL: 24 dBm
Receiver noise figure	NodeB – 5 dB UE – 9 dB
NodeB maximum TX power	DL – 43 dBm
TX power in the CCH channels	DL – 33 dBm
Propagation model	Walfish-Ikegami based
Antenna gain	NodeB – 15 dB UE – 0 dB
Cells radius	R = 500 m, 3 km
Number of cells in the model	19,37
No SHO, ideal power control, uniform subscriber distribution	

3. Sector antenna directions in hexagonal layout

CDMA is a single frequency network (SFN). As we already know its capacity is limited by interference levels. Placing the base stations according to a hexagonal grid we can obtain two totally different borderline cases when it comes to interference, depending on the directions of the sector antennas. Both of these are shown in Fig. 1.

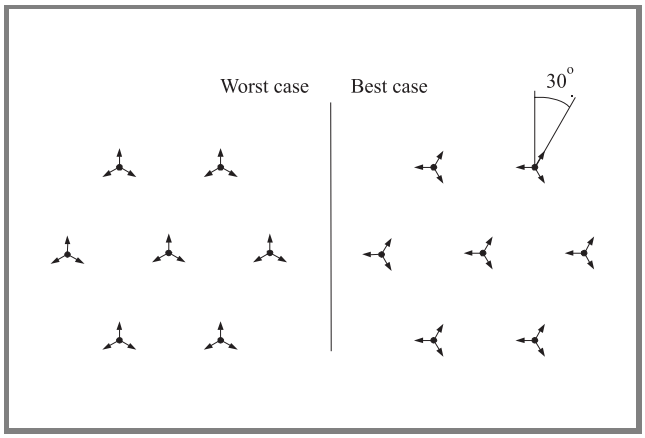

Fig. 1. Best and worst case of antenna directions for CDMA systems.

Figure 2 presents the TCH channel TX power characteristic as a function of the network load. An improper direction of sector antennas can cause a capacity degradation exceeding even 20% and requires an increase of base station TX power from 3 to 6 dB (assuming a uniform distribution of terminals within the test area). The decrease pertains not only to the capacity depending on the finite maximum power of the transmitter (in this case +41 dBm), but also to the *pole capacity*. The graphs shown in Fig. 2 represent average values.

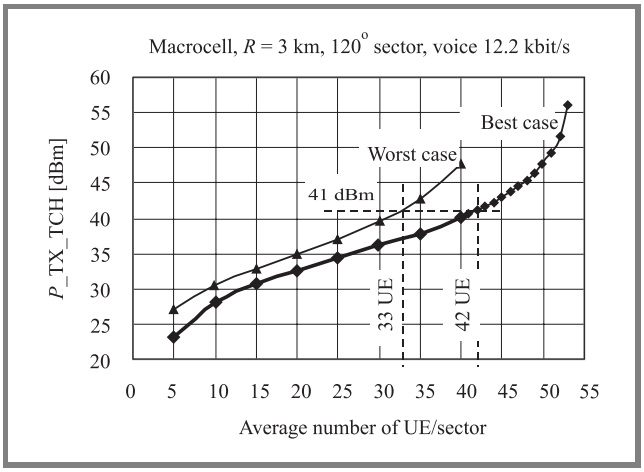

Fig. 2. Base station TX power for best and worst cases.

4. Base station antenna down-tilt

Base station antenna down-tilt is a common practice used in cellular networks. In CDMA networks it becomes especially important as the system performance is limited by interference coming from other cells.

The simulations are based on the characteristics of a Cellwave APX206513-T0 antenna designed for the 1900–2170 MHz frequency band. Its gain is about 15 dB and it gives a beam width of 65° (3 dB). Figure 3 presents the vertical characteristic. This is a typical antenna, which can be used in tri-sector UMTS base stations.

Figure 4 shows the total combined TX power of TCH channels as a function of the antenna down-tilt at three different load levels. The graphs clearly show, that significantly loaded (50 UE/sector) system with high antenna down-tilt (as compared to tilt = 0) have greatly reduced TX power. More detailed characteristics have been shown in Fig. 5.

Figure 5 presents the total combined TX power of TCH channels as a function of the load level for different down-tilts. At a first glance we see an interesting property. Having tilts lower then 5° the total combined TX power in the TCH channels decreases. However, with tilts exceeding 5° this power rises. Thus, the actual capacity of the system decreases because of the finite power limitation of the transmitter. At the same time, the more we tilt the antenna the higher the *pole capacity*. To sum up, with a given

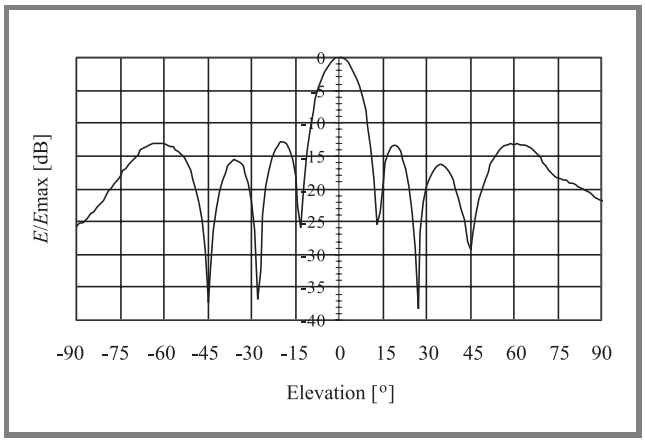

Fig. 3. Vertical characteristic of base station antenna.

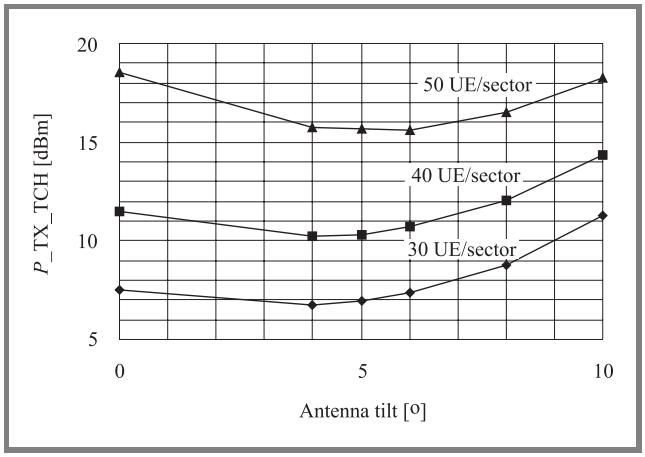

Fig. 4. Base station TX power versus antenna down-tilt.

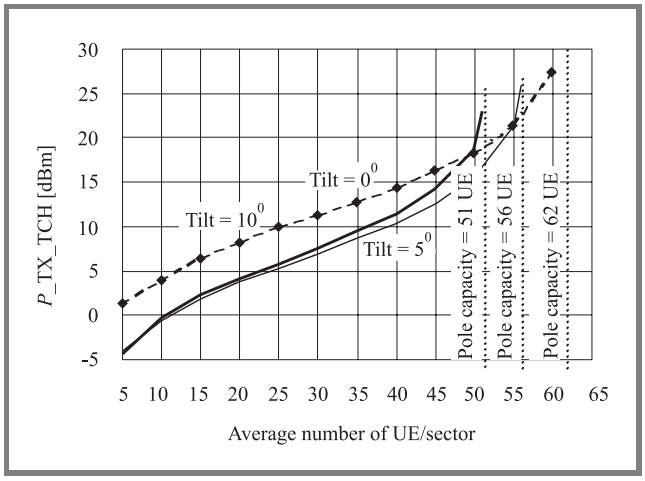

Fig. 5. Base station TX power curves for specified tilt values.

cell load when the antenna is tilted the total combined TX power lowers to a certain borderline value. With further tilting the power level rapidly rises depending on the given antennas characteristic, and the actual capacity decreases. At the same time the theoretical capacity actually rises. Considering the above, if the load is high and the transmitter has appropriate reserve TX power, it is possible to increase the number of available channels by tilting the antenna or choosing an antenna with an appropriate characteristic. The above seems obvious when we take into account the vertical characteristic of an antenna (Fig. 3). The down-tilt causes the antenna directional gain to drop in a direction parallel to the ground surface (at 10 dB for a down-tilt of 10°), thus lowering the level of interference onto the adjacent cells. This in term lowers the value of the F coefficient in formula (1) and thus the pole capacity rises.

5. Irregular base station distribution

One of the environmental parameters, which can be varied by the operator, is base station location. This parameter is especially significant for systems using coded multiple access, as these systems can handle loads of variable and irregular nature. Figure 6 presents capacity loss for base station location irregularity varying from 0% to 30% of the cell radius. Calculations were done for an uplink and a downlink.

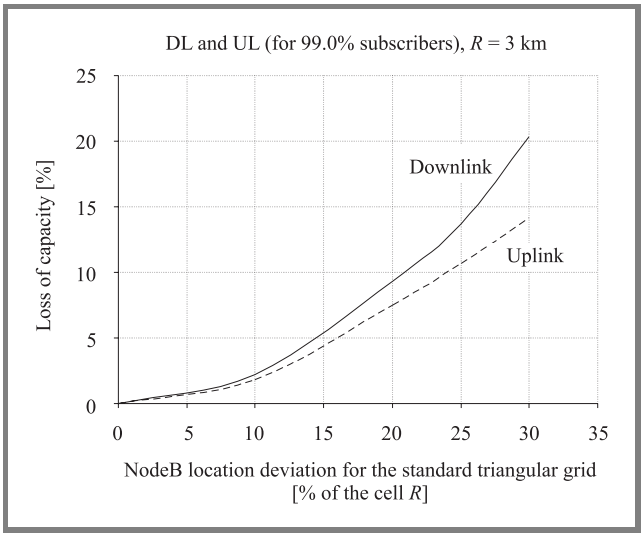

Fig. 6. Cell capacity loss for both link directions as a function of NodeB location deviation.

For a deviation of NodeB location equal to 30% of the cell radius, the number of available channels will be about 14% less as compared to an even base station distribution for an uplink and 20% for a downlink.

6. Summary

The paper presents an influence of site location and antenna tilts onto the operation of UMTS systems. The down-tilt of base station antennas is especially significant for CDMA systems. In order to obtain the best results it is necessary to

have a detailed antenna characteristic for both the horizontal and vertical planes. Improper base station location and/or improper antenna direction can greatly reduce the system capacity. On the other hand, it should also be noted that the UMTS system has cells of various size and hierarchy (macrocells, microcells and picocells), which will allow to significantly improve the system performance in reference to irregular base station locations. Also, the results pertain to a network using a singular bandwidth of 5 MHz.

The conclusions arising from the presented calculations are especially important to engineers involved directly in network planning. It is obvious that in urban areas it is not possible to freely place base stations at any and thus optimal locations. Considering the above, the deviation of base station antenna location in reference to the ideal triangular grid is very important during the network planning process. This data will also allow for easier network scalability under varying and irregularly distributed loads at a given area, especially for single frequency networks as the case of UMTS.

The cellular operators who received the UMTS license are nowadays faced with the fact that WCDMA interface cellular network planning is much more complicated then GSM. Just a few years back it was thought that CDMA type networks will require almost no planning because the coded access method, which dynamically adjusts the system resources within each cell based on the traffic requirement, will allow the network to "plan itself". After detailed analysis of the problem it is evident that the amount of significant parameters influencing the capacity is much larger than in TDMA/FDMA systems. Additionally, minor changes of the system or environmental parameters can influence the parameters of the entire system.

References

[1] 3rd Generation Partnership Project; Technical Specification Group, Radio Access Network; Standard Documents, Release 1999 & Release 2000.

[2] M. J. Nawrocki," WCDMA network planning aspects", in *Proc. Conf. Nat. Radiocommun. Radiodif. Telev. KKRRiT'2000*, Poznań, Poland, June 2000 (in Polish).

[3] D. J. Bem, M. J. Nawrocki, T. W. Więckowski, and R. J. Zieliński, "Modeling methods for WCDMA network planning", in *IEEE VTS Veh. Technol. Conf. VTC'2001*, Rhodes, Greece, May 2001.

[4] K. Sipila, Z. C. Honkasalo, J. Laiho-Steffens, and A. Wacker, "Estimation of capacity and required transmission power of WCDMA downlink based on downlink pole equation", in *IEEE VTS Veh. Technol. Conf. VTC'2000*, Tokyo, Japan, May 2000.

[5] K. Hiltunen and R. De Bernardi, "WCDMA downlink capacity estimation", in *IEEE VTS Veh. Technol. Conf. VTC'2000*, Tokyo, Japan, May 2000.

[6] M. J. Nawrocki, "Influence of base station localization irregularities and subscriber distribution onto UMTS network planning", in *Proc. Conf. Nat. Radiocommun. Radiodif. Telev. KKRRiT'2001*, Poznań, Poland, May 2001 (in Polish).

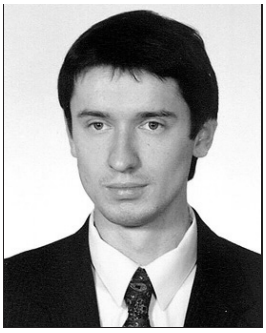

Maciej J. Nawrocki is with the Institute of Telecommunications and Acoustics of the Wrocław University of Technology, Wrocław, Poland, where he works as Assistant Professor in the field of wireless systems. He works on UMTS network modeling, planning and optimization. He received the M.Sc. and Ph.D. degrees in telecommunications in 1997 and 2002, respectively. He is the author of 16 papers presented at international and national conferences as well as 13 unpublished works.

e-mail: Maciej.Nawrocki@pwr.wroc.pl
Institute of Telecommunications and Acoustics
Wrocław University of Technology
Wybrzeże Wyspiańskiego st 27
50-370 Wrocław, Poland

Tadeusz W. Więckowski is with the Institute of Telecommunications and Acoustics of the Wrocław University of Technology, Wrocław, Poland, where he is a Professor in the field of communications systems and electromagnetic compatibility. He has been a Director of the Institute for six years and is currently Vice-Rector of the Wrocław University of Technology. He received the M.Sc. and Ph.D. degrees in telecommunications in 1976 and 1980, respectively. In 1993 he has been habilitated. He is a senior IEEE member, a member of the Association of Polish Electrical Engineers and Organizing Committee of the Wrocław EMC Symposia. He is the author of 144 publications and over 240 unpublished works.

e-mail: Tadeusz.Wieckowski@pwr.wroc.pl
Institute of Telecommunications and Acoustics
Wrocław University of Technology
Wybrzeże Wyspiańskiego st 27
50-370 Wrocław, Poland

Paper

FDTD modeling and experimental verification of electromagnetic power dissipated in domestic microwave ovens

Paweł Kopyt and Małgorzata Celuch-Marcysiak

Abstract — The FDTD (Finite Difference Time Domain) method has proven to be effective in modeling high-frequency electromagnetic problems in telecommunications industry. Recently it has been successfully applied in microwave power engineering. In order to accurately model scenarios typical in this field one has to deal with the movement of objects placed inside cavities. This paper describes a simple algorithm that makes it possible to take into account object rotation – important in simulations of domestic microwave ovens. Results of example simulations are presented and an experimental verification of the simulation tool is performed.

Keywords — electromagnetic simulations, FDTD algorithm, microwave heating.

1. Introduction

Microwave power engineering community has only recently discovered the FDTD and other modeling methods successfully used in telecommunications for years. Like in any other field, also in this application modeling is very beneficial as it cuts down the design costs. In the literature one can find various approaches to model heating devices. The general possibilities and limitations were described in [1]. In [4] the authors used FDTD to model microwave power distribution in a food object placed inside a microwave oven. Simulations and optimisation results of power uniformity in objects passing through a tunnel industrial oven have been presented in [2].

One important feature has been so far overlooked. In real-life heating devices the greater uniformity of power distribution inside the heated objects is often achieved with the object movement inside the cavity while heating is on. In industrial ovens the foodstuffs are simply passing through a cavity on a conveyor belt [2], while in small-scale simpler devices – like domestic microwave oven – the object is placed on a rotating shelf.

The accurate modeling of microwave heating scenarios requires that movement of the objects be taken into account. This paper introduces a simple but effective method to conduct an accurate modeling of an object heated inside a domestic microwave oven with the object rotation. The algorithm itself is presented in Section 2. Section 3 describes various power uniformity criteria. One of those presented is chosen for further use. Section 4 presents the results of simulations and comparison of the introduced method with results obtained without its application. Section 5 discusses comparisons of the FDTD simulations with real-life measurements.

2. Method of simulation

The basic electromagnetic simulation software has been developed for years and currently on the market one can find ready packages of proven reliability and accuracy, successfully used in various problems. Especially, the software based on FDTD method has proven advantageous over other solutions employing FEM method [2]. One of those – QuickWave 3D developed by QWED – with implemented conformal FDTD method [5, 6] is known in microwave power industry. Several papers presenting results obtained with its help have been published and it ranks high on the list of available software suited for microwave power simulation [7].

An additional feature makes it even more suitable to the task – the possibility to define scenario geometry using parametrized macros in the so-called UDO language. This feature together with the possibility to define scripts (tasker files) instructing QuickWave to dump chosen data at a given moment facilitates effective simulation and optimisation of complex problems. It has been successfully used in [3].

That way of conducting simulation has been adopted in our case. The experiments have been conducted with a model of an example microwave oven. The whole geometry of the model, together with excitation and the sample object being heated, have been prepared with a single macro. By modifying its parameters one can place the sample object at any angle inside the oven. Next, using an external routine written in Matlab [8], one can trigger QuickWave simulation several times, each time for a different object position. Calculated dissipated power pattern in the object cross-section will be different for each angle. It means that by collecting the data on dissipated power for each angle and summing them up one can arrive at more accurate information on how evenly the dissipated power is distributed inside the object during heating and rotation.

Table 1
Relative error of the averaging (for sets 7 and 8 the mirroring was used)

Set number	1	2	3	4	5	6	7	8
Step [°]	5	10	20	30	45	60	*)	**)
No. angles	72	36	18	12	8	6	6	7
Effective no. angles	72	36	18	12	8	6	10	12
Error [%]	0	0.0916	0.3043	1.1609	4.0086	5.1448	1.9044	1.1267

*) Angles in set no. 7: 0°, 36°, 72°, 180°, 216°, 252°.
**) Angles in set no. 8: 0°, 30°, 60°, 90°, 180°, 210°, 240°.

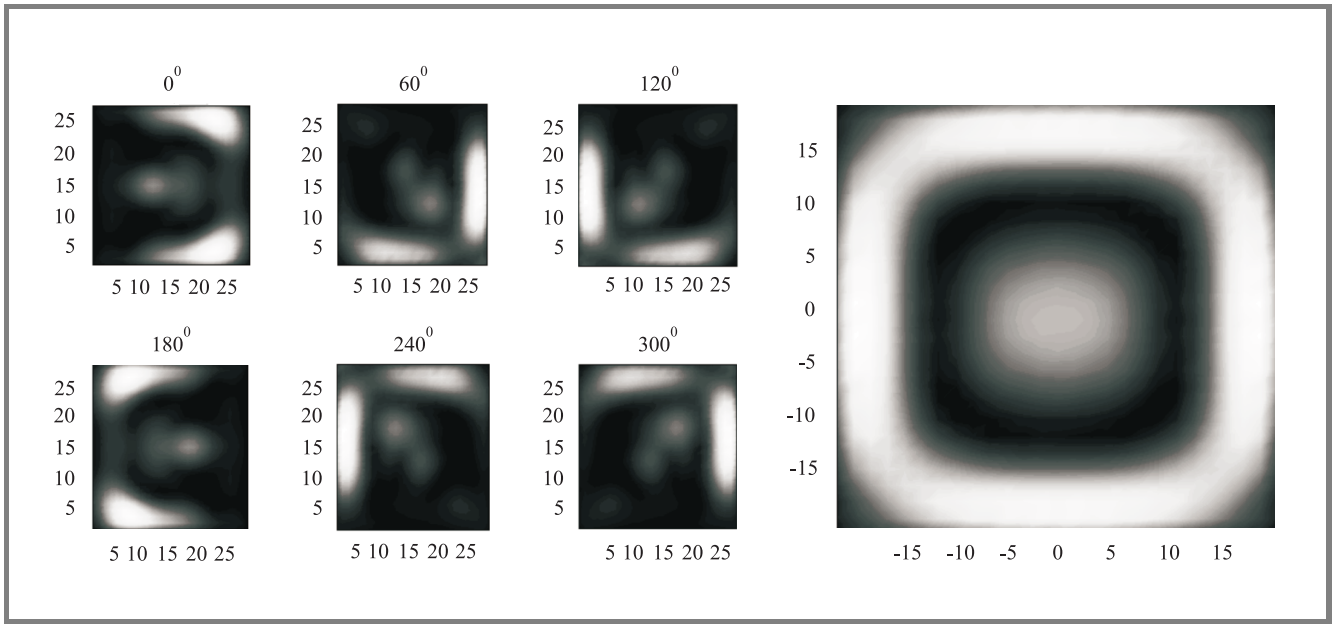

Fig. 1. Dissipated power pattern for six angular positions of the object (from 0 to 300° with the step of 60°).

The FDTD method requires that the model be discretized with small parallelepipeds (or cells). Fields and resulting power distribution are calculated within each such cell. The collected information comes in the form of snapshots of dissipated power in the object's cross-sections. If the object is rotated, the snapshot is rotated as well. Obviously direct summing of the data for different rotation angles is not possible. This task requires that the snapshots of dissipated power be first brought back to their original position – 0 degrees. Since in each case the angle of rotation is known one can achieve this using standard formula for coordinate system rotation applied to each cell:

$$\begin{aligned} x' &= x\cos\alpha + y\sin\alpha, \\ y' &= -\sin\alpha + y\cos\alpha, \end{aligned} \tag{1}$$

where x, y are coordinates of the cell center of the rotated snapshot, while x' and y' are coordinates of the cell center after the back-rotation.

After the back-rotation it is possible to average the dissipated power for all the angular positions of the object. Figure 1 presents six matrices that have been rotated back and are ready for averaging. During all the experiments the object (a parallelepiped $40 \times 40 \times 20$ mm) has been placed centrally on the shelf and rotated around its center. The object is made of meat modeled as material of relative electric permitivity $\varepsilon = 50 - j20$.

The accuracy of the averaging procedure for different number of distinct positions has been tested. As a reference we have used averaged pattern P^5 obtained by summing up power snapshots taken every 5°. Table 1 contains results of comparison between the reference pattern and patterns based on a smaller number of positions. The relative error values have been obtained with the following formula:

$$e(a) = \frac{\sum_{i=1}^{N}\sum_{j=1}^{M}\left(P_{ij}^{5} - P_{ij}^{a}\right)^2}{NM}, \tag{2}$$

where P^a is a pattern whose accuracy we verify against the reference pattern P^5, N and M are the dimensions of the patterns (given in cells).
The error grows as the number of angular positions decreases. There is a way to lower the number of angles without deteriorating the accuracy. We have presented 6 templates in Fig. 1. It is clear that due to the symmetry of the problem one can find pairs of snapshots that are mirrored copies of each other (60° and 300° or 120° and 240°). It is enough to get one result and sum it up twice with and without mirroring. Sets 7 and 8 of data in Table 1 contain angles only from the first and third quarters of the coordinate system, with subsequent mirroring. It is clear that error is low despite the relatively small number of angles, for which the simulations were performed.

3. Power uniformity criteria

Effective comparison of the uniformity of power distribution within different objects requires a carefully chosen criterion. A criterion like that is also necessary in order to conduct an optimization process. We have browsed the available literature and chosen two criteria for further consideration. We have also proposed a new one which seems to be most useful.

- **Differential power difference** – difference between the highest and the lowest value of dissipated power found inside the object (or its cross-section in the case of analyzing the object as a set of two-dimensional layers) [2].
- **Statistical criterion** – standard deviation of the dissipated power distribution normalized by the mean value [4].
- **Integral power criterion** – maximum value of power dissipated in a small volume (surface when we deal with single layers of object) normalized by the total power dissipated in the object (one layer).

The differential power criterion constructed as a simple difference between power dissipated in hottest and coldest spot and used in [2] is not suitable in our case. It takes into account only two points out of many available in object's volume which does not fully describe power distribution in complex two- or three-dimensional geometries.
The statistical criterion seems to be a better choice as all the points (or cells) of the object give contribution to the total value of the criterion. We have conducted some tests of the criterion trying to confirm that it gives results, which agree with intuition. The tests have shown that the criterion cannot be used in our case despite the fact that it has been successfully applied in [3, 4].
The third proposed criterion – the integral power criterion – has been eventually chosen for further experiments. It has been confirmed in tests that it can be treated as accurate description of the power distribution. What is also important is that this criterion is completely based on physical concepts and phenomena (e.g. power dissipated in a specified region) that we want to measure. The criterion is defined with the following formulae:

$$f_p(v) = \max\left(\frac{\int\limits_{S_A(x_0,y_0)} SAR(x,y)\,ds}{\int\limits_{S} SAR(x,y)\,ds}\right), \tag{3}$$

$$f_p(v) = \max\left(\frac{\int\limits_{S_A(x_0,y_0)} -SAR(x,y) + 2E\left(SAR(x,y)\right)\,ds}{\int\limits_{S} SAR(x,y)\,ds}\right), \tag{4}$$

where S is the area of the object's cross-section (if whole volume of the object is taken into account then the integral is calculated over the volume), S_A is the small fraction of the whole area of the object's cross-section, SAR is function describing the distribution of the specific absorption rate (in reality it is discretized due to the nature of the applied simulation method) and E is the symbol of calculating expected value.
It also has one important advantage – it allows taking into consideration not only the value of power dissipated in cold (or hot) spots but also the shape of the power distribution. A sharp peak in power over a small region is not so important as a peak similar in value but spread over a larger region. The tuning of the criterion means changing the S_A area. If it is small in comparison to S then the criterion is tuned to sharp peaks. By making the S_A larger we average the value of power peaks over greater area thus making the influence of such peaks smaller.
There is also another advantage of the integral power criterion. A typical goal of the optimization process is a uniform power distribution within the heated object. Yet from a practical viewpoint, this is usually a secondary goal as it is more important to assure that in the volume of the heated object none of the regions will be heated too much (hot spots elimination) or all the regions' temperature will be high enough (cold spots elimination) to kill pathogens. One can easily modify the criterion for each case. The (3) criterion is to be used in hot spot elimination while (4) should be used to eliminate cold spots. The modification in (4) is simply turning the power distribution around its mean value. Thus all the peaks become valleys and all the valleys (or cold spots) are peaks which the optimization algorithm will try to eliminate.

4. Results of simulation

Using the algorithm described in Section 2 together with the integral power criterion presented in Section 3 two numerical experiments have been conducted. The results

show that taking into account the object rotation can change the resulting dissipated power distribution in heated objects, and consequently the optimum object design.

The experiments have been performed with a modified domestic microwave oven model. On the shelf a sample object has been placed whose shape can be modified with a single parameter. In order to maintain simplicity of the experiments and keep the computation time reasonably short the object's shape can be changed by rounding its corners. The parameter is defined with the following formula:

$$n = \frac{r_c}{0.5a}, \tag{5}$$

where r_c is the radius of the curvature of the object's corners while a is the length of the object's side (the assumption is that the object is equilateral). One can easily introduce other parameters (e.g. ratio of the object's sides). Two example objects of different shapes are presented in Fig. 2.

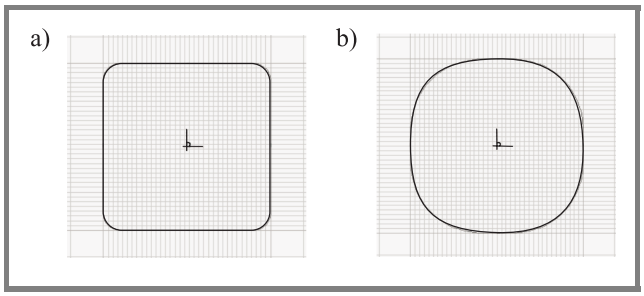

Fig. 2. Two example objects: (a) $n = 0.2$; (b) $n = 0.8$.

The sample object used in the experiments has been made of meat (material density is 1 g/cm^3), its volume has been 300 cm^3, its height – 20 mm. The experiment goal has been to average dissipated power over 6 angles (angle set 7 listed in Table 1) in the plane cutting the sample object at the level of 2, 10 and 18 mm from its base. Then the integral power criterion has been used to calculate the uniformity of the distribution in each layer. The calculations have been repeated for different shapes of the object (different values of n parameter in Eq. (5)). The results are presented in Fig. 3 together with similar data obtained by calculating the uniformity of power distribution for one angle only (0°).

Clearly the object rotation contributes to higher heating uniformity. It is also important that object rotation makes the power distribution less sensitive to the shape of the heated object. From Fig. 3 one can see that when the object rotation has been taken into account, the shape factor influences the uniformity to a much lesser extent as compared to the case in which the rotation has not been employed. Without rotation, we observe one local minimum at $n = 0.8$ and a global minimum at $n = 0.1$.

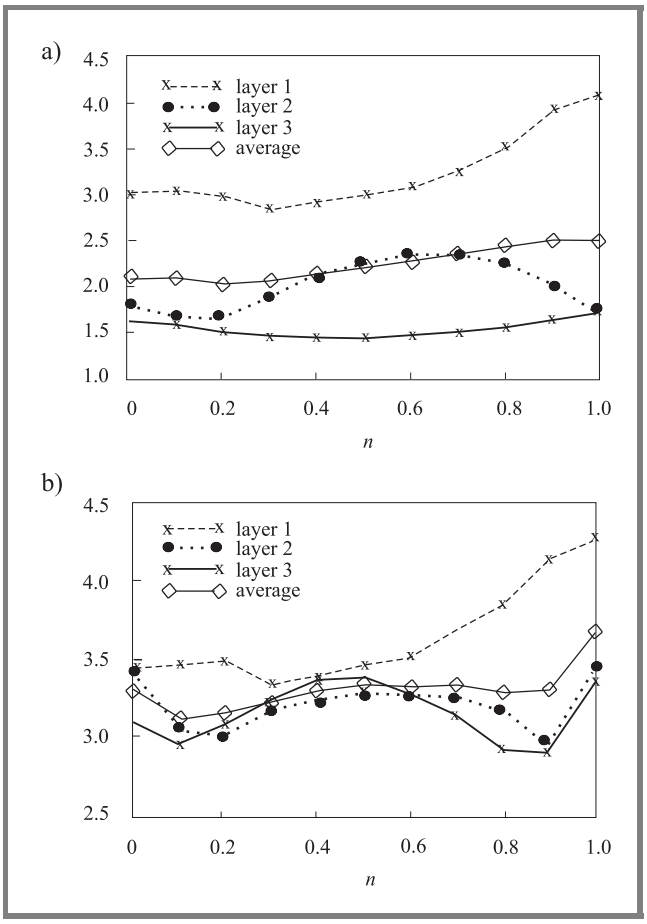

Fig. 3. Comparison of the uniformity (integral power criterion) of dissipated power distribution with (a) object rotation; (b) without rotation.

With rotation, the local minimum disappears, and the global one shifts to $n = 0.2$. This means that the optimum design of a food package would be different in the two cases.

5. Experimental validation of the accuracy of simulation

The accuracy of the simulation software employed to obtain the results described in the previous section has been verified experimentally. The measurement equipment recently acquired by the Institute of Radioelectronics has been employed in the task and presented in Fig. 4. It consists of a microwave oven (by Plazmatronika, www.plazmatronika.pl) with adjustable power level controlled with a PC, and a signal conditioner with set of eight thermometers (by Fiso Systems, www.fiso.com) that can register temperature changes simultaneously.

A set of temperature measurements has been conducted. A sample of bread 60(w) × 60(d) × 20(h) mm has been

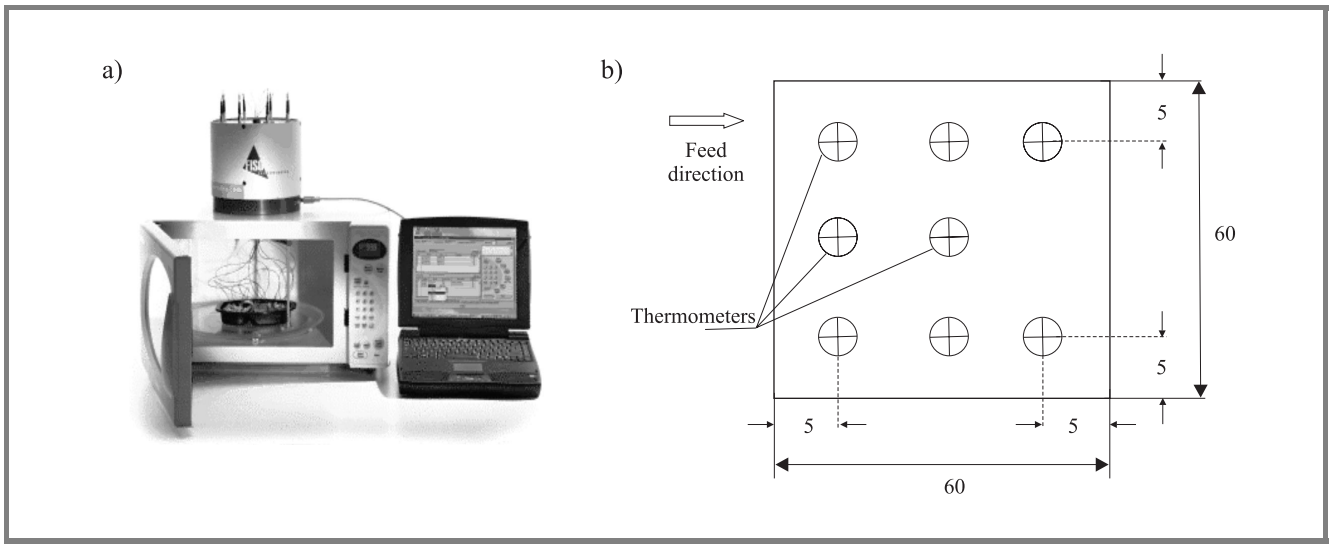

Fig. 4. Measurement system used in verification of the simulation results (a); placement of thermometers in sample (b).

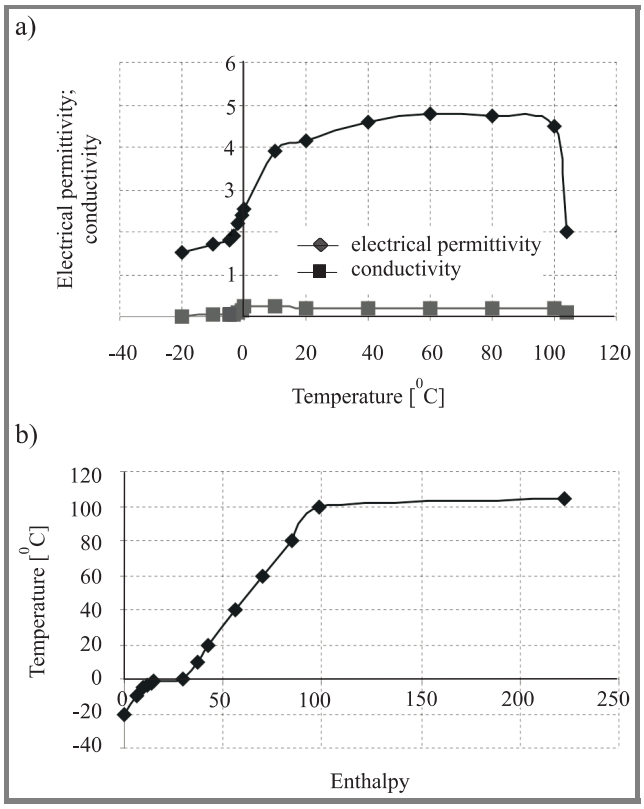

Fig. 5. Data contained in the file describing the media: (a) dependence of the relative electrical permittivity and conductivity [S/m] on the temperature; (b) dependence of the temperature in a cell on the enthalpy in this cell.

placed centrally on the oven turntable. The power level has been set to 100 W and the heating lasted around 5 minutes. Temperature has been registered at 8 locations shown in Fig. 4b, in the middle layer of the sample. Since the main goal of the experiment has been to check the accuracy of the software, we have performed the heating without sample rotation. It has made the computation time much shorter as there has been no need for repeated simulations of the oven with sample at various angular positions.

After the measurements the computer model of the microwave oven has been prepared and a set of simulation results obtained. An additional module – called BHM (basic heating module) [9] – has been used that takes into account the temperature-induced changes of the media parameters. The changes are based on the data stored in an external file containing enthalpy and corresponding media parameters: electrical permittivity, conductivity (losses) as well as temperature. The data stored in the file used in the bread simulation have been presented in Fig. 5.

The BHM module repetitively modifies the media parameters according to the dissipated power and data provided in the file. The total heating time has to be divided into smaller timesteps in order to accurately model the gradual changes of the media parameters. The operations performed in each step have been illustrated in Fig. 6. First, the steady-state needs to be reached in order to calculate the dissipated power envelope in the simulated circuit. Then the lossy materials are being heated for the time equal to the timestep length. After the heating has been done the enthalpy is obtained and the media parameters are modified according to the file, and temperature in each cell is changed.

The comparison of the experimentsal data and the simulation results has been presented in Fig. 7a. The comparison has been made in the hot spot which is just off the sample center. The curves are close to each other with the biggest discrepancy occuring at the beginning of heating process. This can be ascribed to the inertia of the thermometer. The

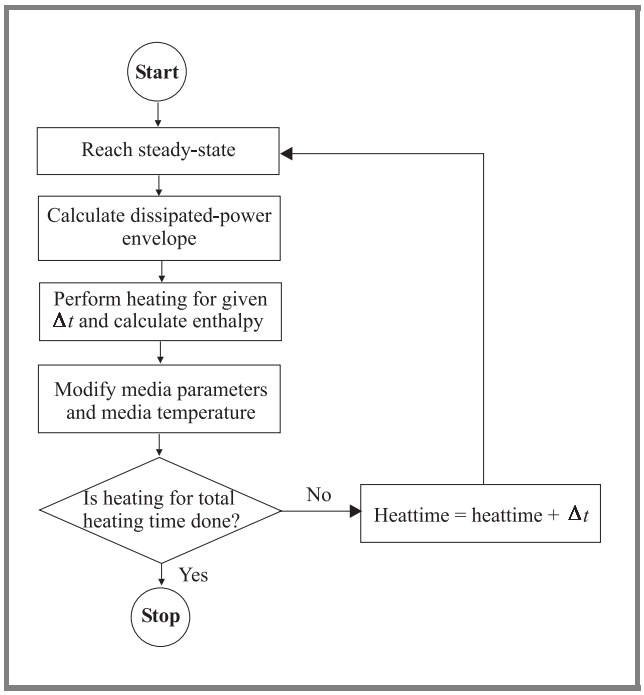

Fig. 6. Operation of the BHM module.

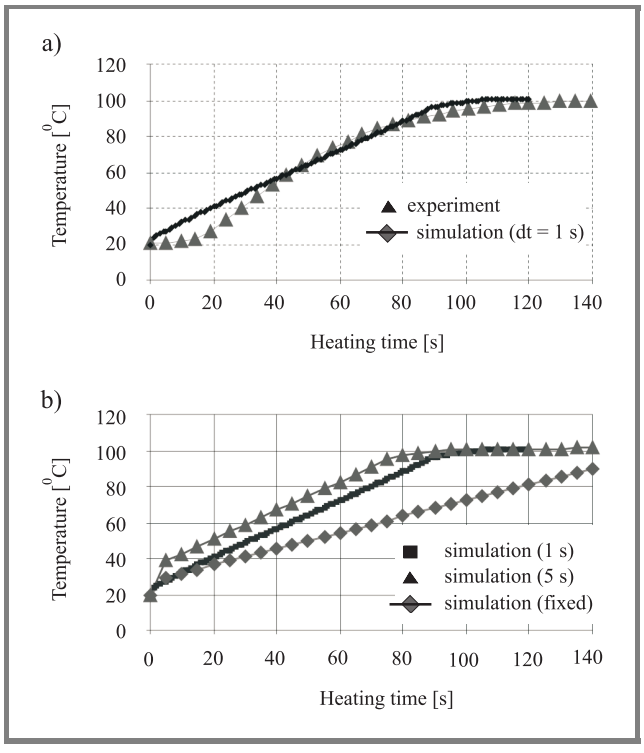

Fig. 7. (a) Comparison of the measurements and the simulation data (in the hot spot); (b) comparison of simulation results (two cases where media parameters where modified with two different heating timesteps – 1 s and 5 s – and one case where media parameters stayed unchanged).

simulation data have been obtained for a heating time step set to 1 s. It has been checked that in this case bigger values can lead to inaccurate data.

The inertia of the thermometers used in the measurements has been checked experimentally. The thermometer has been placed first in a glass filled with water of room temperature (25°C) and then transferred to a glass filled with much hotter water. The output has been registered and we have shown it in Fig. 8. It seems that in case of water the time for the temperature to rise to the correct level is around 4 s. In case of water the contact resistance between the thermometer and the medium is not high. With bread the resistance is much higher so greater inertia can be expected.

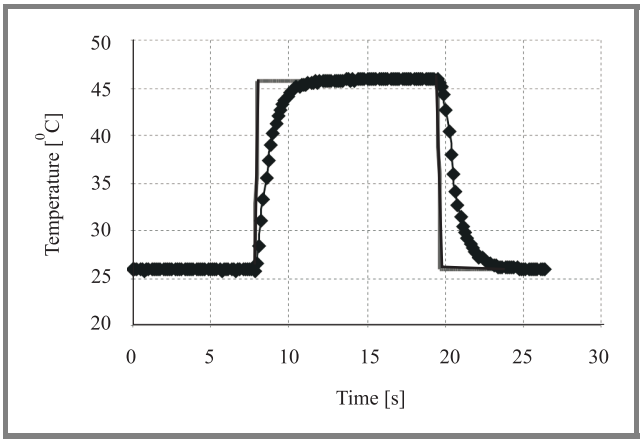

Fig. 8. Response of the thermometer used in experiment (water).

The timestep of the heating is an important factor since choosing too small values will lead to excessively long computation time without any improvement in accuracy. Too big timestep, though, is even more dangerous as it may cause abrupt changes in temperature and, in turn, jumps of the media parameter values which can bring instabilities into the simulations. The data obtained for different timestep values are presented in Fig. 7b. They have been compared with the data obtained without any modification of parameters.

6. Conclusion

We have presented an effective and simple approach to modeling of problems with load rotation, which is an important issue in microwave power applications and has not been previously addressed. It is a post-processing method that is easy to implement with standard mathematical routines found in e.g. Matlab package. We have also considered a couple of examples proving that object rotation may change the dissipated power distribution within the object, and hence optimum geometry of the heating system. This is important in design of microwave ovens and microwaveable food packages. The experimental verification of the simulation tool has been conducted and it has been shown that the accuracy of the computations is high enough to ensure a good agreement with measurements.

Acknowledgement

This work has been performed within EUREKA E!2602 initiative and co-financed by the State Committee for Scientific Research grant no. 134/E-365/SPUB-M/EUREKA/T-10/DZ 206. The authors also kindly acknowledge the helpful discussions with Per Risman, Microtrans AB, on power uniformity criteria and physical parameters of bread as a function of enthalpy.

References

[1] P. O. Risman and M. Celuch-Marcysiak, "Electromagnetic modelling for microwave heating applications", in *13th Int. Conf. MIKON-2000*, Wrocław, Poland, May 2000, pp. 167–182.

[2] M. Sundberg, P. Kildal, and T. Ohlsson, "Moment method analysis of a microwave tunnel oven", *J. Microw. Pow. Electromagn. Ener.*, vol. 33, no. 1, pp. 36–48, 1998.

[3] P. Kopyt, "Optymalizacja układu grzania mikrofalowego pod względem jednorodności rozkładu mocy". Praca magisterska, Wydział Elektroniki i Technik Informacyjnych, Politechnika Warszawska, Warszawa, 2001 (M.Sc. thesis in Polish).

[4] B. Wäppling-Raaholt and P. O. Risman, "FDTD simulation of a microwave heating process: effects of oven parameters on heating uniformity", in *3rd Int. Conf. Predic. Model.*, Leuven, Belgium, Sept. 2000, pp. 271–273.

[5] W. K. Gwarek, "Analysis of an arbitralily-shaped two-dimensional microwave circuits by FD-TD method", *IEEE Trans. Microw. Theory Techn.*, vol. 36, no. 4, pp. 738–744, 1988.

[6] W. K. Gwarek, M. Celuch-Marcysiak, M. Sypniewski, and A. Więckowski, "QuickWave-3D software manual", QWED, Poland, 1999.

[7] V. V. Yakovlev, "Examination of contemporary electromagnetic software capable of modelling problems of microwave heating", in *Proc. 8th Int. Conf. Micro and HF Heating*, Bayreuth, Germany, Sept. 2001, pp. 19–20 (complete paper in *Trends in Microwave and HF Heating*, Springer Verlag, 2001 – to be published).

[8] Matlab 5.1, Mathworks – university licence.

[9] W. K. Gwarek, M. Celuch-Marcysiak, M. Sypniewski, and A. Więckowski, "BHM module", QWED, Poland, 2000.

Paweł Kopyt was born in Warsaw, Poland, on May 15, 1975. He graduated *cum laude* in telecommunications from Warsaw University of Technology, where he received an M.Sc. degree in 2001. At present, he is a Ph.D. student at Institute of Radioelectronics, Warsaw University of Technology. Among his interests are numerical techniques for simulation of electromagnetic and thermal fields and microwave heating.
e-mail: pkopyt@elka.pw.edu.pl
Institute of Radioelectronics
Warsaw University of Technology
Nowowiejska st 15/19
00-655 Warsaw, Poland

Małgorzata Celuch-Marcysiak is an Assistant Professor at the Warsaw University of Technology and Vice-President of QWED company. She received an International Baccalaureate from the United World College of the Atlantic, in 1983, M.Sc. and Ph.D. in electronic engineering from Warsaw University of Technology in 1988 and 1996, respectively. She is one of the main authors of QuickWave electromagnetic simulation software. She contributed to more than 60 technical publications. Her main professional interest is in numerical modeling of electromagnetic problems.
e-mail: m.celuch@ire.pw.edu.pl
Institute of Radioelectronics
Warsaw University of Technology
Nowowiejska st 15/19
00-655 Warsaw, Poland

Paper

Theory of scattering by an array of lossy dielectric, ferrite and conducting cylinders

Michał Polewski and Jerzy Mazur

Abstract — Theory of scattering by lossy dielectric, ferrite and/or conducting cylinders is investigated using a combination of an iterative scattering procedure and the orthogonal expansion method. The addition theorems for vector cylindrical harmonics, which transform harmonics from one coordinate system to another, are presented.

Keywords — iterative scattering, waveguide junctions, conducting and dielectric cylinders.

1. Introduction

Considering the electromagnetic wave scattering from two-dimensional arbitrary obstacles we can observe a two areas of active research. The first approach concerns open problems – obstacles in free space, where the far scattered field patterns can be investigated [1, 2], while the second – closed problems – presents the frequency responses of described structure in a rectangular waveguide [3, 4].

In the last decade, a recursive algorithm has been developed for the scattering by arbitrarily shaped obstacles [1]. Elsherbeni *et al.* [2] proposed an iterative solution for the scattering by M different parallel circular cylinders. Recently, Valero and Ferrando [4] presented the method, which segments the problem into regions that are characterized by their generalized admittance matrices.

In this paper we apply modified iterative scattering procedure, which has been used for open problems [2] and the orthogonal expansion method to describe an equivalent scattered field by lossy dielectric, ferrite and/or conducting cylinders on the surface of a separated interaction region, which then can be used both for open and closed structures. The main advantage of this method is that we can obtain a total scattered field from all cylinders and match it with other incident fields to define scattering matrix of investigating structure. This technique can be applied to analyze a waveguide structures where incident fields are the TE_{m0} mode and open structures to define the far scattered field patterns for E_z-wave excitation.

2. Basic formulation

Consider harmonic E_z-wave excitation in global coordinates as infinite series of Bessel functions of the first kind with unknown coefficients a_n, where the electric field has

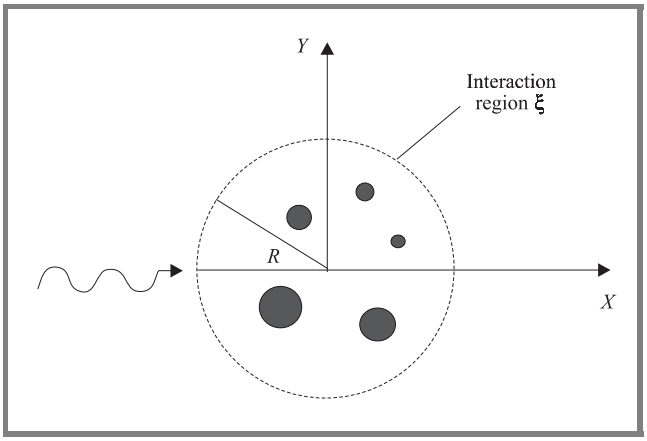

Fig. 1. Cylindrical obstacles in the interaction region excited by E_z-wave.

a z component only with all vectors independent of z of the cylindrical coordinates (ρ, ϕ, z):

$$E_z^{inc(0)} = \sum_{n=-\infty}^{\infty} a_n J_n(k_0\rho) e^{jn\phi}, \tag{1}$$

where k_0 is the wave number in free space.

Now we assume that field (1) excites all of the M homogeneous, lossy dielectric, ferrite or perfectly conducting cylinders (see Fig. 1) and has to be defined in their local coordinates. For the ith cylinder using an addition theorem for Bessel functions [5] we have

$$E_{zi}^{inc(0)} = \sum_{n=-\infty}^{\infty} a_n \sum_{m=-\infty}^{\infty} J_m(k_0 r_i) e^{jm\phi_i} J_{m-n}(k_0 d_{io}) e^{j(n-m)\phi_{io}}, \tag{2}$$

where d_{io}, ϕ_{io} are defined in Fig. 2.

In response to our excitation, a zero order scattered field is created from each of M cylinders by forcing the tangential components of both the electric and magnetic fields, on the surface of each cylinder, to be continuous:

$$E_{zi}^{inc(0)}(r_i, \phi_i) + E_{zi}^{s(0)}(r_i, \phi_i) = E_{zi}^{d(0)}(r_i, \phi_i), \tag{3}$$

$$H_{\phi i}^{inc(0)}(r_i, \phi_i) + H_{\phi i}^{s(0)}(r_i, \phi_i) = H_{\phi i}^{d(0)}(r_i, \phi_i), \tag{4}$$

where r_i is the radius of the ith cylinder.

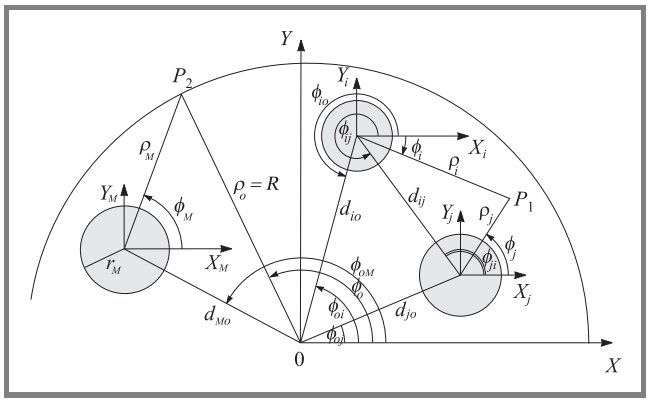

Fig. 2. Notation used for a change of coordinate system for Bessel functions.

The scattered electric field component for the ith cylinder can be expressed as

$$E_{zi}^{s(0)}(\rho_i, \phi_i) = \sum_{n=-\infty}^{\infty} c_{in}^0 H_n^{(2)}(k_0\rho_i) e^{jn\phi_i} \tag{5}$$

while transmitted field component inside the dielectric material of the ith cylinder is given by

$$E_{zi}^{d(0)}(\rho_i, \phi_i) = \sum_{n=-\infty}^{\infty} b_{in}^0 J_n(k_i\rho_i) e^{jn\phi_i}, \tag{6}$$

where c_{in}^0 and b_{in}^0 are the unknown coefficients, $J_n(k_i\rho_i)$, $H_n^{(2)}(k_0\rho_i)$ denotes Bessel and Hankel functions, respectively and $k_i = \omega\sqrt{\varepsilon_{f(i)}\mu_{eff(i)}}$, $\mu_{eff(i)} = (\mu_i^2 - \mu_{a(i)}^2)/\mu_i$, denotes the effective ferrite permeability where μ_i, $\mu_{a(i)}$ are tensor elements. The corresponding magnetic field along ϕ direction can be established from

$$H_\phi = -\frac{1}{j\omega\mu_0\mu_{eff(i)}}\left(\frac{\partial E_z}{\partial\rho} + j\frac{\mu_{a(i)}}{\mu_i\rho}\frac{\partial E_z}{\partial\phi}\right). \tag{7}$$

Applying (2) into Eqs. (3) and (4) and orthogonalizing by $e^{-jm\phi_i}$, the solution is obtained from the point of view of the unknown coefficients c_{in}^0 of the ith cylinder

$$[c_i^0] = [G_i]\cdot[T_{io}]\cdot[a], \tag{8}$$

where $[G_i]$ is shown in (8a) at the top of the following page.

Here the prime symbol denotes the derivative with respect to argument. For dielectric structures we assume that $\mu_{a(i)} = 0$ and $\mu_{eff(i)} = \mu_i = 1$. Transformation of Bessel functions from global coordinates to the local coordinates of the ith cylinder is expressed by matrix

$$[T_{io}] = \left[J_{m-n}(k_0 d_{io})\, e^{j(n-m)\phi_{io}}\right]_{m,n=-\infty}^{\infty} \tag{9}$$

and m, n are rows and columns indexes respectively, while $[a]$ defines a vector

$$[a] = \left[\ldots\ a_{-m}\ \ldots\ a_0\ a_1\ \ldots\ a_m\ \ldots\right]^T. \tag{10}$$

In the next interaction, we use scattered fields from $M-1$ cylinders from the previous interaction as a new incident field on the ith remaining cylinder

$$E_{zi}^{inc(1)} = E_0 \sum_{\substack{j=1\\ j\neq i}}^{M} \sum_{n=-\infty}^{\infty} c_{jn}^0 H_n^{(2)}(k_0\rho_j)\, e^{jn\phi_j}. \tag{11}$$

To transfer the scattered fields from $M-1$ cylinders to the local coordinate of the ith cylinder the Graf's addition theorem for Bessel functions is used [5] (see Eq. (12) at the top of the following page).

In response to our new excitation, the first order ($p = 1$) scattered and transmitted field is created from each of M cylinders like in Eqs. (5) and (6) but with new unknown coefficients c_{in}^1 and b_{in}^1. Using Eqs. (3) and (4) with the first order fields the following solution is obtained:

$$[c_i^1] = [G_i] \sum_{\substack{j=1\\ j\neq i}}^{M} [T_{ij}^H]\cdot[c_j^0], \tag{13}$$

where $[T_{ij}^H] = \left[H_{m-n}^{(2)}(k_0 d_{ij}) e^{j(n-m)\phi_{ij}}\right]_{m,n=-\infty}^{\infty}$ and m, n are rows and columns indexes, respectively. The matrix $[T_{ij}^H]$ provides transformation of Hankel functions of the second kind located in the coordinates of the jth cylinder to the ones located in the coordinates of the ith cylinder.

This approach gives us a next order scattered field and repeated for each individual cylinder leads us to an iterative scattering procedure where the coefficients of the pth interaction depend only on the coefficients of the $(p-1)$th interaction

$$[C^p] = [T^{ij}]\cdot[C^{p-1}]\cdot[a], \tag{14}$$

where

$$[C^p] = \begin{bmatrix} [c_1^p] \\ \cdot \\ [c_i^p] \\ \cdot \\ [c_M^p] \end{bmatrix}, \quad [T_{ij}] = \begin{bmatrix} [0] & \cdot & [T_{1,j}] & \cdot & [T_{1,M}] \\ \cdot & [0] & \cdot & \cdot & \cdot \\ [T_{j,1}] & \cdot & \cdot & \cdot & [T_{j,M}] \\ \cdot & \cdot & [T_{i,j}] & [0] & \cdot \\ [T_{M,1}] & \cdot & [T_{M,j}] & \cdot & [0] \end{bmatrix}$$

for $p = 2, 3, \ldots$ and $[c_i^p]$, $[0]$, $[T_{i,j}]$ are square sub-matrices where

$$[T_{i,j}] = [G_i]\cdot[T_{ij}^H]. \tag{15}$$

Iterative procedure gives us the scattered field from the ith cylinder in its local coordinates as follows

$$[E_{zi}^S] = [H_i^\rho]\cdot[C_i]\cdot[a], \tag{16}$$

where $[C_i] = \sum_{p=0}^{N}[c_i^p]$, $[H_i^\rho] = diag\left(H_m^{(2)}(k_0\rho_i)e^{jm\phi_i}\right)_{m=-\infty}^{\infty}$ and N is the number of interactions.

$$[G_i] = diag\left(\frac{k_0 J_m(k_i r_i) J'_m(k_0 r_i) - J_m(k_0 r_i)\left[\frac{k_i}{\mu_{eff(i)}} J'_m(k_i r_i) - m\frac{\mu_{a(i)}}{\mu_{eff(i)}\mu_i r_i} J_m(k_i r_i)\right]}{H_m^{(2)}(k_o r_i)\left[\frac{k_i}{\mu_{eff(i)}} J'_m(k_i r_i) - m\frac{\mu_{a(i)}}{\mu_{eff(i)}\mu_i r_i} J_m(k_i r_i)\right] - k_0 J_m(k_i r_i) H_m^{(2)\prime}(k_0 r_i)} \right)_{m=-\infty}^{\infty}. \tag{8a}$$

$$H_n^{(2)}(k_0\rho_j)e^{jn\phi_j} = \left\{ \begin{array}{ll} \sum\limits_{m=-\infty}^{\infty} H_{m-n}^{(2)}(k_0 d_{ij}) e^{j(n-m)\phi_{ij}} J_m(k_0\rho_i) e^{jm\phi_i} & \text{for} \quad d_{ij} \geq \rho_i \\ \sum\limits_{m=-\infty}^{\infty} J_{m-n}(k_0 d_{ij}) e^{j(n-m)\phi_{ij}} H_m^{(2)}(k_0\rho_i) e^{jm\phi_i} & \text{for} \quad d_{ij} < \rho_i \end{array} \right\}. \tag{12}$$

Using transformation (12) for $d_{ij} < \rho_o$ the scattered field from each cylinder is transferred to global coordinate system. Therefore the scattered electric field from the ith cylinder on the surface of the interaction region (see Fig. 2) is given as

$$\left[E_{zi}^{SG}\right] = \left[H_i^R\right] \cdot \left[T_{oi}^G\right] \cdot [C_i] \cdot [a], \tag{17}$$

where

$$\left[H_i^R\right] = diag\left(H_m^{(2)}(k_0 R) e^{jm\phi}\right)_{m=-\infty}^{\infty}$$

$$\left[T_{oi}^G\right] = \left[J_{m-n}(k_0 d_{oi}) e^{j(n-m)\phi_{oi}}\right]_{m,n=-\infty}^{\infty}$$

and m, n are rows and columns indexes, respectively.

Writing (17) for electric and magnetic field for each of M cylinders we obtain the following matrix equations:

$$\left[E_z^{SG}\right] = \left[H^R\right] \cdot \left[T^G\right] \cdot [C] \cdot [a], \tag{18}$$

$$\left[H_\phi^{SG}\right] = \tfrac{1}{j\omega\mu_0}\left[H'^R\right] \cdot \left[T^G\right] \cdot [C] \cdot [a], \tag{19}$$

where

$$\left[E_z^{SG}\right] = \left[\left[E_{z1}^{SG}\right] \; . \; \left[E_{zi}^{SG}\right] \; . \; \left[E_{zM}^{SG}\right]\right]^T,$$

$$\left[H_\phi^{SG}\right] = \left[\left[H_{\phi 1}^{SG}\right] \; . \; \left[H_{\phi i}^{SG}\right] \; . \; \left[H_{\phi M}^{SG}\right]\right]^T,$$

and

$$\left[H^R\right] = \begin{bmatrix} [H_1^R] & . & [0] & . & [0] \\ . & . & . & . & . \\ [0] & . & [H_i^R] & . & [0] \\ . & . & . & . & . \\ [0] & . & [0] & . & [H_M^R] \end{bmatrix},$$

$$\left[T^G\right] = \begin{bmatrix} [T_{o1}^G] & . & [0] & . & [0] \\ . & . & . & . & . \\ [0] & . & [T_{oi}^G] & . & [0] \\ . & . & . & . & . \\ [0] & . & [0] & . & [T_{oM}^G] \end{bmatrix}, \quad [C] = \begin{bmatrix} [C_1] \\ . \\ [C_i] \\ . \\ [C_M] \end{bmatrix}.$$

Matrices $\left[H_i^R\right]$, $\left[T_{oi}^G\right]$, $[C_i]$ and $[0]$ are square sub-matrices.

The total scattered electric and magnetic field from all cylinders, can be easy obtained from

$$\left[E_z^{SGT}\right] = [I] \cdot \left[E_z^{SG}\right], \tag{20}$$

$$\left[H_\phi^{SGT}\right] = [I] \cdot \left[H_\phi^{SG}\right], \tag{21}$$

where matrix $[I]$ consists of diagonal sub-matrices $[I_i] = diag(1)_{m=-\infty}^{\infty}$ as shown $[I] = \left[[I_1] \; \ldots \; [I_i] \; \ldots \; [I_M]\right]$.
Now the total field on the surface of the interaction region can be defined as

$$\left[E_z^T\right] = \left[E_z^{inc(0)}\right] + \left[E_z^{SGT}\right], \tag{22}$$

$$\left[H_\phi^T\right] = \left[H_\phi^{inc(0)}\right] + \left[H_\phi^{SGT}\right], \tag{23}$$

where $\left[E_z^{inc(0)}\right]$ and $\left[H_\phi^{inc(0)}\right]$ are diagonal matrices based on (1). To eliminate unknown coefficients (10), a relation between electric and magnetic field on the surface of the interaction region is defined:

$$\left[E_z^T\right] = [Z] \cdot \left[H_\phi^T\right]. \tag{24}$$

Hence, the matrix $[Z]$ is given as

$$[Z] = \left(\left[E_z^{inc(0)}\right] + \left[E_z^{SGT}\right]\right) \cdot \left(\left[H_\phi^{inc(0)}\right] + \left[H_\phi^{SGT}\right]\right)^{-1}. \tag{25}$$

The formulation of the problem in form of $[Z]$ allows to consider both waveguide and open problems assuming the proper excitations.

3. Conclusions

The analysis for scattering by an array of lossy dielectric, ferrite and/or conducting cylinders has been developed using a combination of modified iterative scattering procedure and the orthogonal expansion method. This approach is convenient for investigations of the open and waveguide problems.

References

[1] C. W. Chew, L. Gurel, Y. M. Wang, G. Otto, R. L. Wagner, and Q. H. Liu, "A generalized recursive algorithm for wave scattering solution in two dimensions", *IEEE Trans. Microw. Theory Techn.*, vol. 40, pp. 716–723, 1992.

[2] A. Z. Elsherbeni, M. Hamid, and G. Tian, "Iterative scattering of a Gaussian beam by an array of circular conducting and dielectric cylinders", *J. Electromagn. Wav. Appl.*, vol. 7, no. 10, pp. 1323–1342, 1993.

[3] R. Gesche and N. Löchel, "Two cylindrical obstacles in a rectangular waveguide-resonances and filter applications", *IEEE Trans. Microw. Theory Techn.*, vol. 37, pp. 962–968, 1989.

[4] A. Valero and M. Ferrando, "Full-wave equivalent network representation for multiple arbitrary shaped posts in H-plane waveguide", *IEEE Trans. Microw. Theory Techn.*, vol. 47, pp. 1997–2002, 1999.

[5] M. Abramovitz and I. Stegun, *Handbook of Mathematical Functions*. New York: Dover, 1970.

Michał Polewski, was born in 1975, in Kalisz, Poland. He graduated from the Faculty of Microwave Technology and Optical Telecommunications of the Technical University of Gdańsk (TUG) in 1999. He is currently a Ph.D. student at the Technical University of Gdańsk. His research interests include numerical methods and analysis of wave propagation in waveguides with circular obstacles.
e-mail: mip@eti.pg.gda.pl
Faculty of Electronics, Telecommunications
and Informatics (ETI)
Technical University of Gdańsk
Narutowicza st 11/12
80-952 Gdańsk, Poland

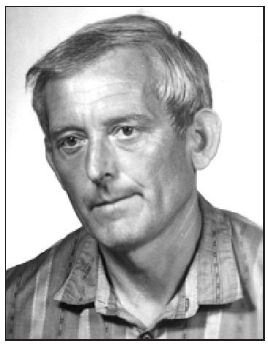

Jerzy Mazur was born in Brno, Czechoslovakia, on March 23, 1946. He graduated from the Technical University of Gdańsk (TUG), Poland, in 1969. He received the Ph.D. and habilitation degrees in electrical communication engineering from TUG in 1976 and 1983, respectively where he is currently a Professor. Since 1992, he has been also a consultant at Telecommunications Research Institute, Division in Gdańsk, Poland. He received Professor title in 1993. His research interests are concerned with electromagnetic field theory and integrated circuits for microwave and millimeter-wave applications.
e-mail: jem@pg.gda.pl
Faculty of Electronics, Telecommunications
and Informatics (ETI)
Technical University of Gdańsk
Narutowicza st 11/12
80-952 Gdańsk, Poland

INFORMATION FOR AUTHORS

The *Journal of Telecommunications and Information Technology* is published quarterly. It comprises original contributions, both regular papers and letters, dealing with a broad range of topics related to telecommunications and information technology. Items included in the journal report primary and/or experimental research results, which advance the base of scientific and technological knowledge about telecommunications and information technology.

The *Journal* is dedicated to publishing research results which advance the level of current research or add to the understanding of problems related to modulation and signal design, wireless communications, optical communications and photonic systems, speech devices, image and signal processing, transmission systems, network architecture, coding and communication theory, as well as information technology. Suitable research-related manuscripts should hold the potential to advance the technological base of telecommunications and information technology. Tutorial and review papers are published by invitation only.

Papers published by invitation and regular papers should contain up to 15 and 8 printed pages respectively (one printed page corresponds approximately to 3 double-space pages of manuscript, where one page contains approximately 2000 characters).

Manuscript: An original and two copies of the manuscript must be submitted, each completed with all illustrations and tables attached at the end of the papers. Tables and figures have to be numbered consecutively with Arabic numerals. The manuscript must include an abstract limited to approximately 100 words. The abstract should contain four points: statement of the problem, assumptions and methodology, results and conclusion, or discussion, of the importance of the results. The manuscript should be double-spaced on only one side of each A4 sheet (210 × 297 mm). Computer notation such as Fortran, Matlab, Mathematica etc., for formulae, indices, etc., is not acceptable and will result in automatic rejection of the manuscript. The style of references, abbreviations, etc., should follow the standard IEEE format.

References should be marked in the text by Arabic numerals in square brackets and listed at the end of the paper in order of their appearance in the text, including exclusively publications cited inside. The **reference entry** (correctly punctuated according to the following rules and examples) **has to contain**.

From journals and other serial publications: initial(s) and second name(s) of the author(s), full title of publication (transliterated into Latin characters in case it is in Russian, possibly preceded by the title in Russian characters), appropriately abbreviated title of periodical, volume number, first and last page number, year. E.g.:

[1] Y. Namihira, „Relationship between nonlinear effective area and modefield diameter for dispersion shifted fibres", *Electron. Lett.*, vol. 30, no. 3, pp. 262–264, 1994.

From non-periodical, collective publications: as above, but after title – the name(s) of editor(s), title of volume and/or edition number, publisher(s) name(s) and place of edition, inclusive pages of article, year. E.g.:

[2] S. Demri, E. Or^{3}owska, „Informational representability: Abstract models versus concrete models" in *Fuzzy Sets, Logics and Reasoning about Knowledge*, D. Dubois and H. Prade, Eds. Dordrecht: Kluwer, 1999, pp. 301–314.

From books: initial(s) and name(s) of the author(s), place of edition, title, publisher(s), year. E.g.:

[3] C. Kittel, *Introduction to Solid State Physics*. New York: Wiley, 1986.

Figure captions should be started on separate sheet of papers and must be double-spaced.

Illustration: Original illustrations should be submitted. All line drawings should be prepared on white drawing paper in black India ink. Drawings in Corel Draw and Postscript formats are preferred. Colour illustrations are accepted only in exceptional circumstances. Lettering should be large enough to be readily legible when drawing is reduced to two- or one-column width – as much as 4:1 reduction from the original. Photographs should be used sparingly. All photographs must be gloss prints. All materials, including drawings and photographs, should be no larger than 175 × 260 mm.

Page number: Number all pages, including tables and illustrations (which should be grouped at the end), in a single series, with no omitted numbers.

Electronic form: A floppy disk together with the hard copy of the manuscript should be submitted. It is important to ensure that the diskette version and the printed version are identical. The diskette should be labelled with the following information: a) the operating system and word-processing software used, b) in case of UNIX media, the method of extraction (i.e. tar) applied, c) file name(s) related to manuscript. The diskette should be properly packed in order to avoid possible damage during transit.

Among various acceptable word processor formats, TEX and LATEX are preferable. The *Journal's* style file is available to authors.

Galley proofs: Proofs should be returned by authors as soon as possible. In other cases, the article will be proof-read against manuscript by the editor and printed without the author's corrections. Remarks to the errata should be provided within two weeks after receiving the offprints.

The copy of the „Journal" shall be provided to each author of papers.

Copyright: Manuscript submitted to this journal may not have been published and will not be simultaneously submitted or published elsewhere. Submitting a manuscript, the authors agree to automatically transfer the copyright for their article to the publisher if and when the article is accepted for publication. The copyright comprises the exclusive rights to reproduce and distribute the article, including reprints and also all translation rights. No part of the present journal may be reproduced in any form nor transmitted or translated into a machine language without permission in written form from the publisher.

Biographies and photographs of authors are printed with each paper. Send a brief professional biography not exceeding 100 words and a gloss photo of each author with the manuscript.

Integration of home digital network and Bluetooth wireless communication system

T. Keller and J. Modelski — *Paper* — 45

Applying the relational modelling and knowledge-based techniques to the emitter database design

J. Dudczyk, J. Matuszewski, and M. Wnuk — *Paper* — 51

Optimal site and antenna location for UMTS - output results of 3G network simulation software

M. J. Nawrocki and T. W. Więckowski — *Paper* — 55

FDTD modeling and experimental verification of electromagnetic power dissipated in domestic microwave ovens

P. Kopyt and M. Celuch-Marcysiak — *Paper* — 59

Theory of scattering by an array of lossy dielectric, ferrite and conducting cylinders

M. Polewski and J. Mazur — *Paper* — 66

National Institute
of Telecommunications
Szachowa st 1
04-894 Warsaw, Poland

Editorial Office

tel. +48(22) 872 43 88
tel./fax: +48(22) 512 84 00
e-mail: redakcja@itl.waw.pl
http://www.itl.waw.pl/jtit